*J Toxicol Pathol 2012; **25**: 63–101*

Report

Histopathology of Incidental Findings in Cynomolgus Monkeys (*Macaca Fascicularis*) Used in Toxicity Studies

Junko Sato[1], Takuya Doi[1], Takeshi Kanno[1], Yumi Wako[1], Minoru Tsuchitani[1], and Isao Narama[2]

[1] Pathology Department, Kashima Laboratory, Nonclinical Research Center, Mitsubishi Chemical Medience Corporation, 14-1 Sunayama, Kamisu, Ibaraki 314-0255, Japan
[2] Department of Pathology, Faculty of Pharmaceutical Sciences, Setsunan University, 45-1 Nagaotouge, Hirakata, Osaka 573-0101, Japan

Abstract. The purpose of our publication is to widely communicate pictures of spontaneous findings occurring in cynomolgus monkeys. Focal lymphoplasmacytic infiltration is commonly seen in the general organs. The frequency and severity of these lesions may be influenced by the administration of drugs with an effect on the immune system. Lymphoplasmacytic infiltration in the lamina propria of the stomach is also frequently seen in cynomolgus monkeys, and it is caused mainly by a *Helicobacter pylori* infection. Various degrees of brown pigments are observed in various organs, and it is possible to distinguish the material of the pigments by its morphological features and site. A focal/segmental glomerular lesion is occasionally seen in a section of the kidney, and the minimal lesion has no influence on the urinalysis. We showed the common glomerular lesions in HE-stained sections, as well as in PAM- or PAS-stained sections, for understanding the details. Young and pubertal monkeys are usually used in toxicity studies; therefore, understanding various maturation stages of the genital system is important. In particular, the female genital system needs to be understood in the morphology, because their cyclic changes are different from other laboratory animals. Thus, we present the normal features of the cyclic changes of the female genital organs. Furthermore, we provide more information on spontaneous findings in cynomolgus monkeys for exact diagnoses in toxicity studies. (DOI: 10.1293/tox.25.63; J Toxicol Pathol 2012; 25: 63–101)

Key words: cynomolgus monkey, spontaneous, incidental, histopathology, background

Introduction

To achieve an accurate pathological evaluation in toxicity studies, it is particularly important to know the background histopathology, that is, to be familiar with pictures of incidental findings. As abundant studies using rats are common in laboratories, toxicological pathologists know the background data of spontaneous lesions in rats and can visualize these histological figures easily. Meanwhile with monkeys, only a few pathologists in limited laboratories have experience with studies using nonhuman primates. Therefore, most pathologists cannot help but depend on the literature or textbooks to participate in the evaluation of monkey studies as a study pathologist or reviewing pathologist[1–7]. In the present state, however, relatively few background data or pictures of incidental findings in monkeys have been published due to the lack of understanding of the importance of publishing incidental findings, which are pathologically or toxicologically insignificant spontaneous lesions with no sign of disease.

Therefore, in this report, we provide pictures of spontaneous lesions in cynomolgus monkeys (*Macaca fascicularis*) that were detected in background data collection studies and ordinary toxicity studies in our laboratory. The figures are grouped and arranged according to the cardiovascular, lymphoid, respiratory, alimentary, urinary, reproductive, endocrine, nervous, musculoskeletal and integumentary systems.

Materials and Methods

A total of 660 cynomolgus monkeys (332 males and 328 females) were subjected to background data collection studies and ordinary toxicity studies conducted in our laboratory from 1998 to 2011. The age range was 2 years and 10 months to 13 years. They were imported from the Philippines (44 males and 50 females), Indonesia (7 males and 7 females), Malaysia (10 females), Vietnam (271 males and 251 females) and China (10 males and 10 females). The animals were housed individually in metal cages (680 × 608

Received: 9 August 2011, Accepted: 12 September 2011
Mailing address: Junko Sato, Kashima Laboratory, Mitsubishi Chemical Medience Corporation, 14-1 Sunayama, Kamisu, Ibaraki 314-0255, Japan
TEL: 81-479-46-2871 FAX: 81-479-46-2874
E-mail. Satou.Junko@ms.medience.co.jp

× 770 mm or 680 × 658 × 770 mm) in conventional rooms air-conditioned at 23 °C to 29 °C with 35% to 75% relative humidity and a 12-hour light/12-hour dark cycle. They were provided with 100 g of commercially available food (CMK-1, CMK-1α or CMK-2, CLEA Japan, Inc.) daily and were also allowed free access to drinking water. The animals were cared for according to the principles outlined in the guides for the care and use of laboratory animals prepared by the Japanese Association for Laboratory Animal Science and our institution.

Organs fixed in 10% neutral phosphate-buffered formalin were embedded in paraffin, and the sections were made and stained with hematoxylin and eosin (HE) for microscopic examination. Selected sections were stained with Warthin-Starry, periodic acid-Schiff (PAS) and periodic acid-methenamine-silver (PAM).

Results

We chose 195 typical findings or rare lesions of the cynomolgus monkeys from the background data collection studies and ordinary toxicity studies conducted in our laboratory, and they are shown as follows. Detailed explanations for these findings are shown in the figure legends.

Fig. 1. Heart: Focal inflammatory cell infiltration in the myocardium
Fig. 2. Heart: Focal myocardial necrosis
Fig. 3. Heart: Proliferation and squamous metaplasia of the epicardial mesothelium
Fig. 4. Heart: Hemorrhage in the endocardium
Fig. 5. Heart: Arterial sclerosis
Fig. 6. Heart: Infarction (Elastica-van Gieson)
Fig. 7. Artery: Arteritis in the mural artery
Fig. 8. Artery: Arteritis in the coronary artery
Fig. 9. Artery: Arteritis in the kidney
Fig. 10. Artery: Arteritis in the intestinal artery
Fig. 11. Artery: Arteritis in the bronchial artery
Fig. 12. Artery: Arteritis in the epididymis
Fig. 13. Mesenteric lymph node: Increased number of pigment-laden macrophages in the sinuses
Fig. 14. Thymus: Involution (physiological atrophy)
Fig. 15. Thymus: Cyst
Fig. 16. Thymus: Ectopic parathyroid tissue
Fig. 17. Thymus: Ectopic muscle tissue
Fig. 18. Thymus: Lymph follicle formation in the medulla
Fig. 19. Thymus: Proliferation of the thymic epithelium
Fig. 20. Thymus: Thymoma (mixed thymoma)
Fig. 21. Spleen: Nodular hyperplasia (lymphoid follicle)
Fig. 22. Spleen: Nodular hyperplasia (red pulp)
Fig. 23. Spleen: Hyalinization of the germinal center
Fig. 24. Spleen: Pigment deposition in the red pulp
Fig. 25. Bone marrow: Lymph follicle formation
Fig. 26. Bone marrow: Pigment deposition
Fig. 27. Nasal cavity: Hyperplasia of the lymph follicle
Fig. 28. Nasal cavity: Mucosal erosion of the turbinate
Fig. 29. Lung: Focal hemorrhage in the alveolus
Fig. 30. Lung: Accumulation of pigment-laden macrophages
Fig. 31. Lung: Anthracotic pigment deposition (anthracosis)
Fig. 32. Lung: Thrombus
Fig. 33. Lung: Accumulation of foam cells in the alveolus
Fig. 34. Lung: Focal infiltration of macrophages in the alveolus
Fig. 35. Lung: Foreign body granuloma
Fig. 36. Lung: Focal hyperplasia of the alveolar epithelium
Fig. 37. Lung: Pulmonary acariasis
Fig. 38. Lung: Osseous metaplasia
Fig. 39. Tongue: Focal inflammatory cell infiltration
Fig. 40. Tongue: Erosion
Fig. 41. Tongue: Edema/reticular degeneration
Fig. 42. Tongue: Foreign body granuloma
Fig. 43. Tongue: Regeneration of the muscle fiber
Fig. 44. Esophagus: Focal inflammatory cell infiltration in the lamina propria
Fig. 45. Stomach: Inflammatory cell infiltration in the lamina propria
Fig. 46. Stomach: Infection by *Helicobacter pylori* in the gastric mucosa
Fig. 47. Stomach: Infection by *Helicobacter heilmannii* in the gastric mucosa
Fig. 48. Stomach: Erosion
Fig. 49. Duodenum: Pigment deposition
Fig. 50. Duodenum: Ectopic pancreatic tissue
Fig. 51. Duodenum: Necrosis of the muscle layer
Fig. 52. Ileum (Jejunum): Increase in goblet cells
Fig. 53. Rectum: Dilatation of the crypt
Fig. 54. Salivary gland: Focal inflammatory cell infiltration
Fig. 55. Salivary gland: Focal fibrosis
Fig. 56. Salivary gland: Hydropic degeneration of acinar cells
Fig. 57. Salivary gland: Salivary calculus and inflammatory cell infiltration
Fig. 58. Liver: Eosinophilic inclusion bodies in hepatocytes
Fig. 59. Liver: Accumulation of glycogen in hepatocytes
Fig. 60. Liver: Diffuse fatty change of hepatocytes
Fig. 61. Liver: Focal fatty change of hepatocytes
Fig. 62. Liver: Focal necrosis of hepatocytes
Fig. 63. Liver: Microgranuloma
Fig. 64. Liver: Focal inflammatory cell infiltration
Fig. 65. Liver: Pericholangitis
Fig. 66. Liver: Pigment deposition in Kupffer cells
Fig. 67. Gall bladder: Inflammatory cell infiltration in the lamina propria
Fig. 68. Pancreas: Ectopic splenic tissue
Fig. 69. Pancreas: Lobular atrophy of the acinus
Fig. 70. Pancreas: Hydropic degeneration of acinar cells
Fig. 71. Pancreas: Apoptosis of acinar cells
Fig. 72. Pancreas: Decrease in zymogen granules
Fig. 73. Pancreas: Chronic pancreatitis
Fig. 74. Pancreas: Chronic pancreatitis
Fig. 75. Pancreas: Focal inflammatory cell infiltration

Fig. 167. Adrenal: Decreased lipid droplets in cortical cells
Fig. 168. Adrenal: Mineralization in the corticomedullary junction
Fig. 169. Adrenal: Pigment deposition in the corticomedullary junction
Fig. 170. Adrenal: Pigment deposition in the cells of the zona reticularis
Fig. 171. Adrenal: Adrenohepatic fusion
Fig. 172. Adrenal: Focal inflammatory cell infiltration
Fig. 173. Brain (Spinal cord): Melanin pigment deposition in the meninx and vascular wall (perivascular tissue)
Fig. 174. Brain: Hemosiderin pigment deposition in the meninx or cerebral cortex
Fig. 175. Brain: Focal inflammatory cell infiltration in the meninx
Fig. 176. Brain: Focal inflammatory cell infiltration in the choroid plexus
Fig. 177. Brain: Focal perivascular inflammatory cell infiltration
Fig. 178. Spinal cord: Mineralization in the meninx
Fig. 179. Spinal cord: Mineralization in the arterial wall
Fig. 180. Spinal cord: Pigment deposition in neuronal cells
Fig. 181. Sciatic nerve: Renaut body
Fig. 182. Sciatic nerve: Focal inflammatory cell infiltration
Fig. 183. Sciatic nerve: Focal fibrosis
Fig. 184. Eye: Focal inflammatory cell infiltration in the conjunctiva
Fig. 185. Eye: Focal inflammatory cell infiltration in the ciliary body
Fig. 186. Eye: Cataract
Fig. 187. Eye: Disarrangement of retinal structures
Fig. 188. Lacrimal gland: Focal inflammatory cell infiltration
Fig. 189. Lacrimal gland: Melanin pigment deposition
Fig. 190. Skeletal muscle: Focal inflammatory cell infiltration
Fig. 191. Skeletal muscle: Focal fibrosis
Fig. 192. Skin: Focal inflammatory cell infiltration in the dermis
Figs. 193–195. Stress-induced lesions

Discussion

In veterinary pathology and toxicological pathology, many textbooks have been published, and information concerning the disease pathology in rodents and dogs is readily available. However, the publications referring to spontaneous lesions are substantially fewer in cynomolgus monkeys than those in other laboratory animals. Furthermore, publications showing pictures of spontaneous nonneoplastic lesions exhaustively as a histopathology atlas cannot be found except for a color atlas of diseases in nonhuman primates[7]. Therefore, we provided many pictures of spontaneous lesions in cynomolgus monkeys that were detected in background data collection studies and ordinary toxicity studies in our laboratory.

The common lesions of the heart, such as focal inflammatory cell infiltration in the myocardium (Fig. 1), focal myocardial necrosis (Fig. 2), proliferation and squamous metaplasia of the epicardial mesothelium (Fig. 3), hemorrhage in the endocardium (Fig. 4), and arterial sclerosis (Fig. 5) have been previously reported[8,9].

Arteritis in cynomolgus monkeys is usually observed in one or a few organs/tissues, and systemic arteritis is rare. There is a case report of polyarteritis nodosa in a cynomolgus monkey[10]. Morphologically, the features of arteritis in the previous report are similar to those in Figs. 7–11.

Testicular spermatogenesis of cynomolgus monkeys was reported in detail by Dreef *et al*.[11]. The female monkey genital system needs to be understood morphologically because the cyclic changes are different from those of other laboratory animals. Cyclic changes in the ovaries of nonhuman primates during the menstrual cycle were reported in detail by Koering[12], and common lesions in the female reproductive system such as deciduosis (Fig. 133)[13], mineralization (Fig. 134)[13], ectopic ovarian tissue (Fig. 139)[13,14] and adenomyosis and endometriosis (Fig. 140)[13,15] were reported previously. Ovarian tumors occasionally occur in monkeys, and some case reports refer to those in cynomolgus monkeys, including a report of mucinous cystadenoma (Fig. 138) in cynomolgus monkeys[16].

Concerning the common lesions of cynomolgus monkeys, we introduced the reports of multinucleated epithelial cells in collecting tubules (Fig. 91)[17], eosinophilic droplets in the transitional epithelium (Fig. 107)[18], adenohepatic fusion (Fig. 171)[19] and focal inflammatory cell infiltration in the ciliary body (Fig. 185)[20].

Concerning the rare lesions of young cynomolgus monkeys, we also introduced the reports of thymoma (Fig. 20)[21] and cataract (Fig. 186)[22] in the Journal of Toxicologic Pathology.

Indeed, not all lesions have been comprehended in various textbooks or journals. Therefore, we have to keep collecting background data continuously. These background lesions may not have an effect on the results of toxicity studies but should be taken into account along with their potential to influence safety assessment in drug administration.

Acknowledgments: The authors thank Dr. Tokuma Yanai and Dr. Kimiaki Hirakawa for their critical reviews and Dr. Dai Nakae for helpful advice and support on preparing the manuscript. The authors also thank Mr. Steve Yamakami and Ms. Azumi Takahashi for language editing.

References

1. Bennett BT, Abee CR, and Henrickson R. Nonhuman Primates in Biomedical Research Diseases. Academic Press, San Diego. 1998.
2. Jones TC, Mohr U, and Hunt RD. Nonhuman Primates I. Springer-Verlag, Berlin. 1993.
3. Jones TC, Mohr U, and Hunt RD. Nonhuman Primates II.

Springer-Verlag, Berlin. 1993.
4. Takayama S, Fukushima S, and Thorgeirsson UP. Atlas of Spontaneous and Chemically Induced Tumors in Non-human Primates. Japan Scientific Societies Press, Tokyo. 2000.
5. Benirschke K, Garner FM, and Jones TC. Pathology of Laboratory Animals. Springer-Verlag, New York. 1978.
6. Chamanza R, Marxfeld HA, Blanco AI, Naylor SW, and Bradley AE. Incidences and range of spontaneous findings in control cynomolgus monkeys (*Macaca fascicularis*) used in toxicity studies. Toxicol Pathol. **38**: 642–657. 2010. [Medline] [CrossRef]
7. The Society of Primate Diseases and Pathology. Color Atlas of Diseases in Non-human Primates. The Corporation for Production and Research of Laboratory Primates, Ibaraki. 2011.
8. Keenan CM, and Vidal JD. Standard morphologic evaluation of the heart in the laboratory dog and monkey. Toxicol Pathol. **34**: 67–74. 2006. [Medline] [CrossRef]
9. Vidal JD, Drobatz LS, Holliday DF, Geiger LE, and Thomas HC. Spontaneous findings in the heart of Mauritian-origin cynomolgus macaques (*Macaca fascicularis*). Toxicol Pathol. **38**: 297–302. 2010. [Medline] [CrossRef]
10. Porter BF, Frost P, and Hubbard GB. Polyarteritis nodosa in a cynomolgus macaque (*Macaca fascicularis*). Vet Pathol. **40**: 570–573. 2003. [Medline] [CrossRef]
11. Dreef HC, Van Esch E, and De Rijk EPCT. Spermatogenesis in the cynomolgus monkey (*Macaca fascicularis*): a practical guide for routine morphological staging. Toxicol Pathol. **35**: 395–404. 2007. [Medline] [CrossRef]
12. Koering MJ. Cyclic changes in ovarian morphology during the menstrual cycle in Macaca mulatta. Am J Anat. **126**: 73–101. 1969. [Medline] [CrossRef]
13. Cline JM, Wood CE, Vidal JD, Tarara RP, Buse E, Weinbauer GF, De Rijk EPCT, and Van Esch E. Selected background findings and interpretation of common lesions in the female reproductive system in macaques. Toxicol Pathol. **36**: 142s–163s. 2008. [Medline] [CrossRef]
14. Kuwamura Y, Kakehi K, Hirakawa K, and Miyajima H. Ectopic uterine ovarian tissue in cynomolgus monkeys. Toxicol Pathol. **34**: 220–222. 2006. [Medline] [CrossRef]
15. Ito T, Sakamaki Y, Fujii E, Misawa Y, Suzuki M, and Sugimoto T. Endometriosis in a rhesus monkey. J Toxicol Pathol. **14**: 313–315. 2001. [CrossRef]
16. Sato J, Kokoshima H, and Tsuchitani M. Ovarian mucinous cystadenoma with smooth muscle proliferation in a cynomolgus monkey (*Macaca fascicularis*). Vet Pathol. **45**: 379–382. 2008. [Medline] [CrossRef]
17. Seaman WJ. Multinucleated epithelial cells of renal collecting tubules in macaques. Vet Pathol. **23**: 87–88. 1986. [Medline]
18. Burek JD, Van Zwieten MJ, and Stookey JL. Cytoplasmic inclusions in urinary bladder epithelium of the rhesus monkey. A histochemical, light- and electron-microscopic study. Vet Pathol. **9**: 212–220. 1972. [Medline] [CrossRef]
19. Mousa S, and Van Esch E. Two cases of adreno-hepatic fusion in cynomolgus monkeys (*Macaca fascicularis*). Toxicol Pathol. **32**: 511–513. 2004. [Medline] [CrossRef]
20. Sinha DP, Cartwright ME, and Johnson RC. Incidental mononuclear cell infiltrate in the uvea of cynomolgus monkeys. Toxicol Pathol. **34**: 148–151. 2006. [Medline] [CrossRef]
21. Kotani Y, Sato J, Wako Y, and Tsuchitani M. Mixed thymoma in a young cynomolgus monkey (*Macaca fascicularis*). J Toxicol Pathol. **23**: 141–145. 2010. [CrossRef]
22. Sasaki Y, Kodama R, Iwashige S, Fujishima J, Yoshikawa T, Kamimura Y, and Maeda H. Bilateral cataract in a cynomolgus monkey. J Toxicol Pathol. **24**: 69–73. 2011. [CrossRef]

All the figures of this report are released in color in J-STAGE and PubMed Central.

Figs. 3–5, 9–12, 14, 18, 21–23, 33, 35–37, 39–41, 44–48, 50, 53–54, 57–59, 61, 72–74, 81, 83–85, 87, 92, 94–95, 108–112, 114–116, 118, 120–121, 134–140, 145, 148–150, 153–156, 158, 160, 165–170, 174–175, 177, 179–181, and 185–188: Reprinted with permission of Mitsubishi Chemical Medience Corporation (MCM). Color Atlas; Histopathology of the Cynomolgus Monkey. MCM. 2006.

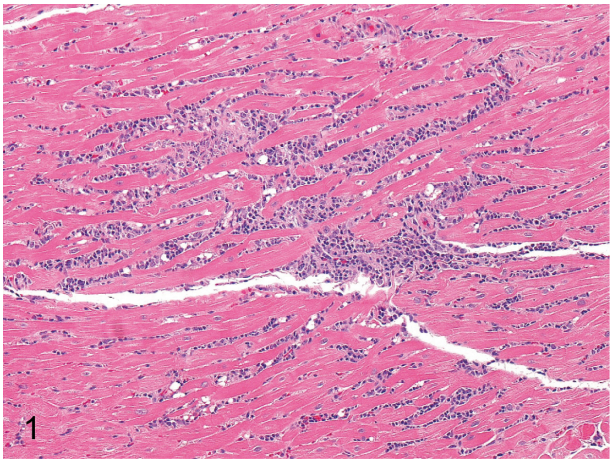

Fig. 1. Heart: Focal inflammatory cell infiltration in the myocardium. Focal infiltration of inflammatory cells mainly consisting of lymphocytes is frequently seen in the myocardium. This lesion is occasionally accompanied by focal myocardial necrosis.

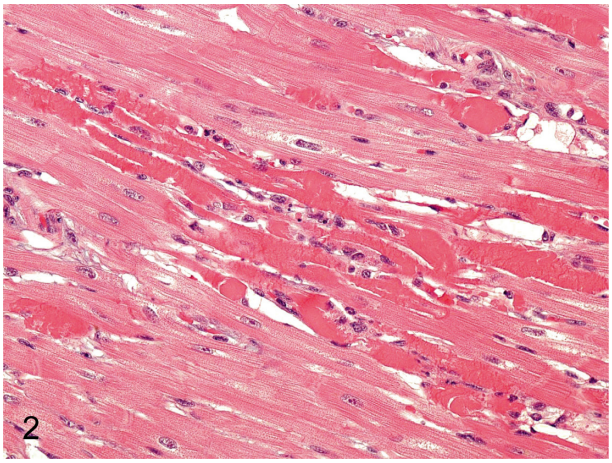

Fig. 2. Heart: Focal myocardial necrosis. Focal myocardial necrosis occurs occasionally, but a large focus like this case is rare. This lesion must be distinguished from artifacts because a similar figure is also formed due to inadequate handling of the heart during necropsy and tissue preparation.

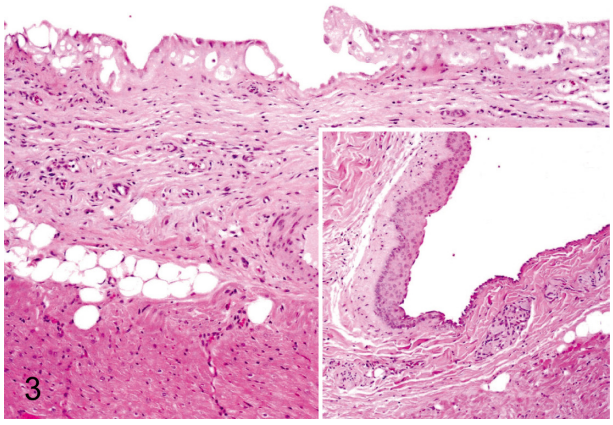

Fig. 3. Heart: Proliferation and squamous metaplasia of the epicardial mesothelium. Focal proliferation of single layered mesothelial cells occurs occasionally in the atrium (atrial auricle). Squamous metaplasia also occurs in the same area, but the incidence is low. They are thought to be reactive changes to some physical irritation.

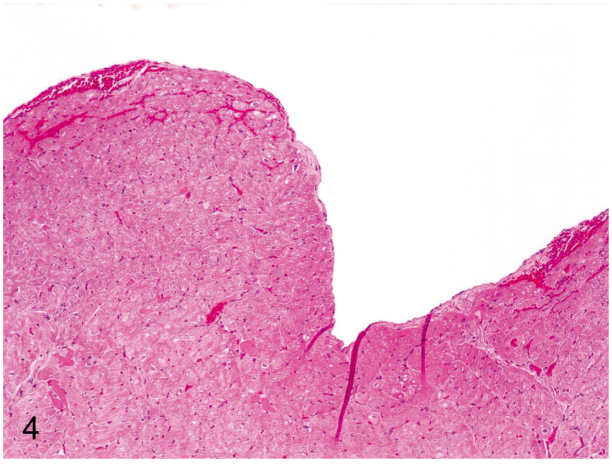

Fig. 4. Heart: Hemorrhage in the endocardium. Focal and mild hemorrhage in the endocardium and subendocardium is considered mainly to be an agonal change.

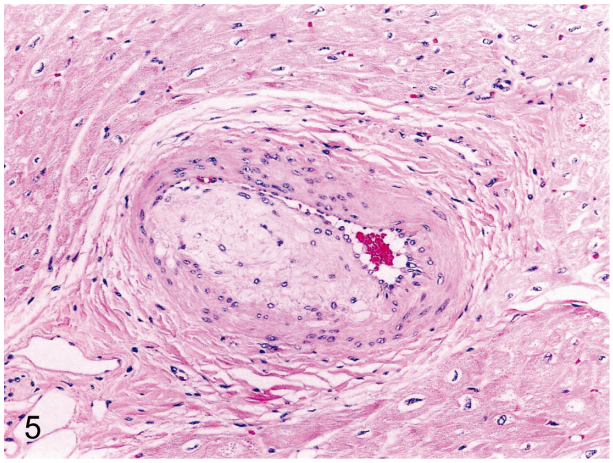

Fig. 5. Heart: Arterial sclerosis. Intimal and medial thickening of the arterial wall with duplication of the elastic lamina is rare in the coronary and mural arteries.

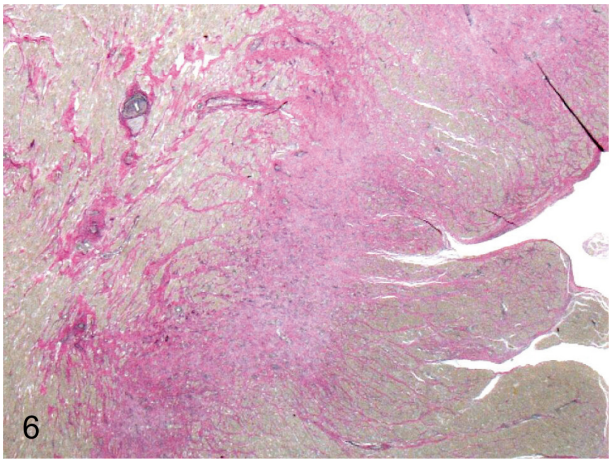

Fig. 6. Heart: Infarction (Elastica-van Gieson). This lesion is associated with arterial sclerosis (Fig. 5), presumably because of ischemia by arterial stenosis accompanied by a thickening of the wall.

Artery: Arteritis (Figs. 7–12)

The term of arteritis refers to various inflammatory changes of the arterial wall. Endarteritis, periarteritis and panarteritis are used to describe the affected part, and polyarteritis is used for multiple lesions. Various adjectives are added to describe the morphological characteristics such as acute arteritis, necrotizing arteritis, polyarteritis nodosa or granulomatous arteritis. Multiple synonyms have been used to describe the same changes. The most frequent locations are the heart, intestine and epididymis. Arteritis is usually observed in one or a few organs/tissues, and systemic arteritis is rare in cynomolgus monkeys.

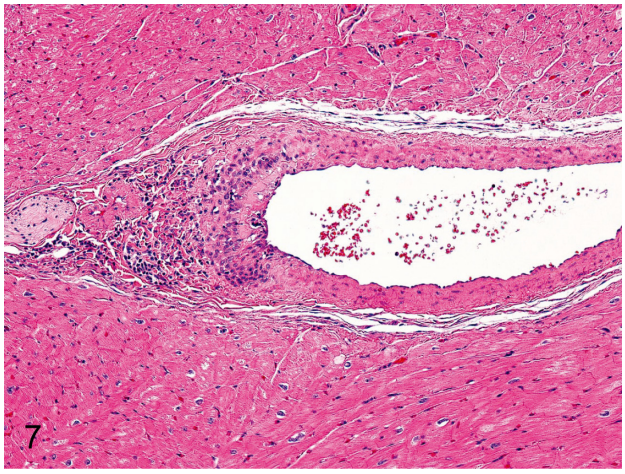

Fig. 7. Artery: Arteritis in the mural artery. Inflammatory cells infiltrate focally in the tunica intima and adventitia of the mural artery.

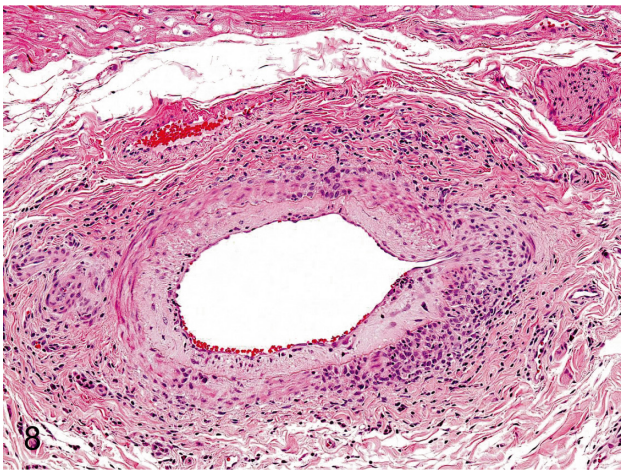

Fig. 8. Artery: Arteritis in the coronary artery. Panarteritis consists of intimal thickening and infiltration of lymphocytes from the tunica intima to the adventitia. The incidence and grade of arteritis in coronary arteries are remarkably lower in cynomolgus monkeys than in Beagles.

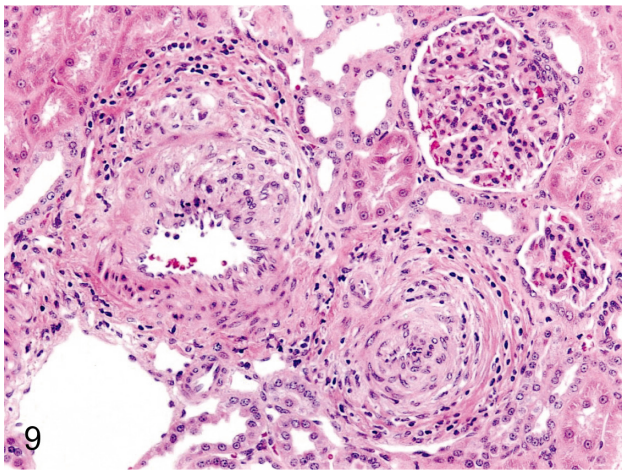

Fig. 9. Artery: Arteritis in the kidney. Panarteritis nodosa is seen relatively frequently in the intrarenal arteries, especially the arcuate arteries, in cynomolgus monkeys.

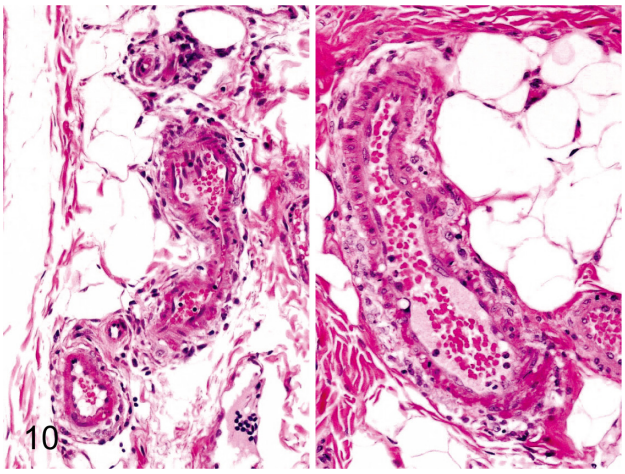

Fig. 10. Artery: Arteritis in the intestinal artery. Arteritis in the submucosa of the intestinal tract is characterized by fibrinoid necrosis of the tunica media and mild inflammatory cell infiltration in the adventitia.

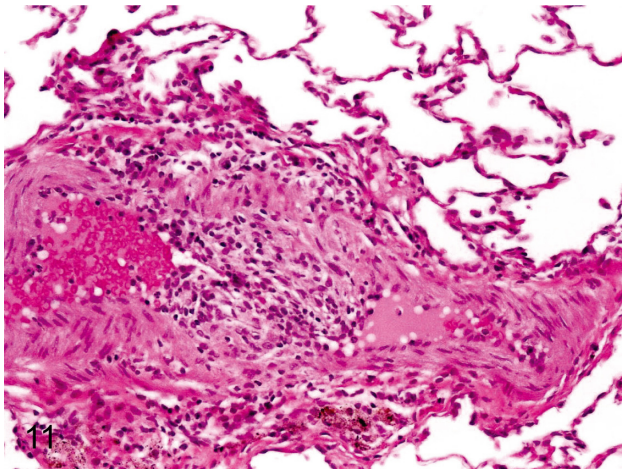

Fig. 11. Artery: Arteritis in the bronchial artery. Arteritis in the bronchial artery is characterized by thickening of the tunica intima and inflammatory cell infiltration in the tunica intima and adventitia.

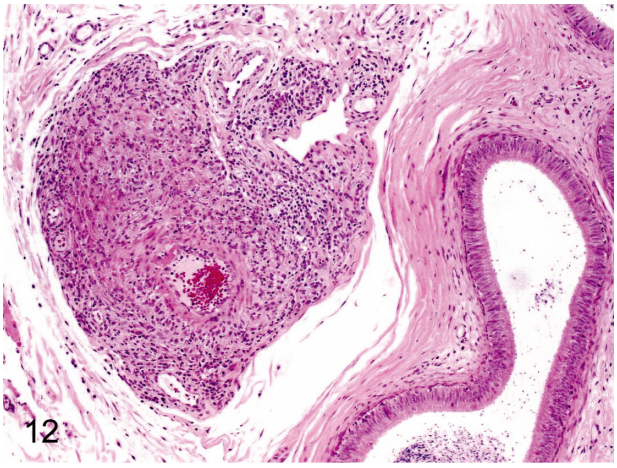

Fig. 12. Artery: Arteritis in the epididymis. The epididymal artery is a relatively frequent site for arteritis or periarteritis.

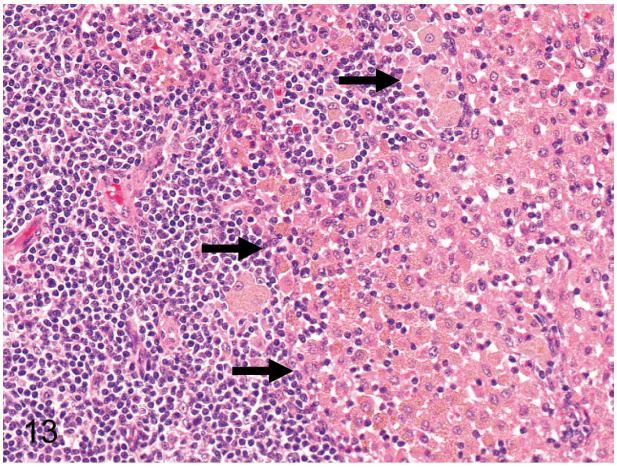

Fig. 13. Mesenteric lymph node: Increased number of pigment-laden macrophages in the sinuses. Accumulation of a large number of histiocytes containing yellow-brown pigment is common in the sinuses of the mesenteric lymph nodes. This pigment is thought to be lipid-related.

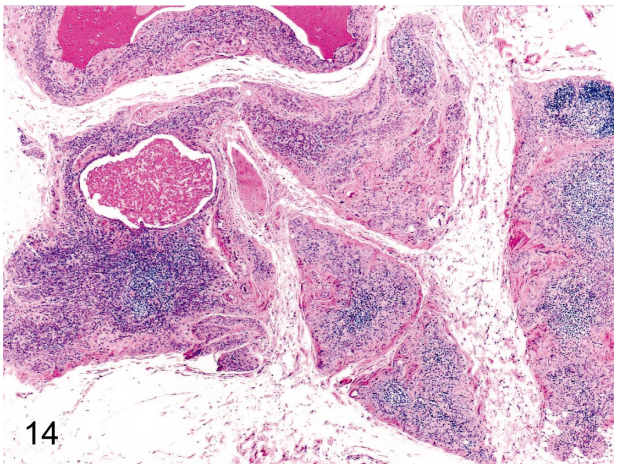

Fig. 14. Thymus: Involution (physiological atrophy). Decreases in lymphoid cells from both the cortex and medulla cause a reduction in organ size and weight. The thymus generally starts to involute from about 4 or 5 years old in cynomolgus monkeys. Thymic involution manifests in females slightly later than in males.

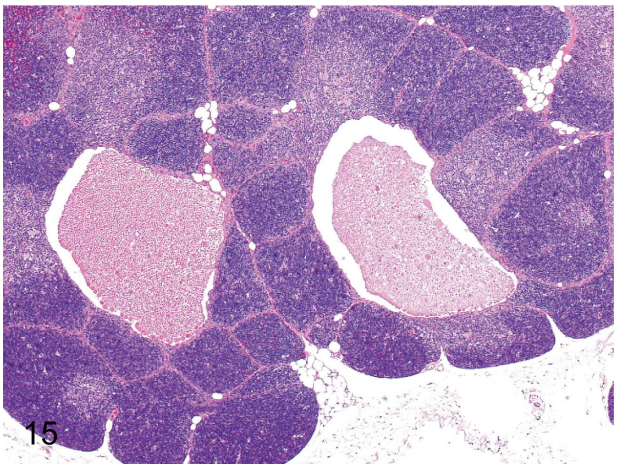

Fig. 15. Thymus: Cyst. Thymic cysts are remnants of embryonic ducts connecting the parathyroid and thymus. The cysts are lined by a partially ciliated cuboidal epithelium and contain eosinophilic and proteinic substances that are the same as those in the parathyroid cysts (Fig. 157).

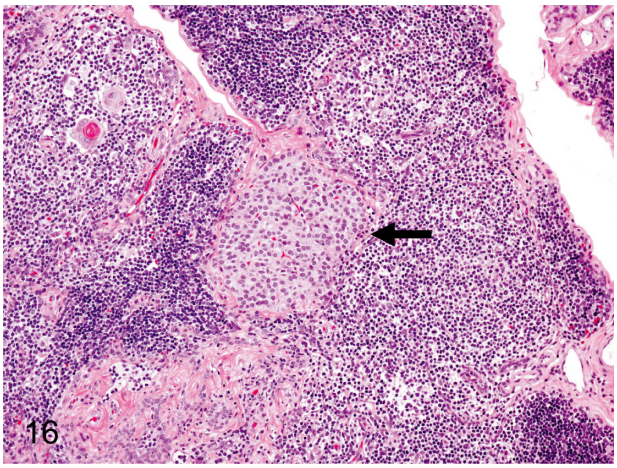

Fig. 16. Thymus: Ectopic parathyroid tissue. As the parathyroid and thymus share the same primordium, the third pharyngeal pouch, it is comprehensible that the thymic tissue contains a mass of parathyroid cells.

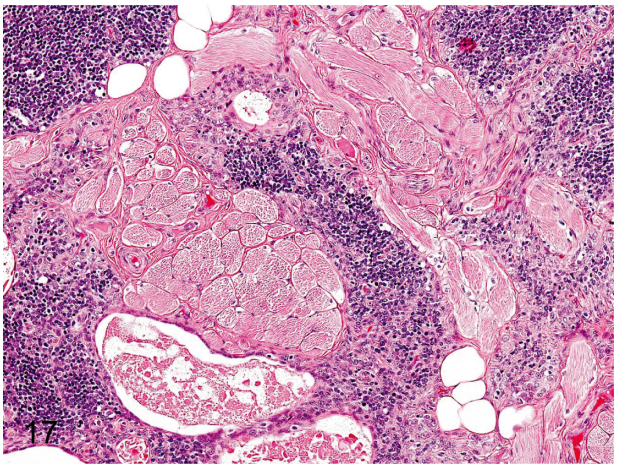

Fig. 17. Thymus: Ectopic muscle tissue. Some bundles of skeletal muscle fibers are mingled within the thymic parenchyma. It is thought to be a hamartoma or aberrant muscle tissue.

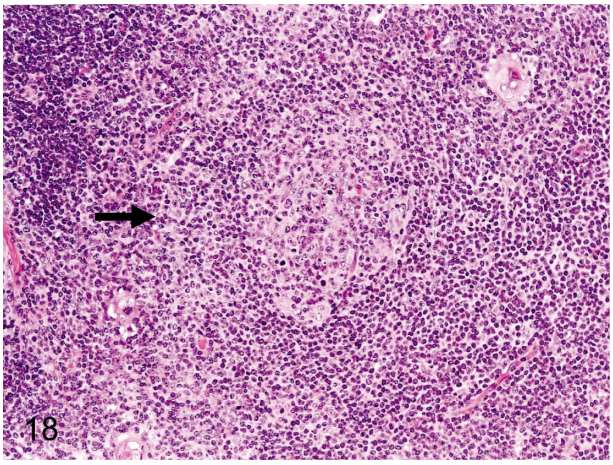

Fig. 18. Thymus: Lymph follicle formation in the medulla. Germinal center formation in the thymic medulla in cynomolgus monkeys is seen less frequently than in Beagles. Increases in the number of follicles above the normal variance may suggest an immunologic failure or overresponse.

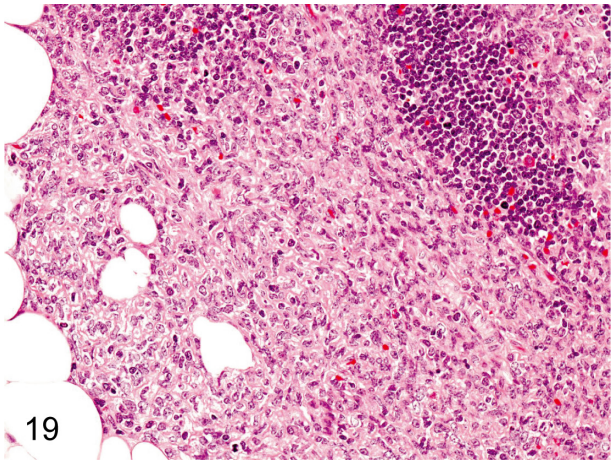

Fig. 19. Thymus: Proliferation of the thymic epithelium. Proliferation of the thymic epithelium is probably associated with thymic atrophy (involution).

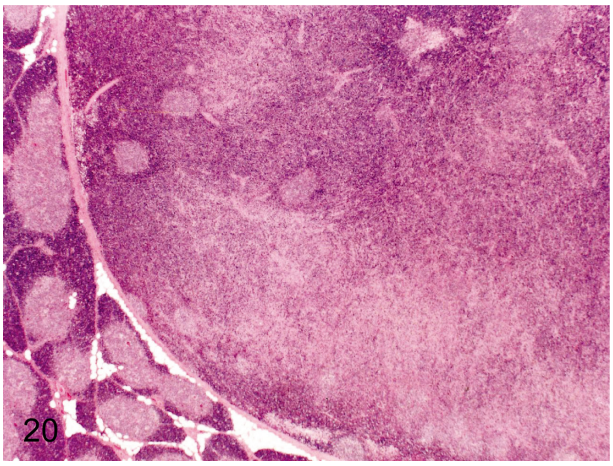

Fig. 20. Thymus: Thymoma (mixed thymoma). Neoplastic lesions including thymoma are rare in cynomolgus monkeys used in toxicologic studies. This thymoma was found as a mass with a diameter of 1.5 cm in the thymus. The detailed morphologic features of this case were reported.

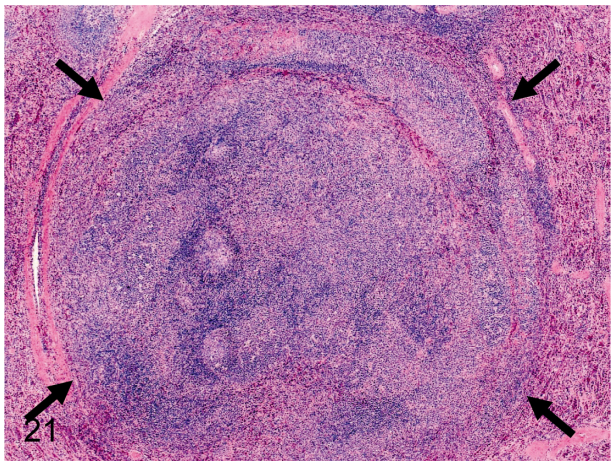

Fig. 21. Spleen: Nodular hyperplasia (lymphoid follicle). There is no capsule around the lesion, but the lesion slightly compresses the normal splenic tissues. This change consists of lymphocytic follicular hyperplasia with/without other splenic components. The other follicles are normal. There is no evidence to support that these lesions progress to lymphoma.

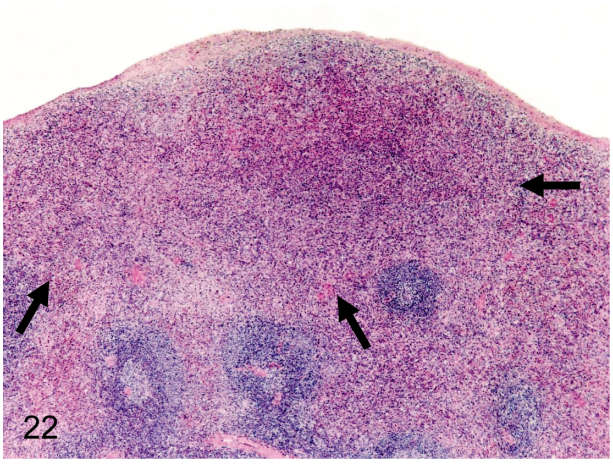

Fig. 22. Spleen: Nodular hyperplasia (red pulp). Grossly, the lesion is detected as a protruded white patch in the subcapsular part. The border of the lesion and peripheral normal parenchyma is unclear. The hyperplastic area is composed of proliferated cells of plural types consisting of normal red pulp.

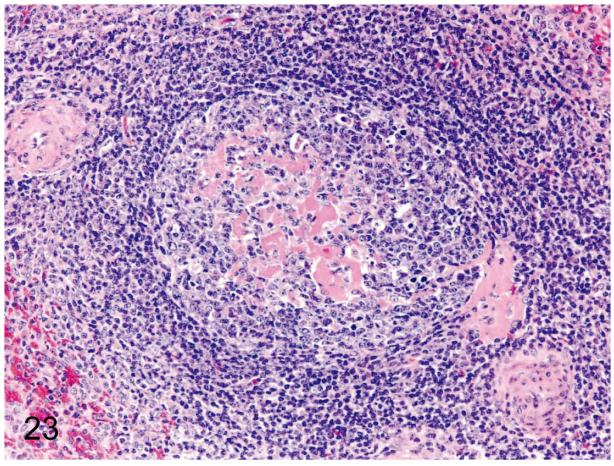

Fig. 23. Spleen: Hyalinization of the germinal center. Hyalinization (deposition of eosinophilic substances) is frequently seen in germinal centers of follicles in cynomolgus monkeys.

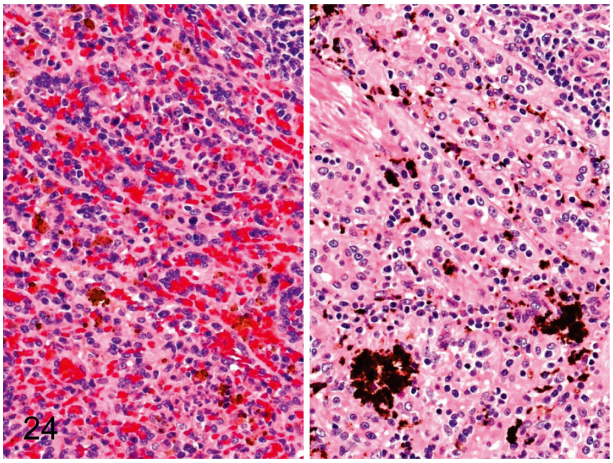

Fig. 24. Spleen: Pigment deposition in the red pulp. Brown or black pigments occasionally deposit in the red pulp. For the most part, brown pigments are hemosiderin (left), and black ones are unidentified (right). We have confirmed that the unidentified pigment is not melanin, lipofuscin, malaria pigment or formalin pigment using some special stains (unpublished data).

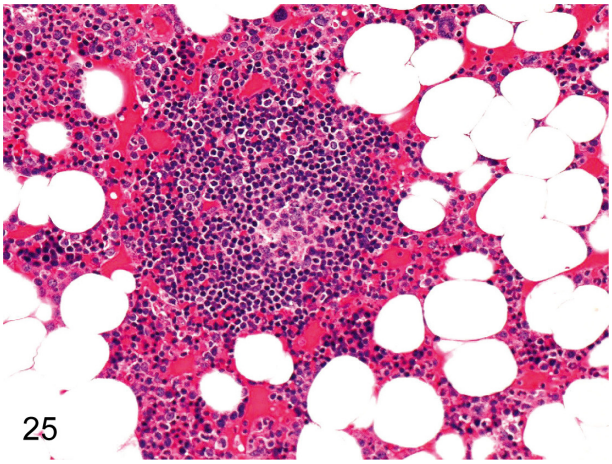

Fig. 25. Bone marrow: Lymph follicle formation. Accumulation of lymphocytes is occasionally seen in the femur and sternum bone marrow. It generally takes the appearance of a primary follicle.

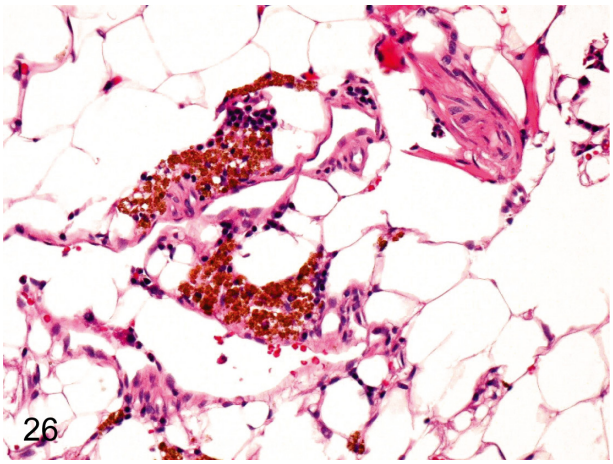

Fig. 26. Bone marrow: Pigment deposition. Accumulation of yellow-brown pigments occurs occasionally in the perivascular area of bone marrow tissue. These pigments are confirmed to be hemosiderin by special staining or reactions on the slide.

Fig. 27. Nasal cavity: Hyperplasia of the lymph follicle. The lymphoid tissue prominently developed in the nasal septa in this case, although lymphocytic infiltration is always seen in the lamina propria of the septal or turbinate mucosa.

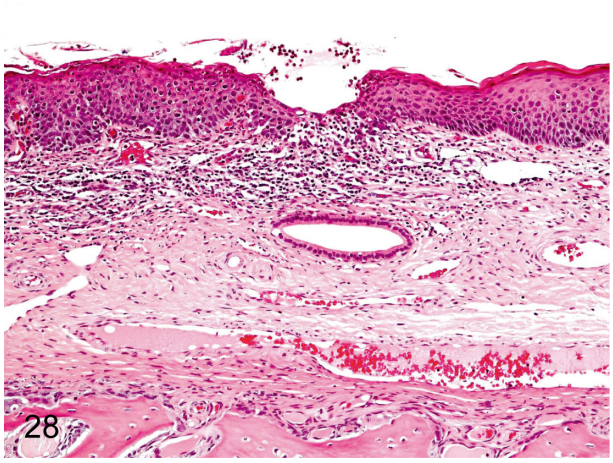

Fig. 28. Nasal cavity: Mucosal erosion of the turbinate. Slight erosion, focal inflammation and/or focal squamous metaplasia of the respiratory epithelium are occasionally seen in the nasal septum and turbinate and are caused by an inserted nasogastric catheter used for the intragastric administration.

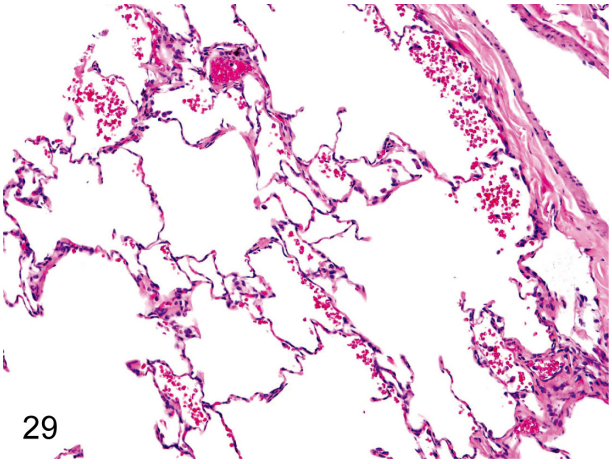

Fig. 29. Lung: Focal hemorrhage in the alveolus . Focal hemorrhage is usually seen in the alveoli. Hemorrhage without inflammatory cell infiltration may be related to certain aspects of death.

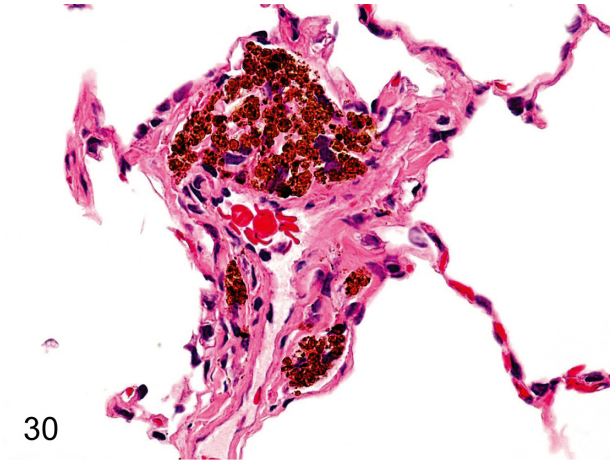

Fig. 30. Lung: Accumulation of pigment-laden macrophages. Accumulation of macrophages containing yellow-brown pigments (probably hemosiderin) is rarely seen in the perivascular interstitium or alveolar wall. These hemosiderin depositions are presumably due to extravasation of blood or congestion caused by some abnormality of vessels, cardiac function or blood coagulation.

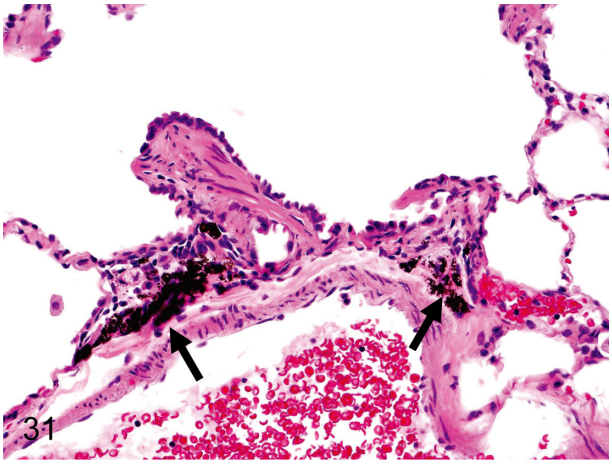

Fig. 31. Lung: Anthracotic pigment deposition (anthracosis). Fine black pigments are deposited in the interstitium around the bronchi in almost all cynomolgus monkeys. This change is not followed by inflammatory reactions or fibrosis.

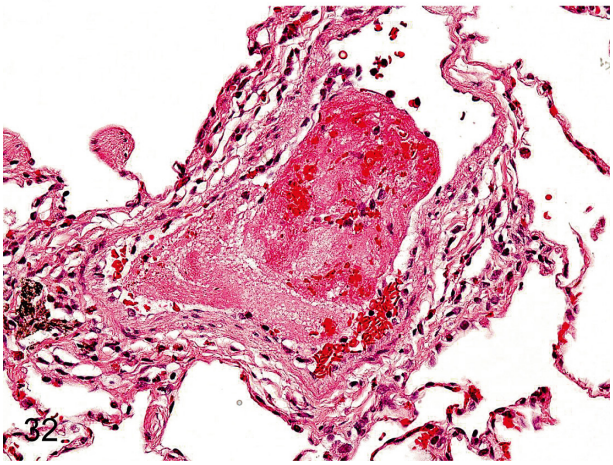

Fig. 32. Lung: Thrombus. Thrombus occasionally occurs in the pulmonary vessels, especially under the influence of intravenous injection.

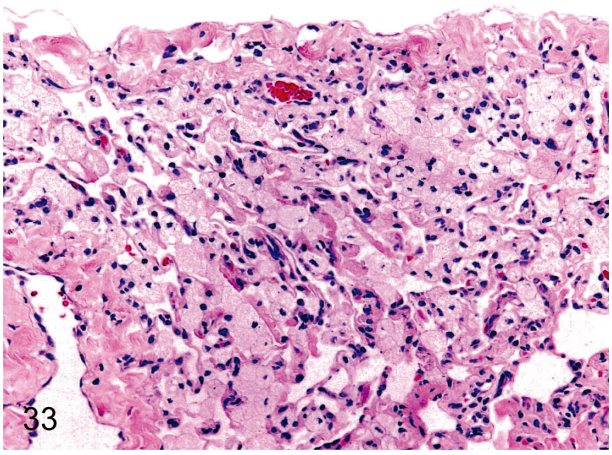

Fig. 33. Lung: Accumulation of foam cells in the alveolus. Foam cells occasionally accumulate in the alveoli without other inflammatory cell infiltration.

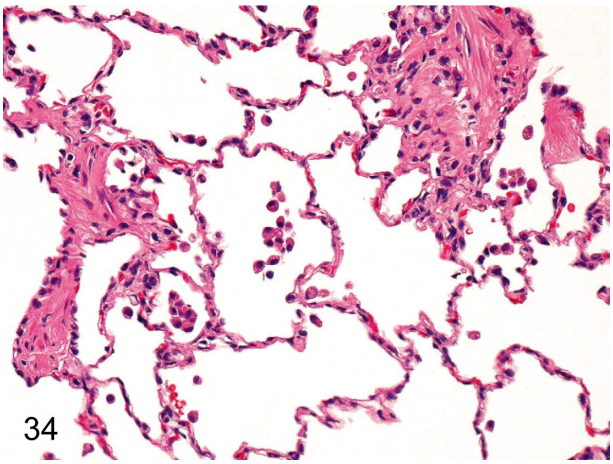

Fig. 34. Lung: Focal infiltration of macrophages in the alveolus. Focal and slight infiltration of macrophages is usually seen in the alveoli.

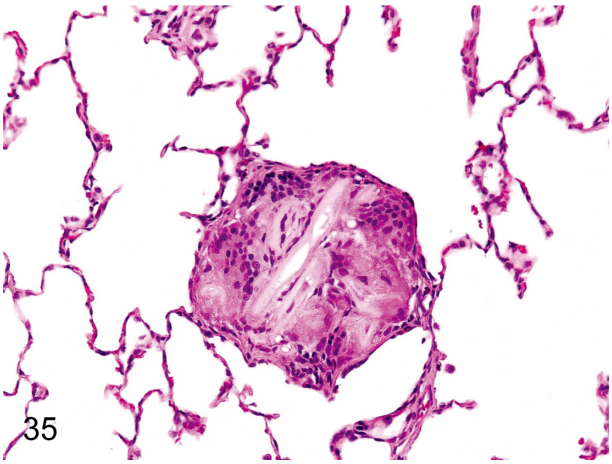

Fig. 35. Lung: Foreign body granuloma. Multinucleated giant cells are engulfing some foreign bodies. This change may have resulted from aspiration of stomach contents or food particles.

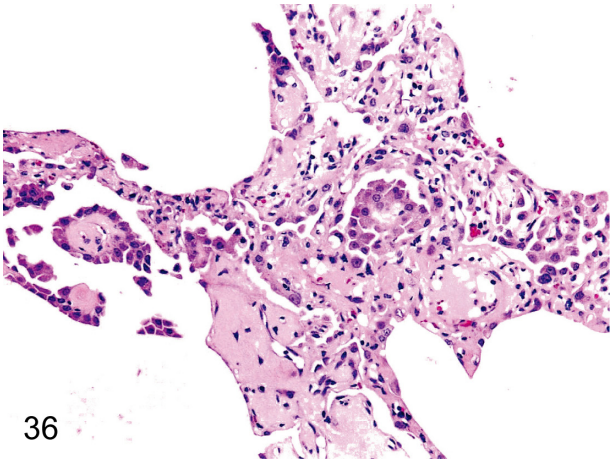

Fig. 36. Lung: Focal hyperplasia of the alveolar epithelium. Focal epithelial hyperplasia with fibrous thickening of the alveolar wall is rarely seen.

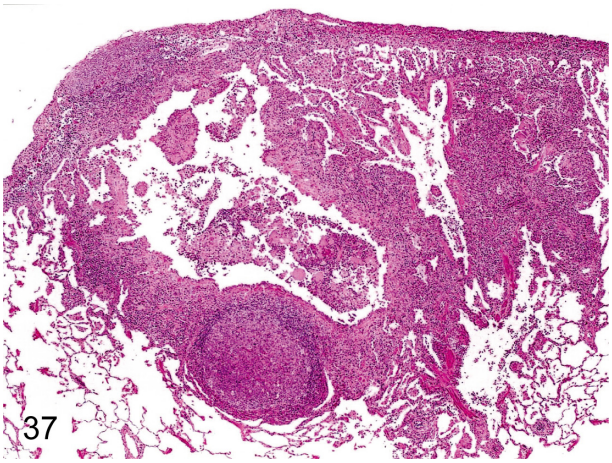

Fig. 37. Lung: Pulmonary acariasis. Gross findings show small yellow or pale green nodules in the lungs. Microscopically, characteristic findings such as dilatation of the bronchial or bronchiolar lumen, thickening of the bronchial wall and inflammatory cell infiltration around the bronchus, lymphoid hyperplasia and brown pigment deposition strongly suggest pulmonary acariasis even if there is no acarid.

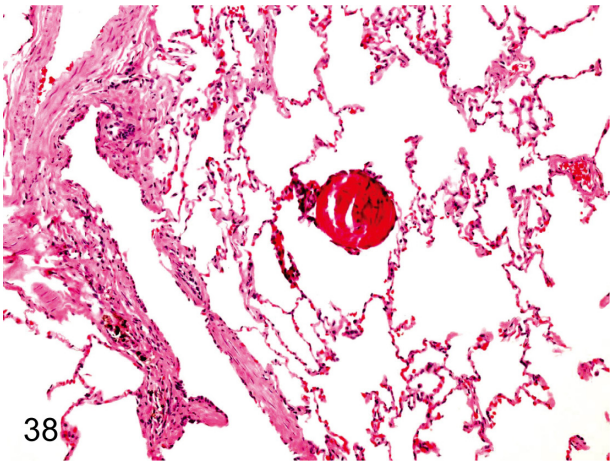

Fig. 38. Lung: Osseous metaplasia. Osseous metaplasia presumably caused by differentiation from fibroblasts to osteoblasts occurs occasionally in the lung alveolar wall. The incidence in cynomolgus monkeys is lower than that in other laboratory animals.

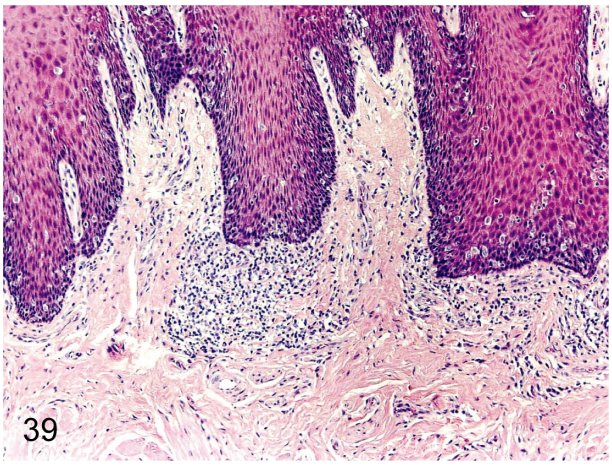

Fig. 39. Tongue: Focal inflammatory cell infiltration. Lymphoplasmacytic infiltration is usually seen in the lamina propria, especially in the lingual papillae.

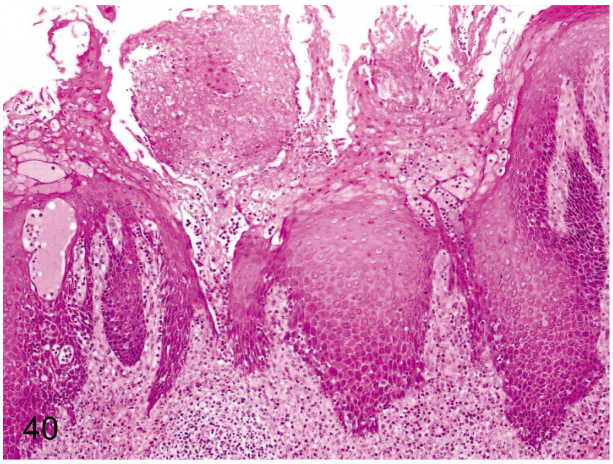

Fig. 40. Tongue: Erosion. Erosion of the squamous epithelium and inflammatory cell infiltration occur occasionally. This change might be caused by some physical irritation.

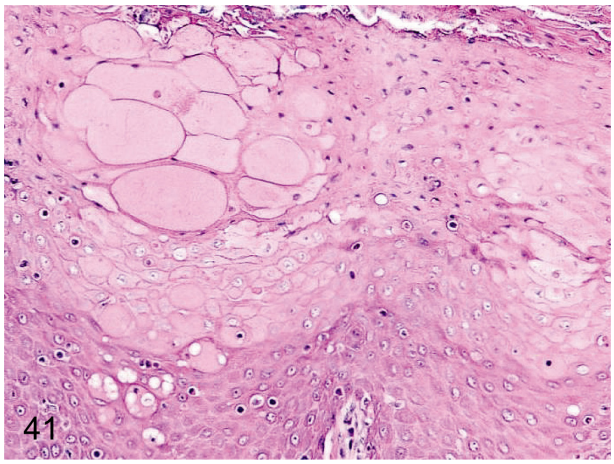

Fig. 41. Tongue: Edema/reticular degeneration. These changes are characterized by swelling of prickle cells, intercellular edema and cell infiltration. Most likely, it is a stage of the degenerative change such as erosion.

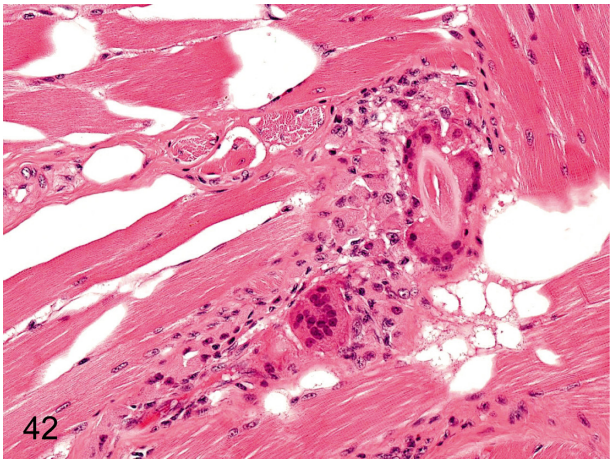

Fig. 42. Tongue: Foreign body granuloma. Foreign body granuloma caused by a fragment of hair stuck on the tongue occasionally occurs in the lamina propria or muscle layer.

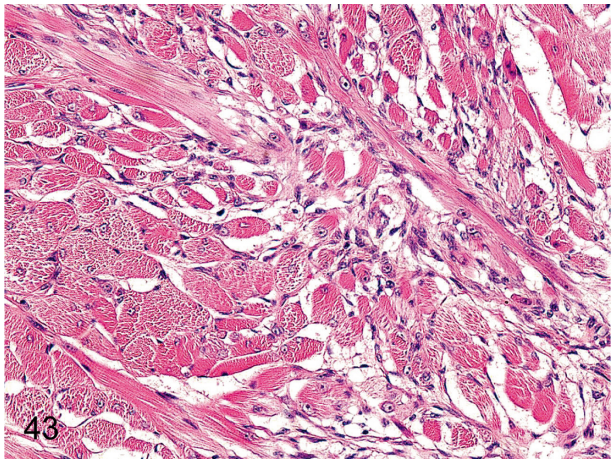

Fig. 43. Tongue: Regeneration of the muscle fiber. Focal regenerative changes of muscle fibers occur occasionally in the lateral tongue muscle layer.

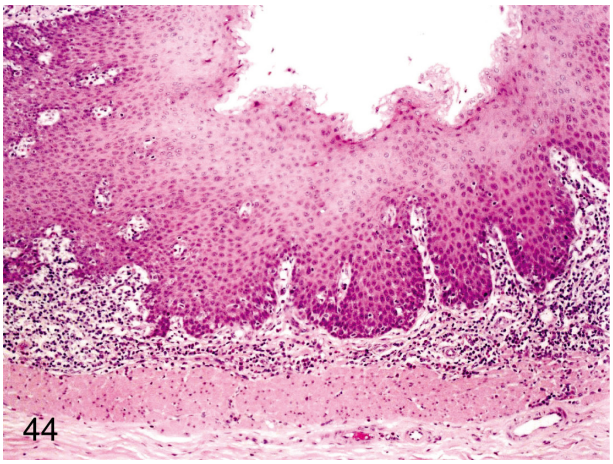

Fig. 44. Esophagus: Focal inflammatory cell infiltration in the lamina propria. Focal lymphoplasmacytic infiltration is common in the lamina propria.

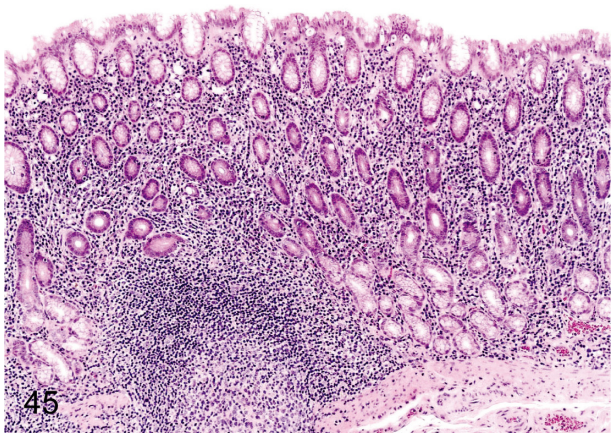

Fig. 45. Stomach: Inflammatory cell infiltration in the lamina propria. Lymphoplasmacytic infiltration in the lamina propria of the fundus and pylorus, so-called gastritis, is frequently seen in cynomolgus monkeys and is seen accompanied by regeneration of the mucosal epithelium. These changes occur occasionally associated with a *Helicobacter pylori* infection.

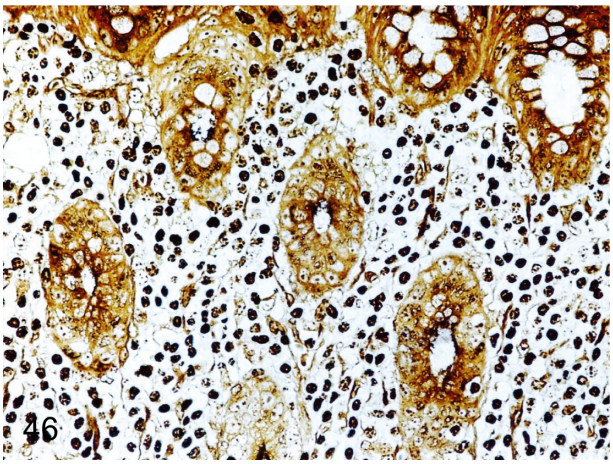

Fig. 46. Stomach: Infection by *Helicobacter pylori* in the gastric mucosa. Many fine bacteria are seen in mucosal crypts in a Warthin-Starry-stained section with inflammatory changes. The detailed morphology of *Helicobacter pylori* and relation between the gastritis and Helicobacter infection have been reported (J Toxicol Pathol. 14: 45-49. 2001).

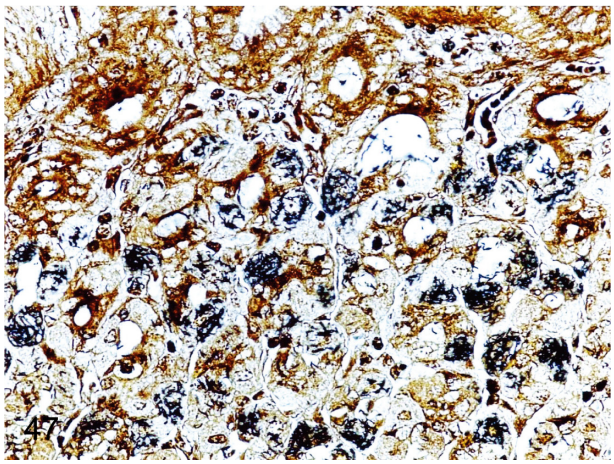

Fig. 47. Stomach: Infection by *Helicobacter heilmannii* in the gastric mucosa. Some fine bacteria are detected in parietal cells in a Warthin-Starry-stained section without any inflammatory changes in the infected mucosa.

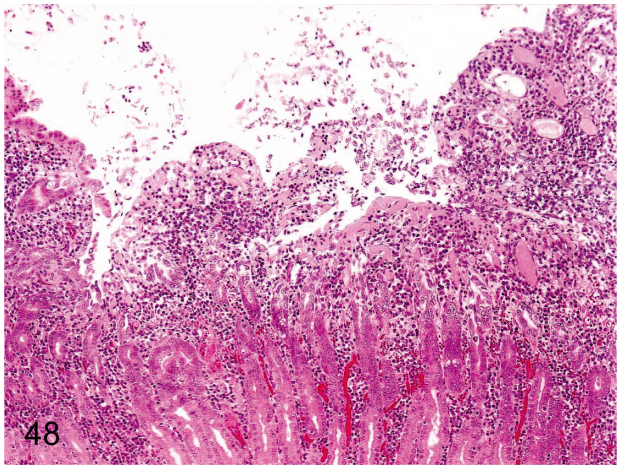

Fig. 48. Stomach: Erosion. Erosion accompanied by gastritis occurs even in monkeys kept under nonstressed conditions, but usually the lesions are small.

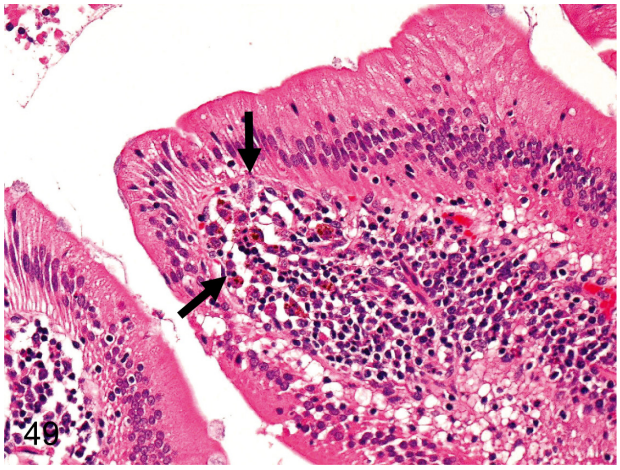

Fig. 49. Duodenum: Pigment deposition. Brown pigment-laden macrophages accumulate in the lamina propria at the top of the villi. Slight pigmentation is usually seen in the duodenal lamina propria of cynomolgus monkeys, but an increase in the number of pigment macrophages might also occur following administration of certain pigmented compounds.

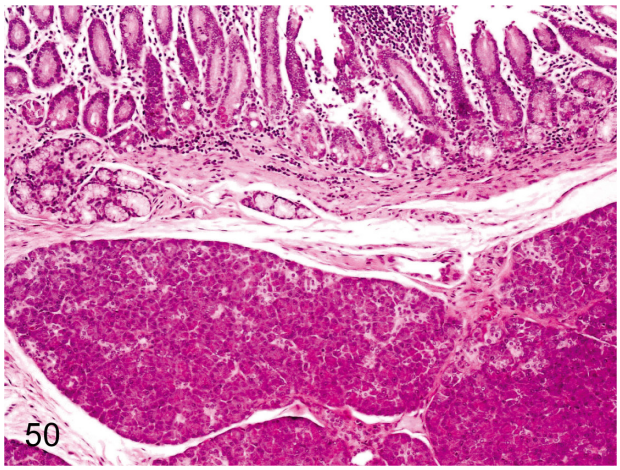

Fig. 50. Duodenum: Ectopic pancreatic tissue. Ectopic pancreatic tissue occurs occasionally in the submucosa near the major papilla of Vater.

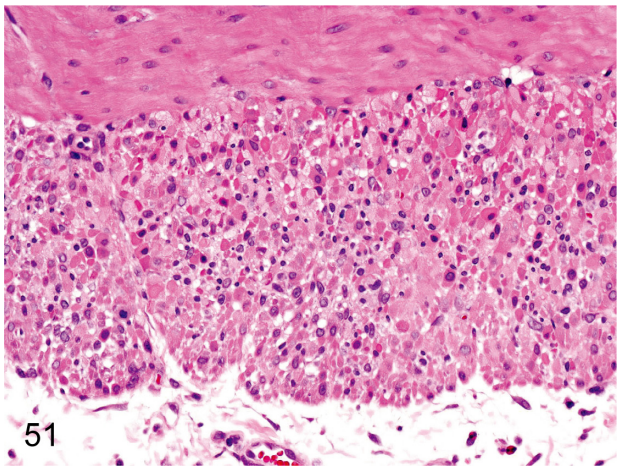

Fig. 51. Duodenum: Necrosis of the muscle layer. Focal muscle fiber necrosis occurs occasionally in the whole intestinal tract, especially in the duodenum.

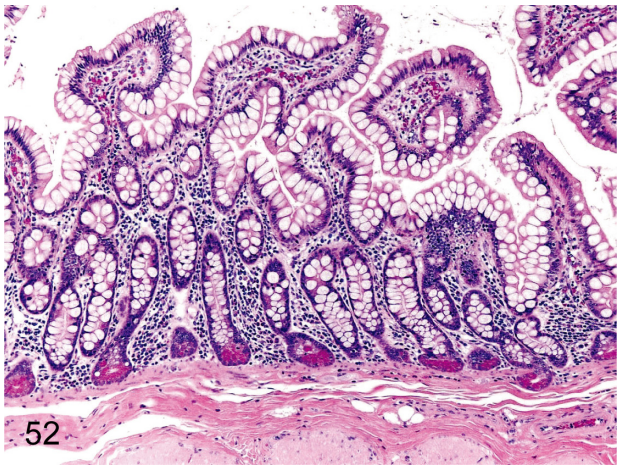

Fig. 52. Ileum (Jejunum): Increase in goblet cells. The population of jejunal and ileal goblet cells varies among individuals.

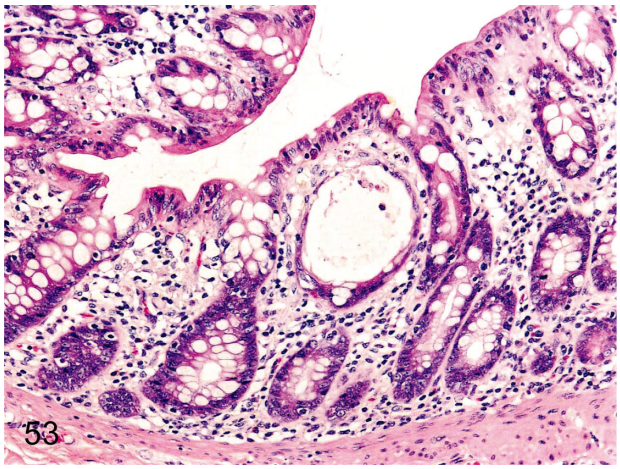

Fig. 53. Rectum: Dilatation of the crypt. Dilatation of a crypt filled with/without cell debris or infiltrated cells is frequently seen. This change is localized in not only the rectum but other parts of the intestinal tract.

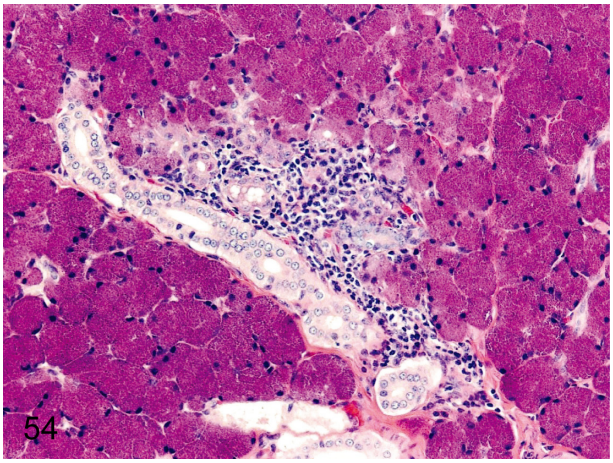

Fig. 54. Salivary gland: Focal inflammatory cell infiltration. Focal lymphoplasmacytic infiltration, occasionally accompanied by lymph follicle formation, is common around the ducts or acini.

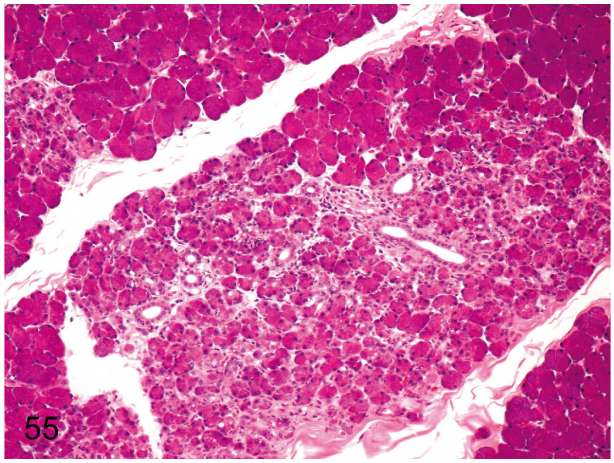

Fig. 55. Salivary gland: Focal fibrosis. Focal fibrosis with atrophy and loss of acini occurs occasionally.

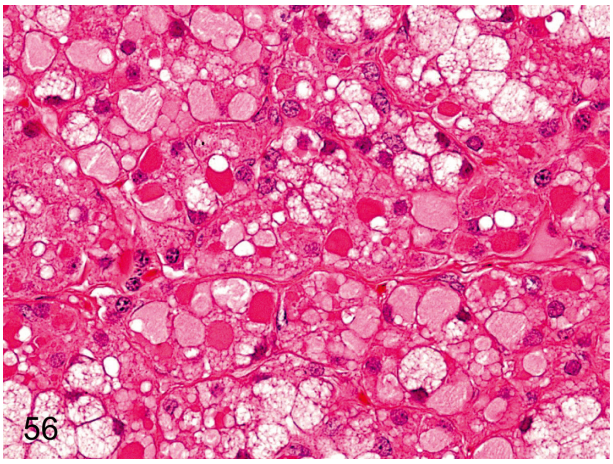

Fig. 56. Salivary gland: Hydropic degeneration of acinar cells. Accumulation of pale eosinophilic substances in acinar cells is rare. Similar changes are caused by dilatation of the endoplasmic reticulum filled with low electron density amorphous substances. This change occurs occasionally in other exocrine or endocrine glands. See also Figs. 70 and 155.

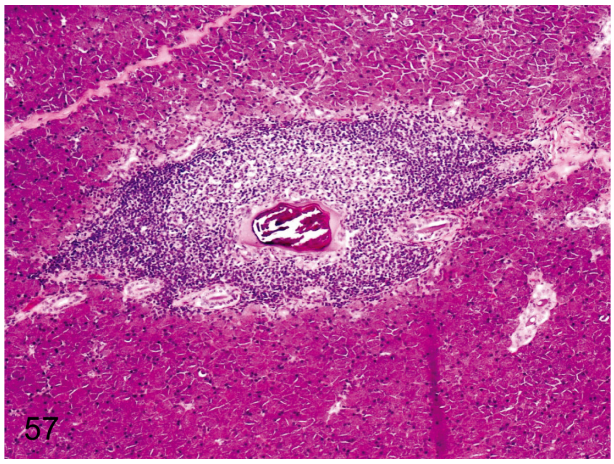

Fig. 57. Salivary gland: Salivary calculus and inflammatory cell infiltration. Small mineralized calculus occurs occasionally in a duct of a relatively large caliber and is frequently accompanied by lymphoplasmacytic infiltration in the surrounding parenchyma.

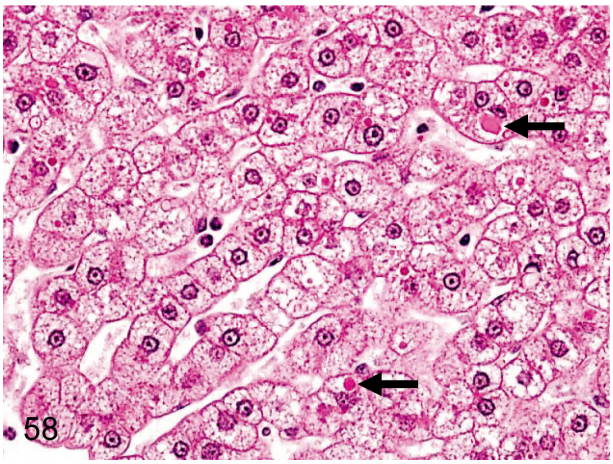

Fig. 58. Liver: Eosinophilic inclusion bodies in hepatocytes. Some hepatocytes include eosinophilic droplets in the cytoplasm. This change occurs less frequently in cynomolgus monkeys than in Beagles. These bodies are considered to be blood plasma due to rise of the internal pressure in the sinusoids or increased permeability of the hepatic cell membrane.

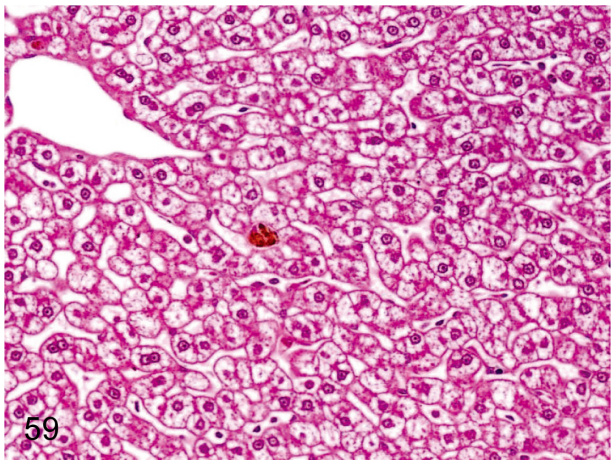

Fig. 59. Liver: Accumulation of glycogen in hepatocytes. Centrilobular hepatocytes in cynomolgus monkeys usually contain a lot of glycogen. This change is characterized by a clear appearance of the hepatic cytoplasm after formalin fixation.

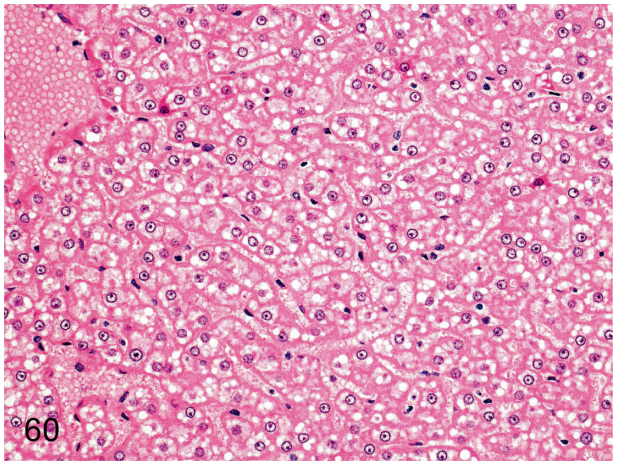

Fig. 60. Liver: Diffuse fatty change of hepatocytes. Small lipid droplets (clear vacuoles) are scattered in the hepatocytes in all zones.

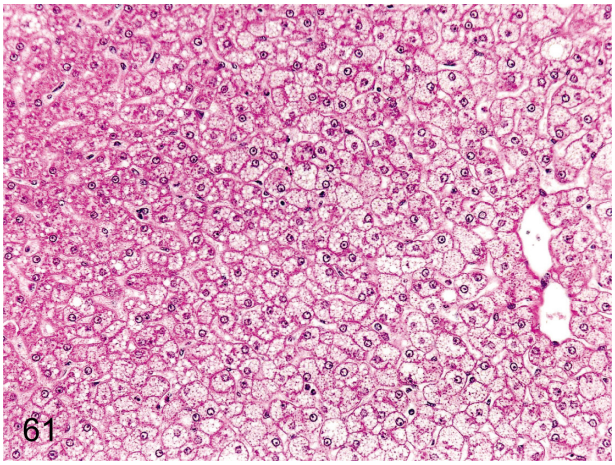

Fig. 61. Liver: Focal fatty change of hepatocytes. This change tends to occur in the border of the right and left central lobes, and it is thought to be tension lipidosis. Fine vacuoles can be seen in the hepatocytes.

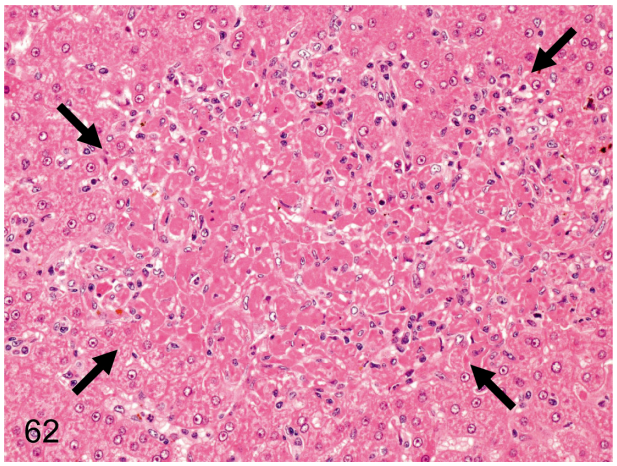

Fig. 62. Liver: Focal necrosis of hepatocytes. A necrotic focus of hepatocytes with inflammatory cell infiltration occurs occasionally without any apparent cause.

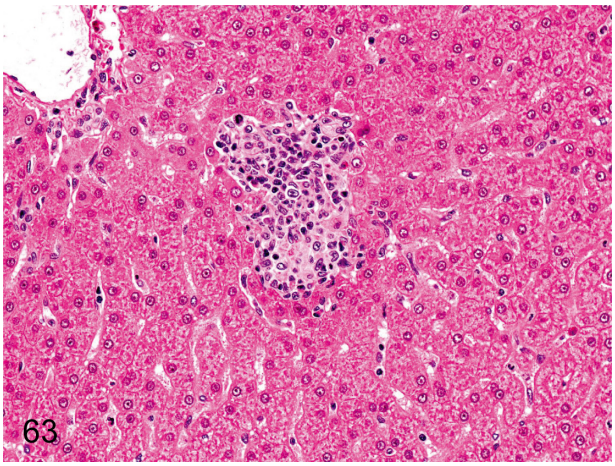

Fig. 63. Liver: Micrograniuloma. Micrograniuloma consists of accumulation of inflammatory cells, mainly of macrophages, lymphocytes and small number of neutrophils, and may be associated with minute necrosis of hepatocytes. Micrograniulomas are of much lower incidence in cynomolgus monkeys than in other laboratory animals.

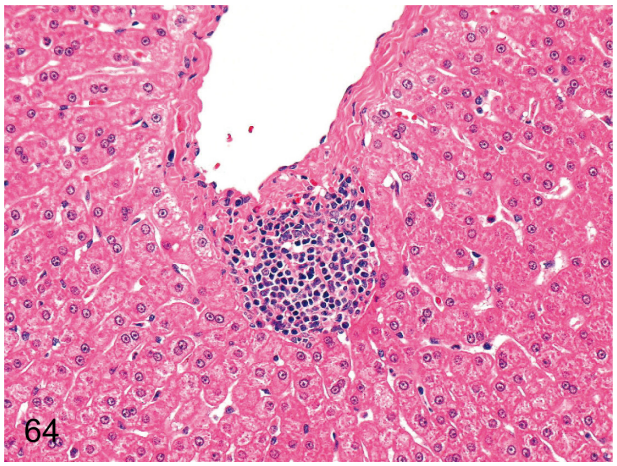

Fig. 64. Liver: Focal inflammatory cell infiltration. This inflammatory focus consists of lymphoplasmacytes and is mainly accumulated in the Glisson's sheath or around the central vein.

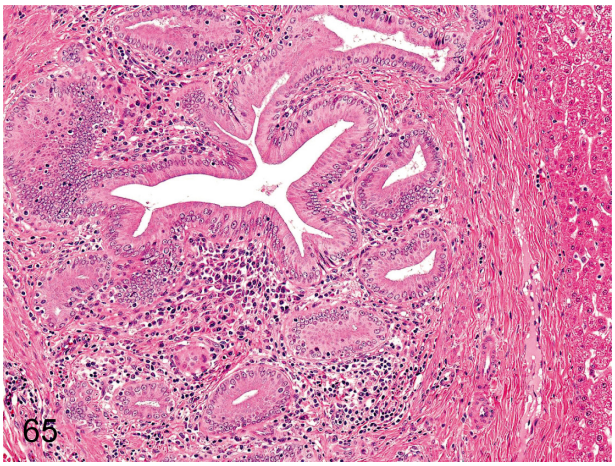

Fig. 65. Liver: Pericholangitis. Inflammatory cells occasionally infiltrate around the bile ducts. If the inflammatory cells are predominantly eosinophils, parasitic infection might be considered as one of the causes.

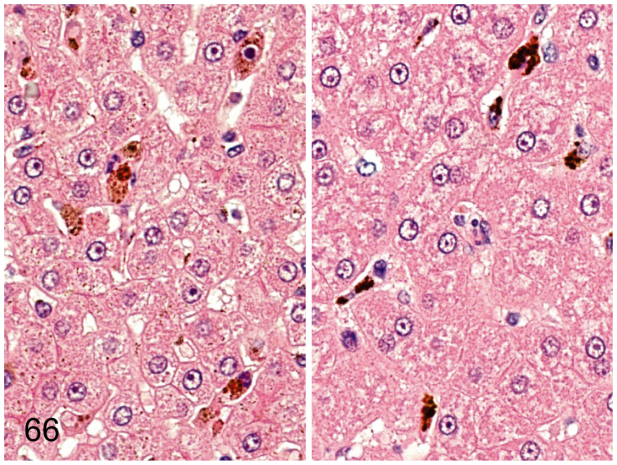

Fig. 66. Liver: Pigment deposition in Kupffer cells. Kupffer cells occasionally engulf brown or black pigments in the sinusoid. Brown pigments are presumably hemosiderin (left), and black ones (right) are unidentified pigments like those described in the spleen.

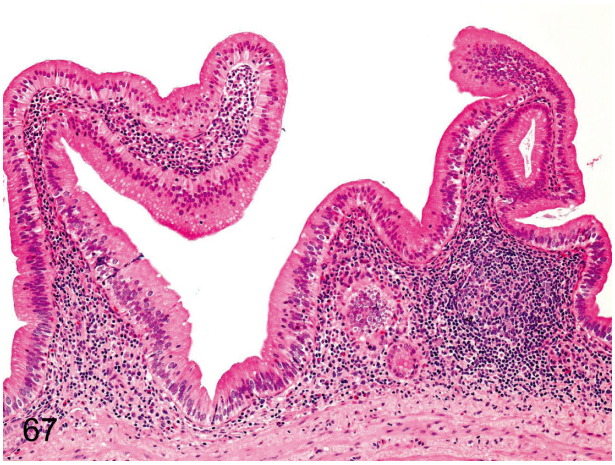

Fig. 67. Gall bladder: Inflammatory cell infiltration in the lamina propria. Development of the lymphoid tissue in the lamina propria occurs occasionally, and slight lymphoplasmacytic infiltration is constant in almost all cynomolgus monkeys.

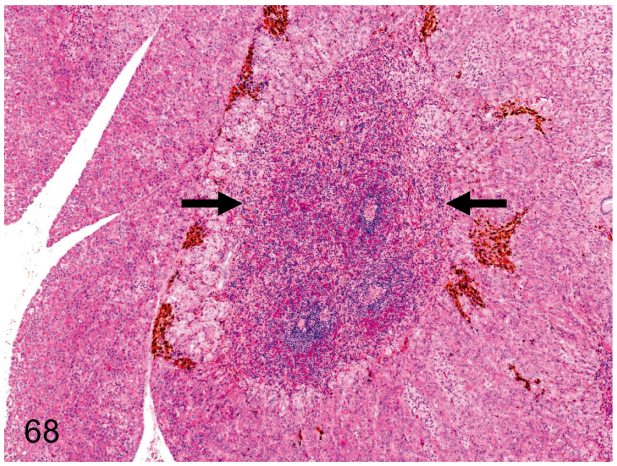

Fig. 68. Pancreas: Ectopic splenic tissue. Splenic tissue consisting of red and white pulp is contained in the pancreatic parenchyma without a fibrous capsule.

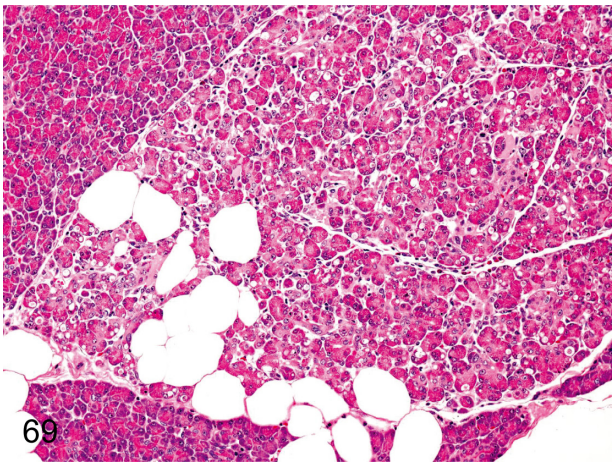

Fig. 69. Pancreas: Lobular atrophy of the acinus. Lobular atrophy consisting of shrinkage and loss of acini with interstitial fibrosis can be seen occasionally in the exocrine pancreas.

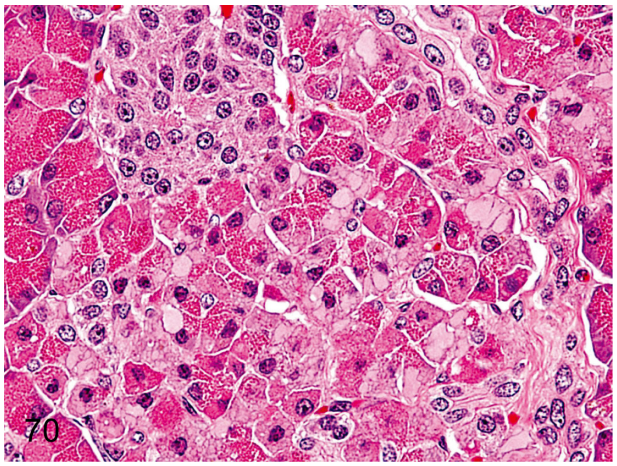

Fig. 70. Pancreas: Hydropic degeneration of acinar cells. A decrease in zymogen granules and accumulation of pale eosinophilic substances in acinar cells are rare. Similar changes are caused by dilatation of the endoplasmic reticulum filled with low electron density amorphous substances. See also Figs. 56 and 155.

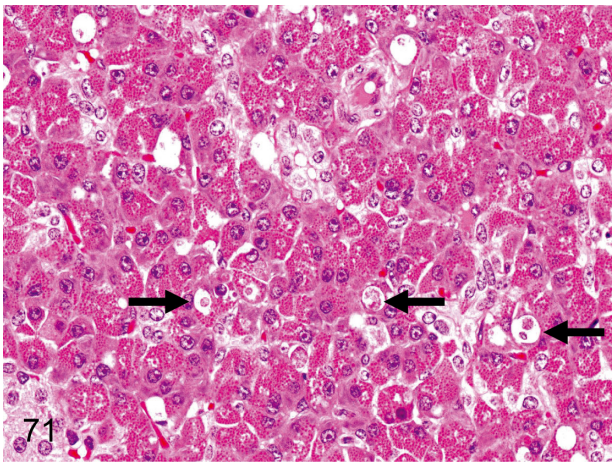

Fig. 71. Pancreas: Apoptosis of acinar cells. Apoptosis of acinar cells is relatively rare in the pancreas of cynomolgus monkeys, in contrast to the larger number and higher frequency in Beagles.

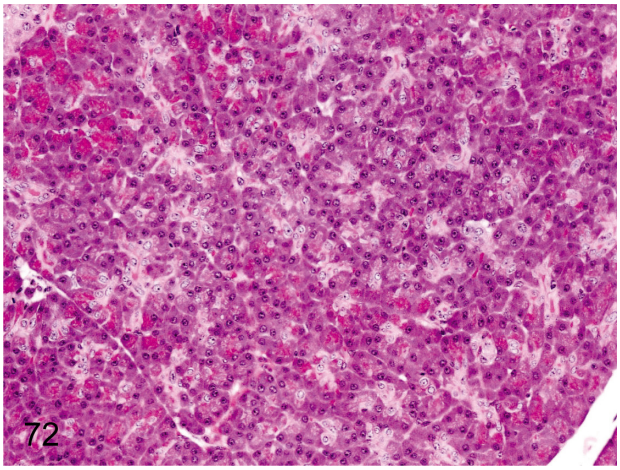

Fig. 72. Pancreas: Decrease in zymogen granules. Although a decrease of zymogen granules is thought to be a stress-related change, it rarely occurs in animals under normal conditions. The gross appearance shows discoloration of the whole pancreas.

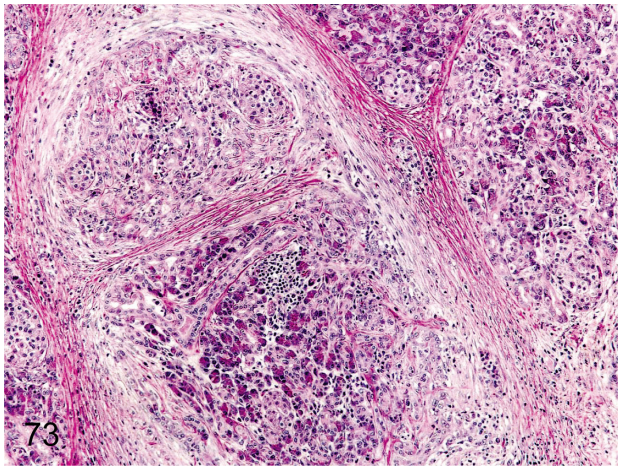

Fig. 73. Pancreas: Chronic pancreatitis. The histopathologic features of chronic pancreatitis consist of necrosis and loss of acinar cells, dense fibrosis and lymphoplasmacytic infiltration in the exocrine pancreas, although the islets usually remain intact in the lesions. On autopsy, the pancreas is firm and nodular. The incidence of chronic pancreatitis is very rare.

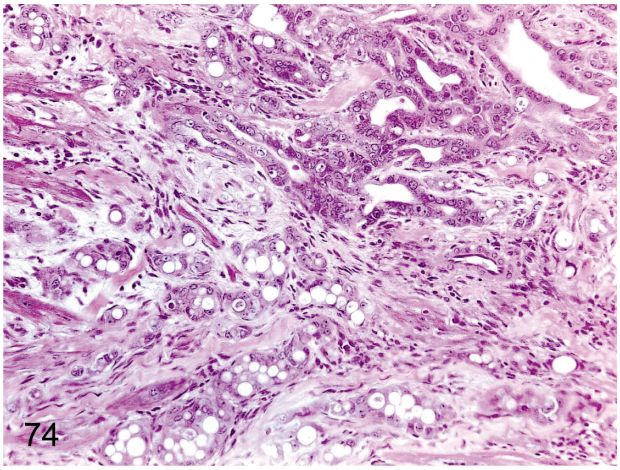

Fig. 74. Pancreas: Chronic pancreatitis. The same case as Fig. 73. Many ductal structures are lined by cuboidal epithelial cells proliferating within a densely fibrotic area.

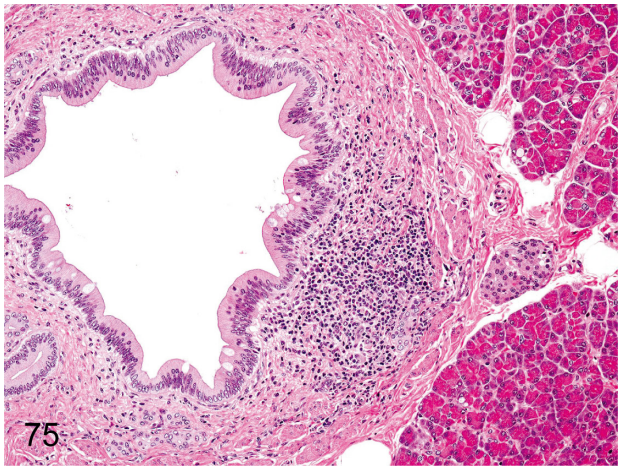

Fig. 75. Pancreas: Focal inflammatory cell infiltration. Focal lymphoplasmacytic infiltration occurs occasionally in the interstitium of the pancreas, especially around the pancreatic duct.

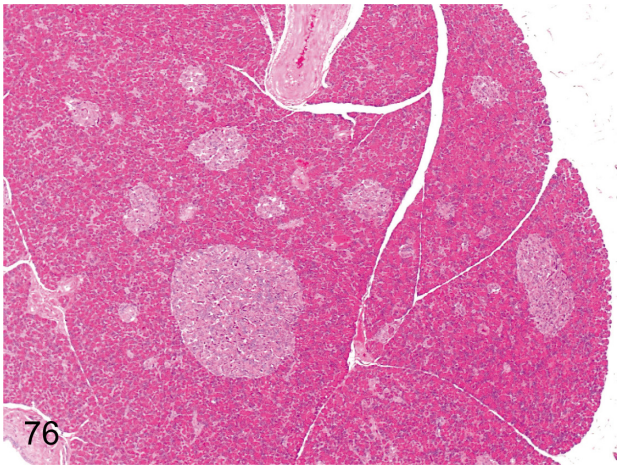

Fig. 76. Pancreas: Large pancreatic islets. The size of the pancreatic islets varies considerably in cynomolgus monkeys. Large-sized islets are common even in normal animals.

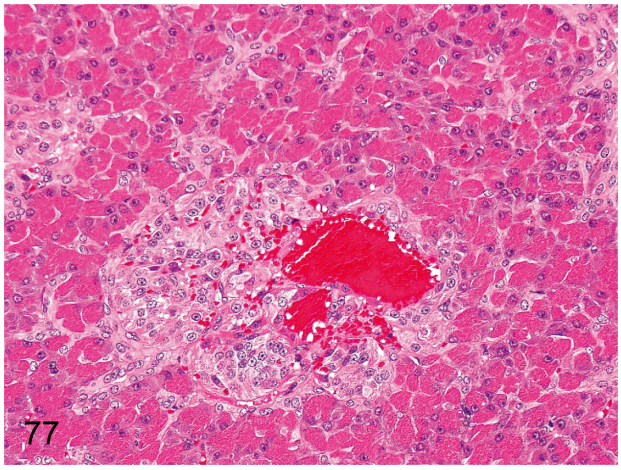

Fig. 77. Pancreas: Angiectasis in islets. The capillary of the islets is associated with dilatation and congestion. Spontaneous occurrence of this change is very rare. It has been described that similar angiectasis was induced in cynomolgus monkeys treated with an antineoplastic immunomodulator.

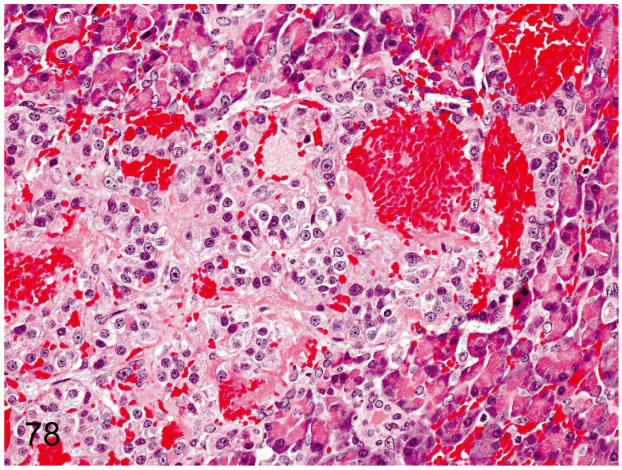

Fig. 78. Pancreas: Hemorrhage in islets. Focal hemorrhage is rare in islets, presumably due to some focal damage of the islet cells or vessel wall.

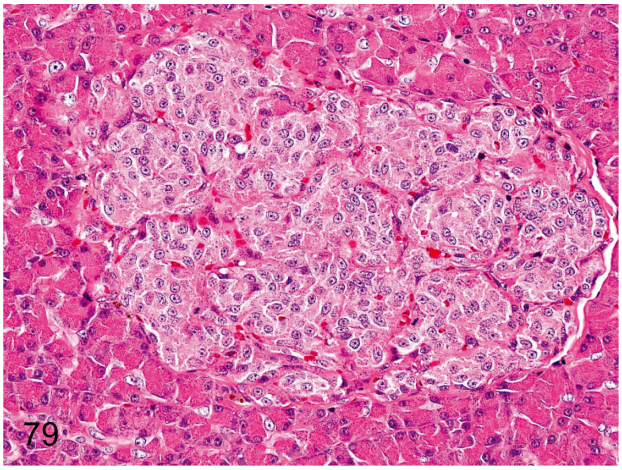

Fig. 79. Pancreas: Fibrosis of islets. The islet tissue is lobulated into multiple compartments by fibrous septa, presumably due to some focal damage of the islets such as in Fig. 78. This change is rare in young cynomolgus monkeys.

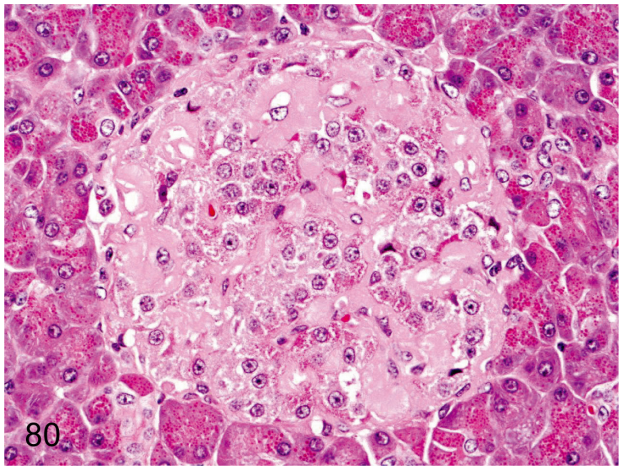

Fig. 80. Pancreas: Amyloidosis. Weakly eosinophilic amorphous material deposits around the capillaries of an islet with loss of a fairly large number of islet cells. Islet amyloidosis occurs occasionally in aged cynomolgus monkeys but is rare in young ones.

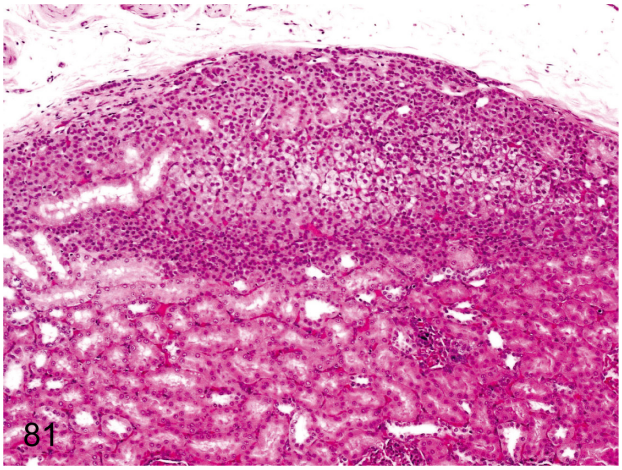

Fig. 81. Kidney: Ectopic adrenocortical tissue. Adrenocortical tissue rarely exists in the subcapsular renal cortex. Embryologically, both primordia of the renal and adrenal tissues are adjacent to each other.

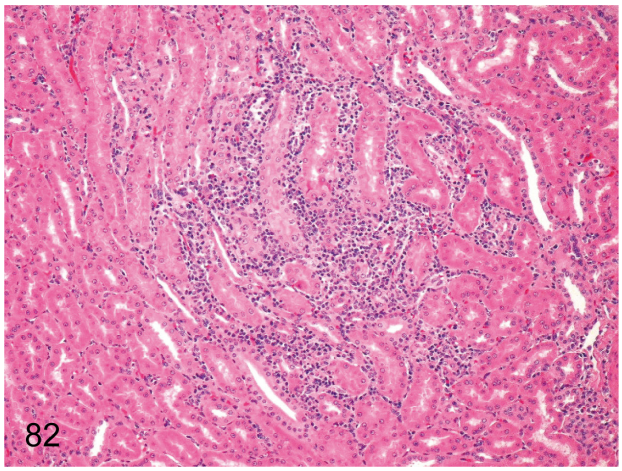

Fig. 82. Kidney: Focal inflammatory cell infiltration in the interstitium. Focal lymphoplasmacytic infiltration is common in the interstitium; usually the lesion size is small.

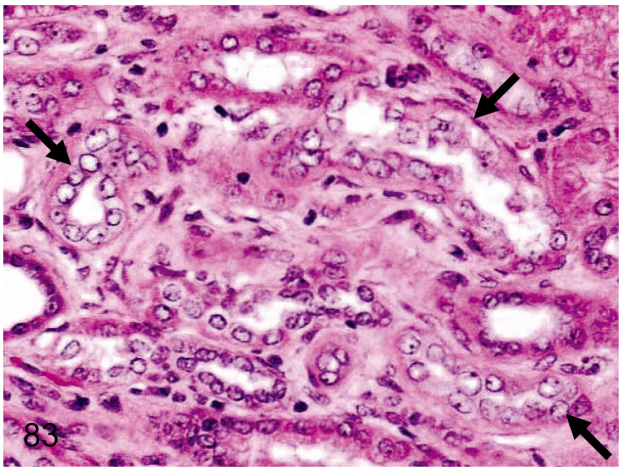

Fig. 83. Kidney: Regeneration of the tubular epithelium. Focal regenerative changes of damaged tubules are detected as basophilic tubules with a high nuclear density in the renal cortex or outer medulla. The incidence is lower in cynomolgus monkeys than in other laboratory animals.

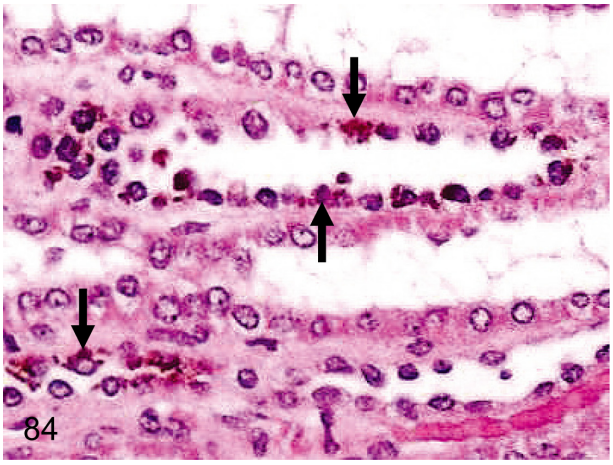

Fig. 84. Kidney: Brown pigment deposition in the tubular epithelium. Brown pigment deposition is frequently seen in the tubular epithelium, mainly in the Henle's tubules and straight portions of proximal tubules. The deposited pigment is considered to be lipofuscin.

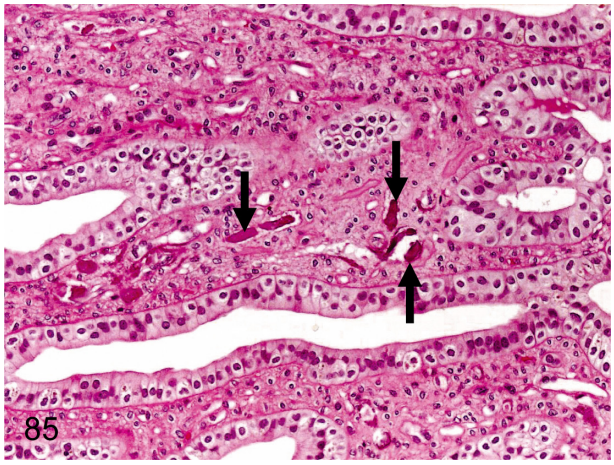

Fig. 85. Kidney: Mineralization. Small mineralization is usually seen in the interstitium of the renal papilla and also occurs occasionally in the cortex and outer medulla. Renal mineralization is found in various laboratory animals but to a lesser extent in cynomolgus monkeys.

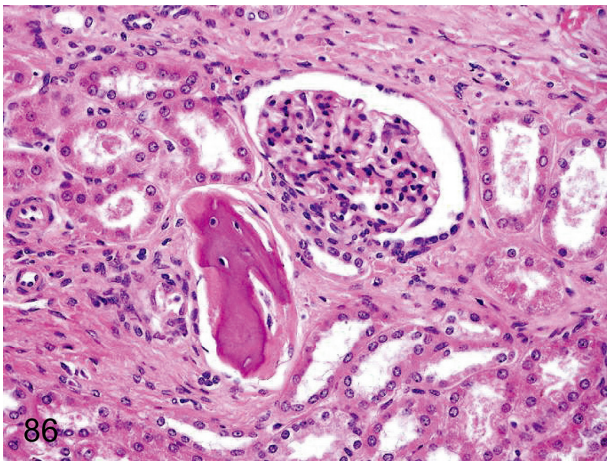

Fig. 86. Kidney: Osseous metaplasia. Osseous metaplasia rarely occurs in the interstitium or the parenchyma and glomerulus.

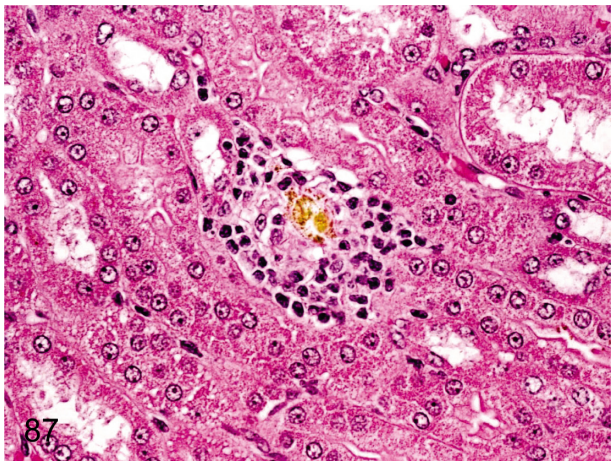

Fig. 87. Kidney: Crystal deposition.A yellowish lucent crystal formed in the tubule causes epithelial damage and inflammatory cell infiltration. This crystal is oxalate calculus. Oxalate is contained in various plants eaten by wild cynomolgus monkeys, and oxalate crystals are common among them but are very rare in animals bred for laboratory use.

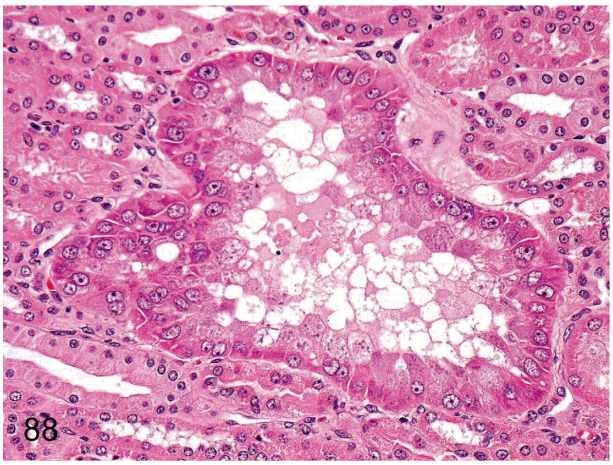

Fig. 88. Kidney: Focal hyperplasia/hypertrophy of the tubular epithelium. Hyperplasia of renal tubular epithelial cells may be caused by repeated tubular damage. This figure shows single cell layered renal tubular hyperplasia, which shows an increase in the number of epithelial cells and hypertrophy of nuclei and cytoplasm.

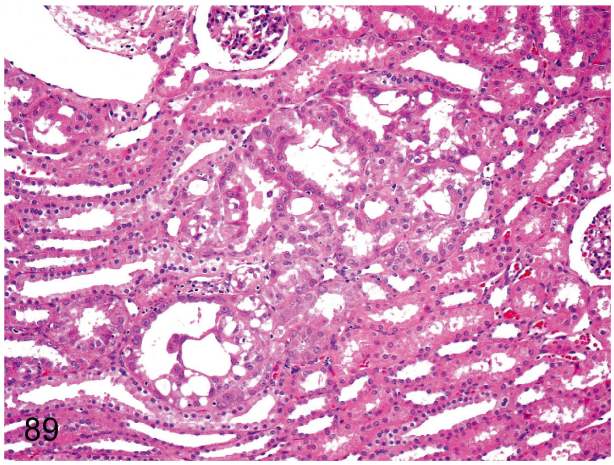

Fig. 89. Kidney: Atypical hyperplasia of the tubular epithelium. This figure shows focal hyperplasia of stratified tubular epithelia with cellular atypia. The pathogenesis of this lesion is probably the same as that described in Fig. 88. There is no evidence to suggest that these lesions ever progress to renal tumor.

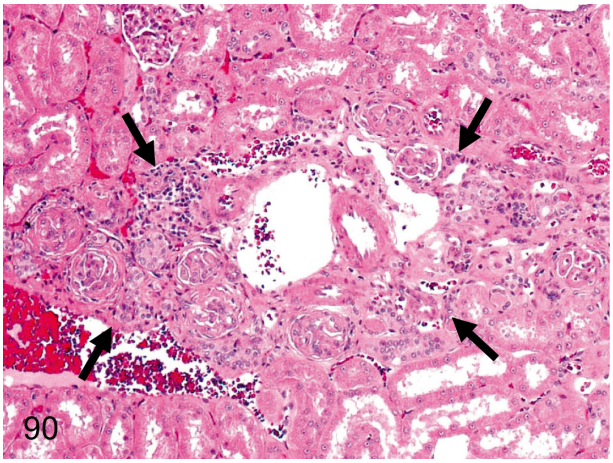

Fig. 90. Kidney: Scar (Nephrosclerotic lesion). A renal scar consists of obsolescent glomeruli, interstitial fibrosis and inflammatory cell infiltration.

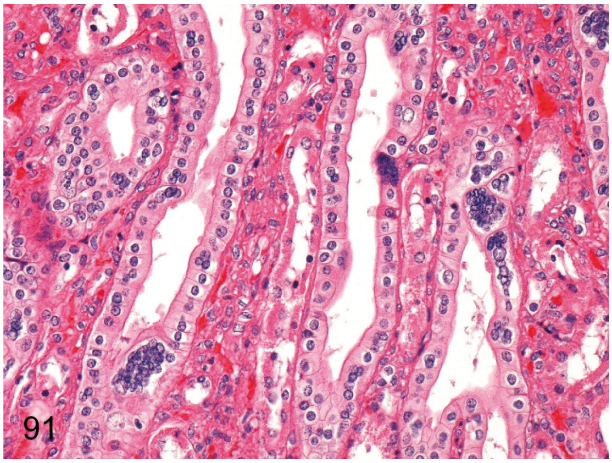

Fig. 91. Kidney: Multinucleated epithelial cells in the collecting tubules. This change occurs in collecting tubules of the renal papilla in some cynomolgus monkeys, although its pathological meaning and pathogenesis are unknown.

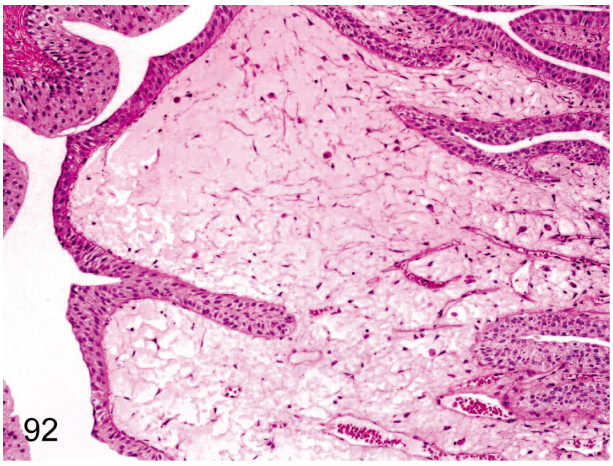

Fig. 92. Kidney: Edema of the renal papilla. Interstitial edema without inflammation is frequently seen in the renal papilla but is restricted to a small area.

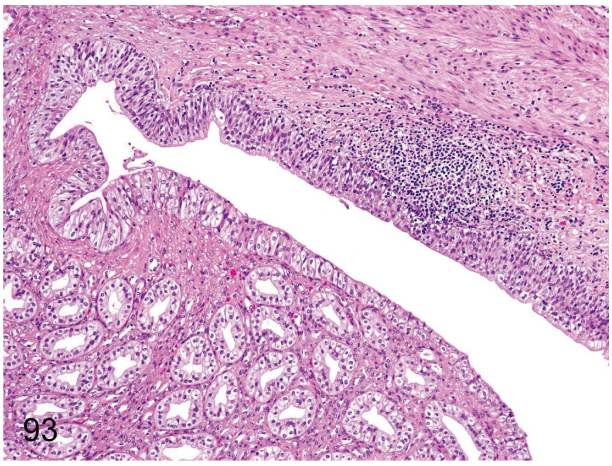

Fig. 93. Kidney: Pyelitis. Inflammatory cell infiltration occurs occasionally in the pelvis. Pyelitis may progress to pyelonephritis (Fig. 94) by ascending spread of inflammation.

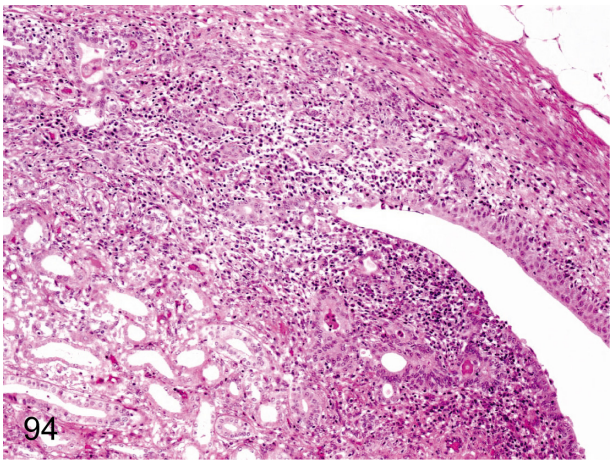

Fig. 94. Kidney: Pyelonephritis. Inflammatory cells rarely infiltrate any mucosal regions of the pelvis and papillary interstitium with tubular damage and regeneration.

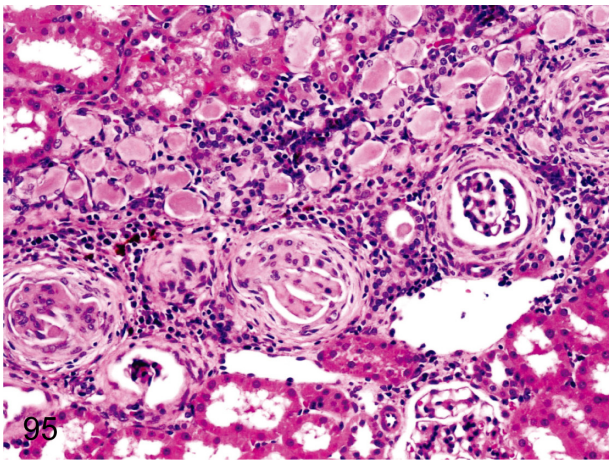

Fig. 95. Kidney: Cortical lesion associated with chronic pyelonephritis. Focal lesions distributed along the nephron suggest ascending spread of inflammatory lesions from the pelvis. Chronic pyelonephritis is tubulointerstitial nephritis consisting of fibrosis and inflammatory cell infiltration in the interstitium, tubular atrophy and thyroid-like appearance, extra-afferent fibrosis of the Bowman's capsule and obsolescent glomeruli.

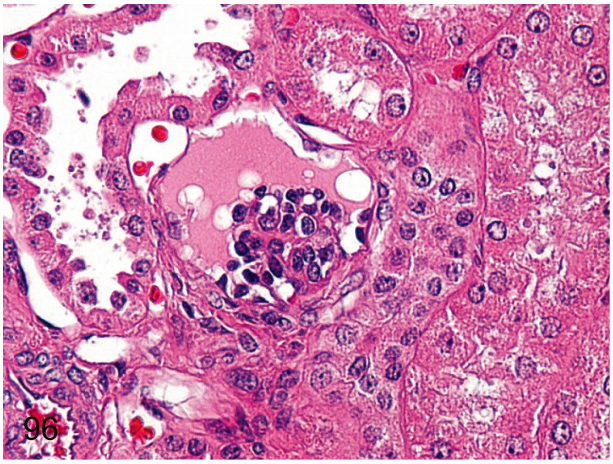

Fig. 96. Kidney: Immature glomerulus. Capillary formation is indistinct, whereas epithelial cells are prominent in an immature glomerulus. Immature glomerulus is seen more frequently in the outer layer of the cortex, reflecting the delayed maturation of the glomeruli in the outer cortex than in the deep layer.

Kidney: Solitary glomerular lesions (Figs. 97–102)

These lesions are usually seen in cynomolgus monkeys but are solitary (one or two abnormal glomeruli in one section). The details of these changes are not understood because every one of the lesions is stained eosinophilic in HE sections.

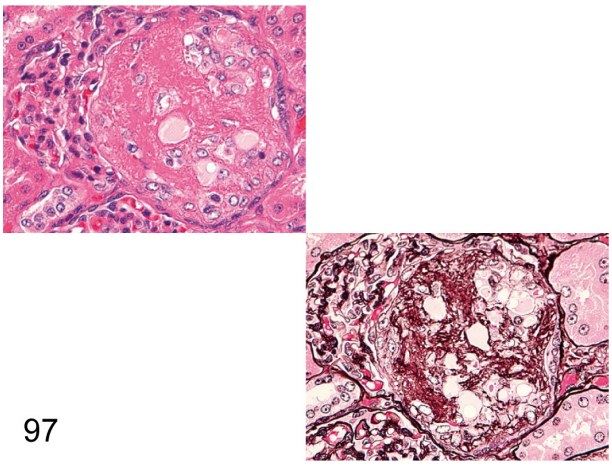

Fig. 97. Kidney: Segmental sclerosis of the glomerulus (HE and PAM). A segmental eosinophilic nodule containing some mesangial cells is frequently seen in one or a few glomeruli in an HE section. PAM staining makes it easy to demonstrate marked proliferation of mesangial cells and increase in mesangial matrix and the collapse of capillary loops. The lesion is similar to those in so-called glomerular sclerosis.

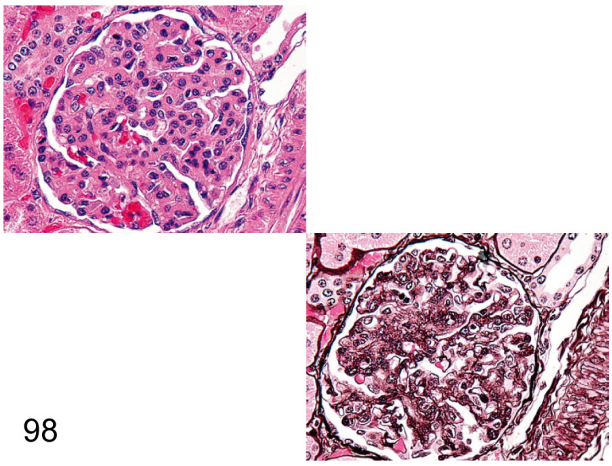

Fig. 98. Kidney: Global sclerosis of the glomerulus (HE and PAM). Global proliferation of mesangial cells with increased matrix is prominent along the glomerular tuft, and capillary loops are not visible presumably because of mesangial proliferation into the capillary loops.

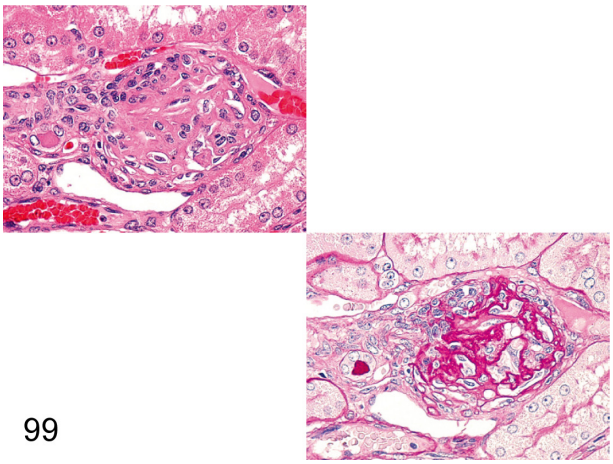

Fig. 99. Kidney: Obsolescent glomerulus (HE and PAS). One or a few obsolescent glomeruli in a section of the kidney are frequently seen in cynomolgus monkeys. This lesion is commonly accompanied by interstitial fibrosis and tubular atrophy, suggesting local ischemia as the pathogenic cause.

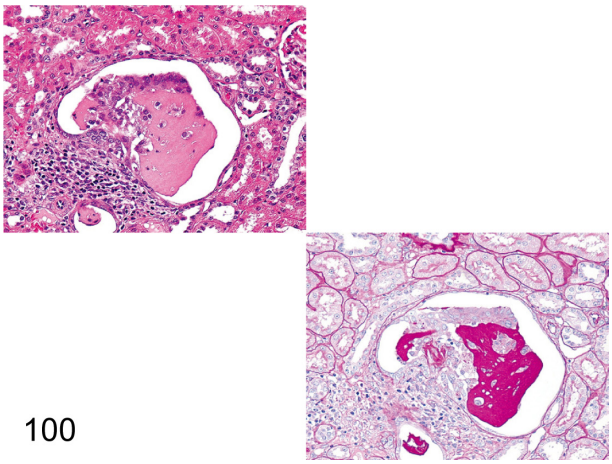

Fig. 100. Kidney: Hyalinosis of the glomerulus (HE and PAS). Some parts of glomerulus are replaced by eosinophilic substances in an HE section. So-called hyalinosis is characterized by the eosinophilic substance consisting of a serum glycoprotein that reacts positively for PAS reaction and negatively for PAM stain.

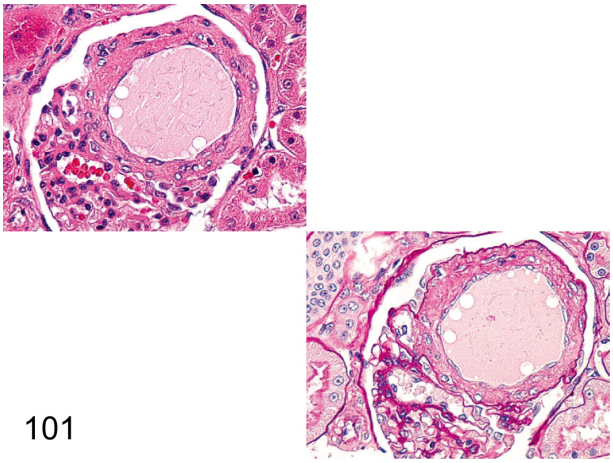

Fig. 101. Kidney: Angiectasis of the glomerular capillary (HE and PAS). The capillary is remarkably dilated and surrounded by increased mesangial matrix. The change is usually seen, but the pathogenesis is unknown.

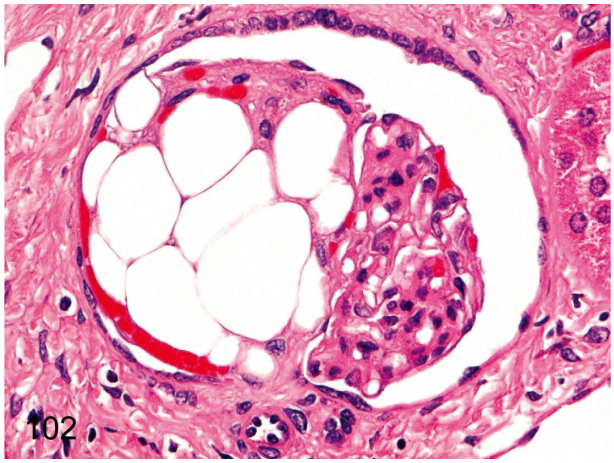

Fig. 102. Kidney: Fatty metaplasia of the glomerulus. Some large lipid droplets are contained in a glomerulus. The histopathologic feature differs from the glomerular lipidosis in Beagles in some respects such as the lack of closely packed fine vacuoles and eosinophilic droplets. Fat droplets are similar to mature adipose tissues in cynomolgus monkeys.

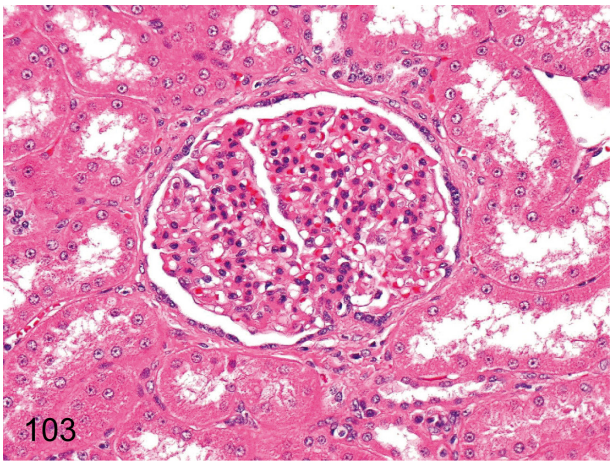

Fig. 103. Kidney: Mesangial proliferative glomerulonephritis (HE). Diffuse markedly enlarged glomeruli are conspicuous in this disease. Albuminuria was found in this case. This lesion is rare in young cynomolgus monkeys.

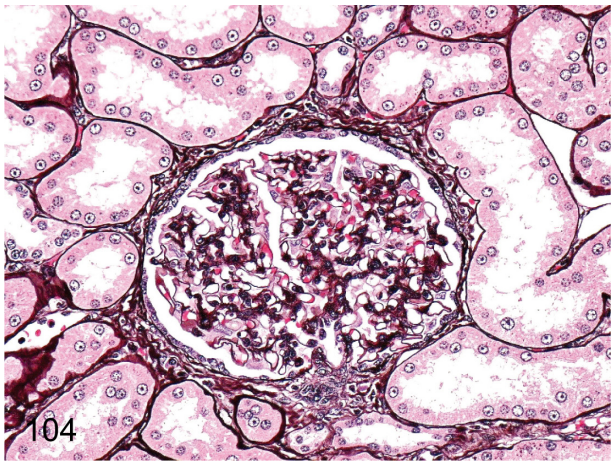

Fig. 104. Kidney: Mesangial proliferative glomerulonephritis (PAM). Proliferation of mesangial cells along the glomerular tufts and thickening of the Bowman's capsule are revealed with PAM stain.

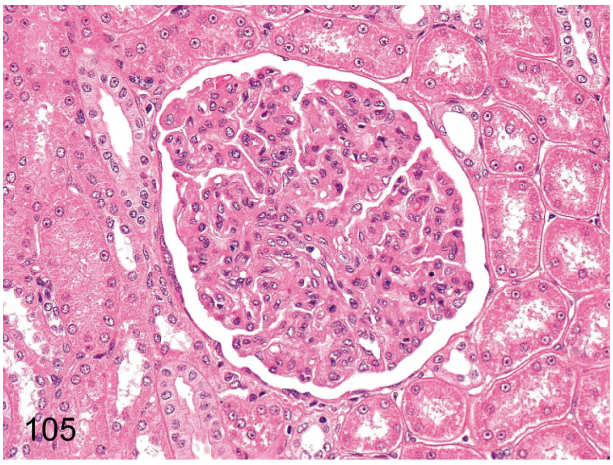

Fig. 105. Kidney: Mesangiocapillary glomerulonephritis (HE). The glomeruli are strikingly enlarged and show lobulation due to the proliferation of mesangial cells and increase in mesangial matrix toward the peripheral area in an HE section. Diffuse glomerulonephritis is rare in young cynomolgus monkeys.

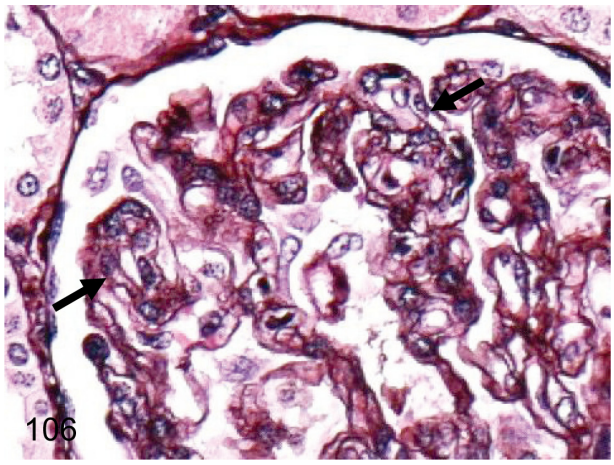

Fig. 106. Kidney: Mesangiocapillary glomerulonephritis (PAM). The characteristic features of mesangiocapillary glomerulonephritis, such as the double contour (arrows) of the basement membranes caused by mesangial interposition, are observed in a PAM-stained section. Though membranoproliferative glomerulonephritis is generally used to refer to this lesion, there is no thickening of the basement membranes by electron microscopy.

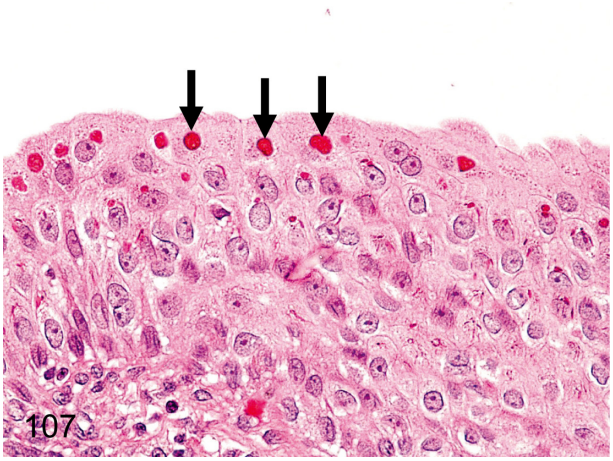

Fig. 107. Kidney (pelvis): Eosinophilic droplets in the transitional epithelium. Eosinophilic droplets in transitional epithelium occur occasionally in the renal pelvis and bladder. These droplets were confirmed as keratohyalin granules in previous reports.

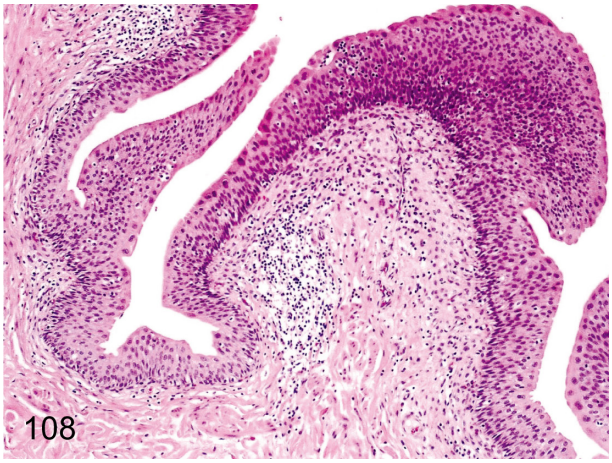

Fig. 108. Urinary bladder: Focal inflammatory cell infiltration in the lamina propria. Focal lymphoplasmacytic infiltration is frequently seen in the lamina propria. The lymphocytes accumulate around small arteries.

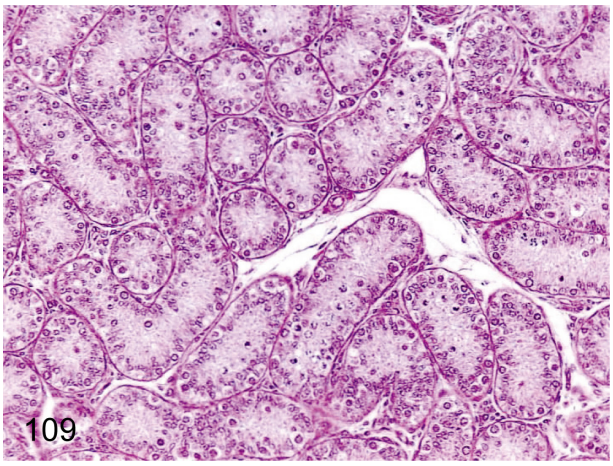

Fig. 109. Testis: Immature (Grade 3). Testes of relatively young monkeys used in toxicologic studies show various stages of maturation with some variability between individuals. We divide immature testes into four grades. Seminiferous tubules consisting of Sertoli cells, spermatogonia and a few spermatocytes are grade 3 (Fig. 109), which is the most usual grade for animals 3 years of age or much younger. The features of grade 4, the most immature grade, consist of only Sertoli cells and undifferentiated spermatogonia.

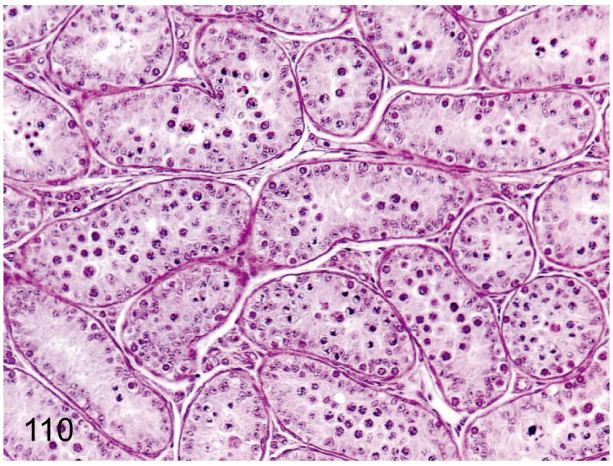

Fig. 110. Testis: Immature (Grade 2). In most seminiferous tubules, epithelia are developing up to spermatocytes. This stage is the most usual in 3- to 4-year-old animals.

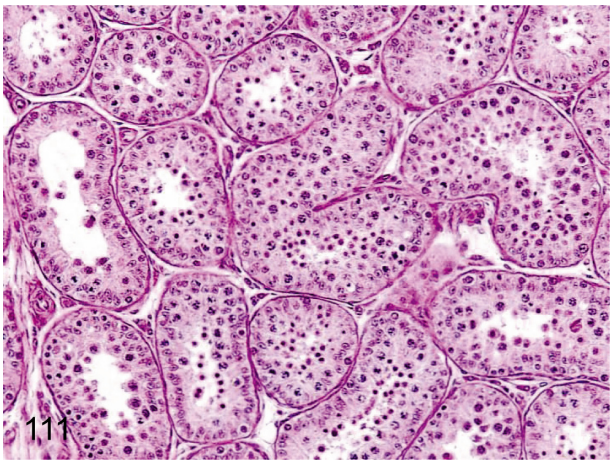

Fig. 111. Testis: Immature (Grade 1). The number of spermatozoa is very low, whereas development up to spermatids completes in almost all seminiferous tubules. This stage is the most usual in 4- to 5-year-old animals.

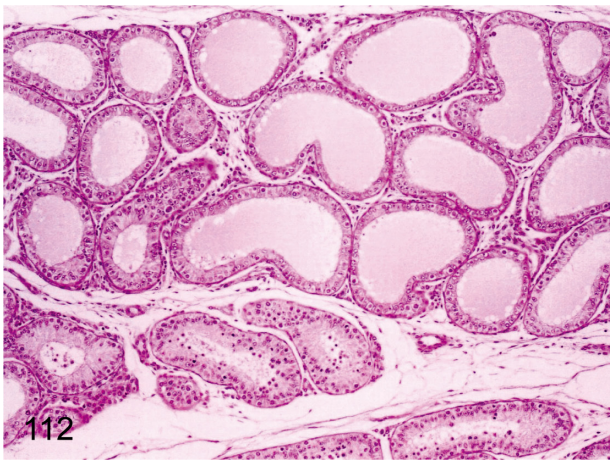

Fig. 112. Testis: Segmental dilatation of the seminiferous tubules. Seminiferous tubules consisting of Sertoli cells, spermatogonia, and spermatocytes are occasionally dilated segmentally in the mature testis.

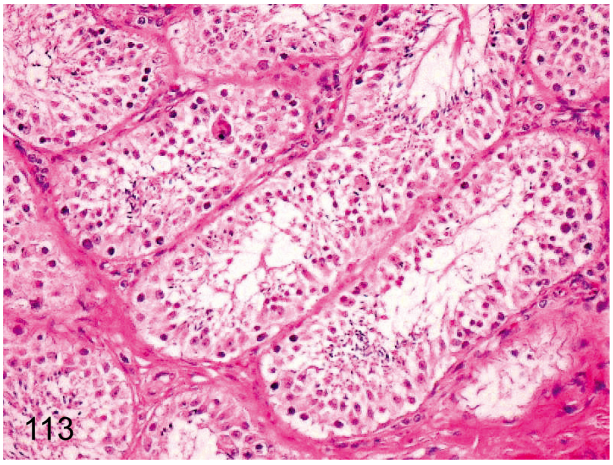

Fig. 113. Testis: Prepubertal testis. Occasional multinucleated giant cell formation and/or aggregation of round spermatogonia occur in the seminiferous tubules in the prepubertal testis. It may be difficult to distinguish these spontaneously occurring changes from some chemical- or drug-induced changes in the seminiferous tubules.

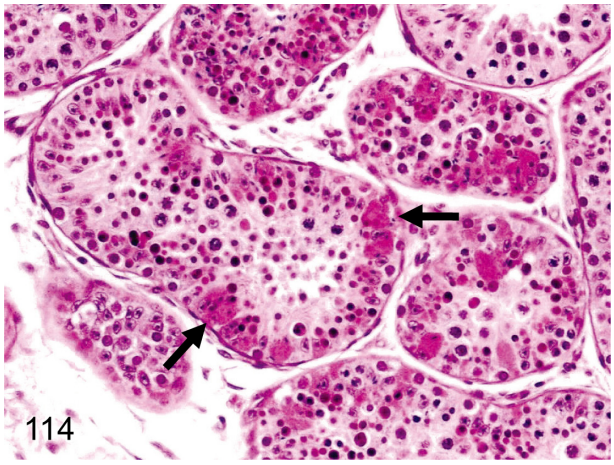

Fig. 114. Testis: Swelling with eosinophilic changes of the Sertoli cells. Swelling with eosinophilic changes of Sertoli cells is rare in the testis. The enlarged Sertoli cells engulfed the degenerative seminiferous epithelia.

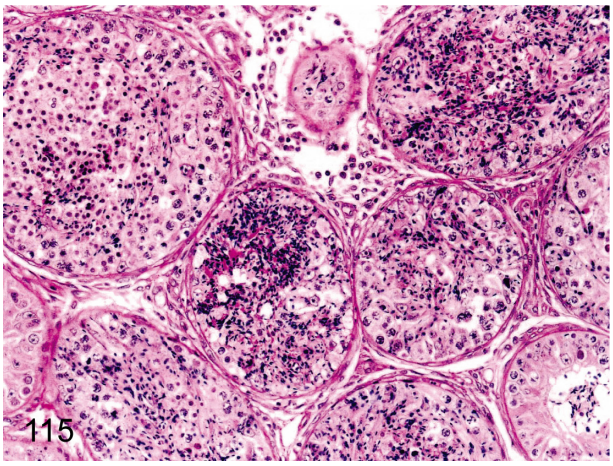

Fig. 115. Testis: Spermatocele. Focal accumulation of spermatozoa occasionally occludes the seminiferous tubules. This change is caused by disturbance of spermatozoa flow due to degenerative changes of the seminiferous tubule.

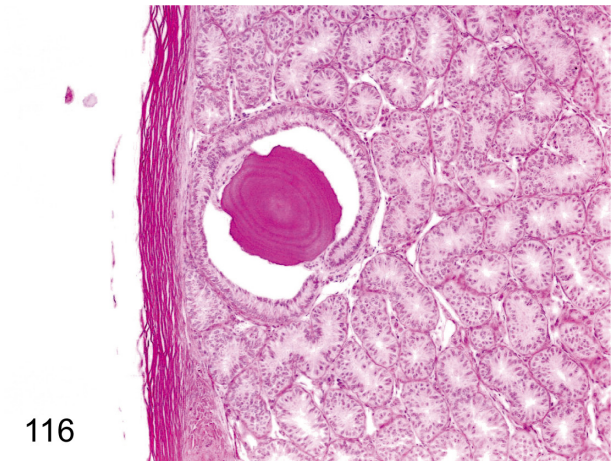

Fig. 116. Testis: Corpus amylaceum. A concentric laminated eosinophilic body is rare in the interstitium of the testis. This body is thought to be derived from degenerated cells or secretions containing protein, and it does not have any important pathological significance.

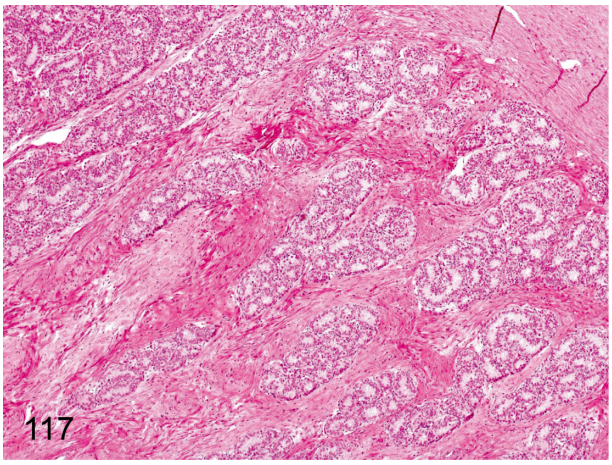

Fig. 117. Testis: Increase in stromal collagen fiber. A focal increase in collagen fiber occurs occasionally in the testicular stroma. The change can be seen in all phases of maturation but cannot be seen in the mature testis. It is not a scar accompanied by damage to the seminiferous tubules.

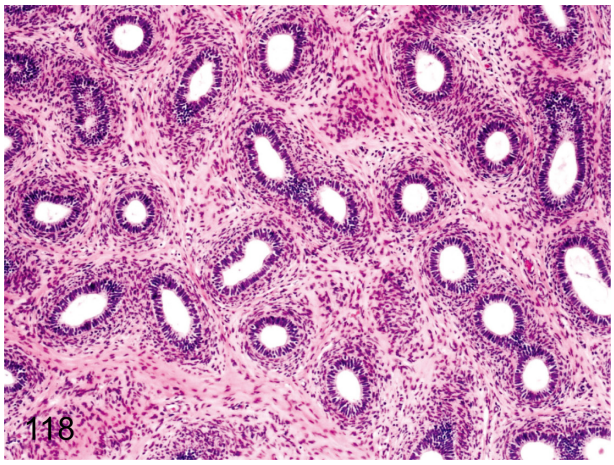

Fig. 118. Epididymis: Immature. The ductal epithelia are small and flat, and lumens are narrow. The interstitium also consists of immature fibrous tissue with higher nuclear density. Maturation of the epididymis closely correlates with the degree of testes maturation.

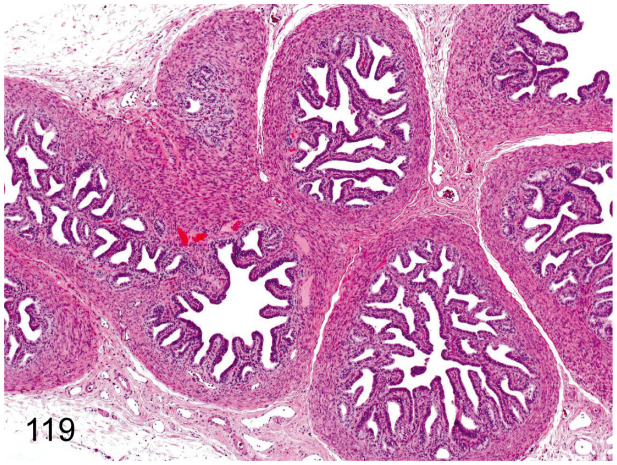

Fig. 119. Seminal vesicle: Immature. The glandular epithelia are low cuboidal, and each fold is also small. There is no secretion in the seminal vesicle. Maturation of the seminal vesicle also closely correlates with the degree of testes maturation.

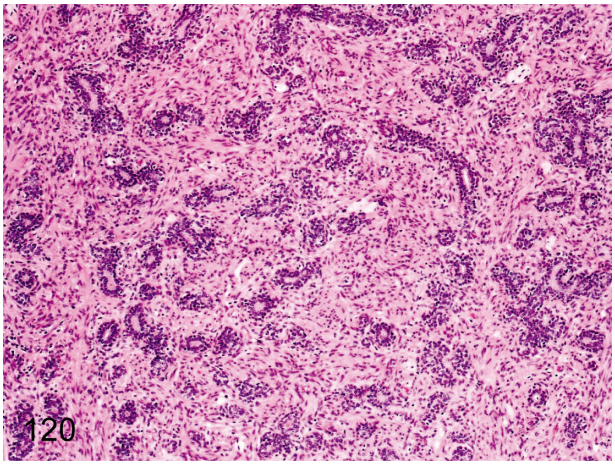

Fig. 120. Prostate: Immature. The glandular epithelia are small and flat, and lumens are narrow because of no prostatic secretion. Maturation of the prostate also closely correlates with the degree of testes maturation.

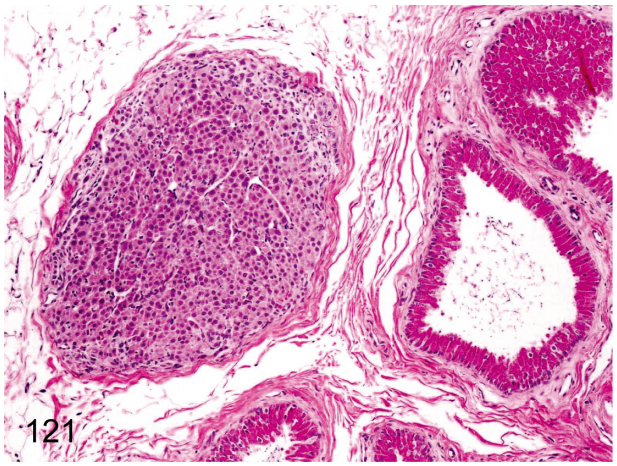

Fig. 121. Epididymis: Ectopic adrenocortical tissue. Remnants of adrenocortical tissue are rare in adipose tissue near the epididymis. Embryologically, both primordia of the reproductive organ and adrenocortical tissue are adjacently located to each other.

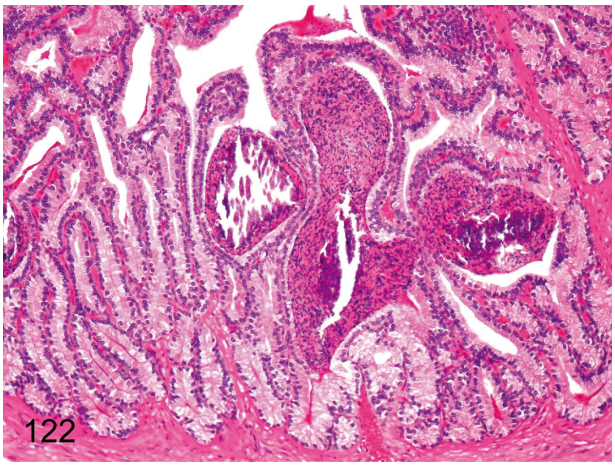

Fig. 122. Seminal vesicle: Spermatocele. Focal accumulation of spermatozoa (spermatocele) occurs occasionally in the seminal vesicle of monkeys after genital maturation, and the accumulated spermatozoa might often be mineralized.

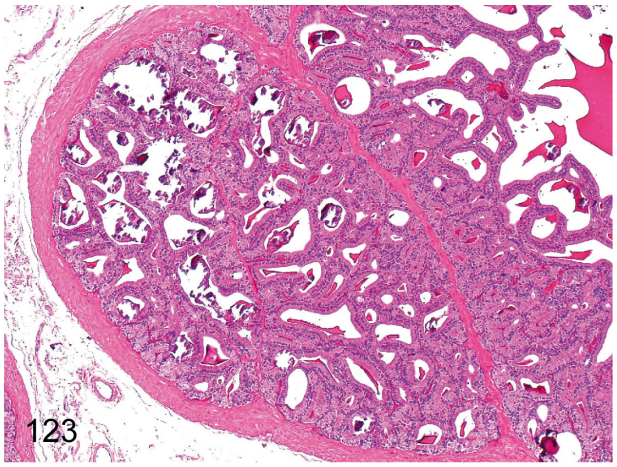

Fig. 123. Seminal vesicle: Mineralization of secretions. Mineralization of secretions is frequently seen in monkeys after genital maturation.

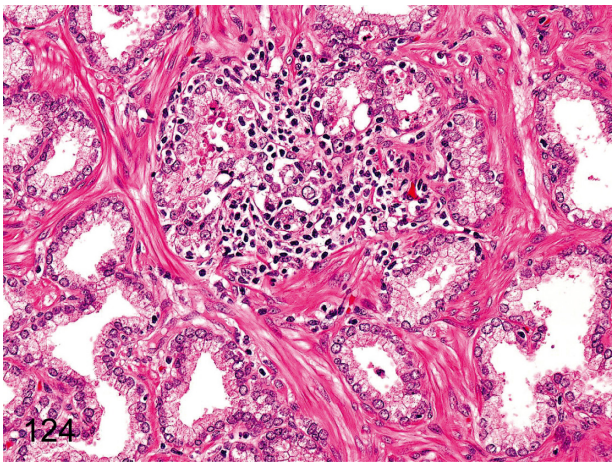

Fig. 124. Prostate: Focal inflammatory cell infiltration. Lymphoplasmacytes occasionally infiltrate in the interstitium focally.

Cyclic changes in female reproductive system (Figures 125–130).

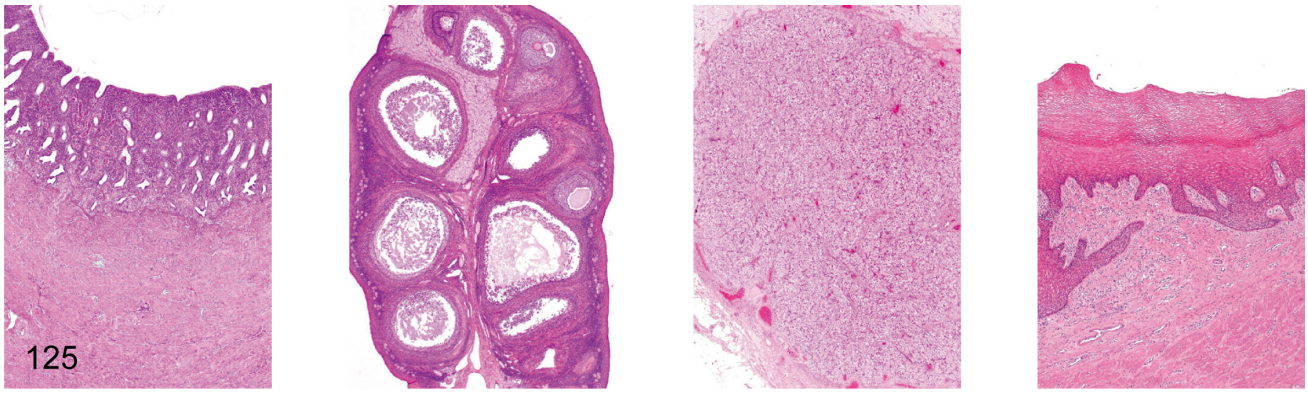

Fig. 125. Female reproductive system: Early follicular phase. Uterus, ovary (containing dominant follicle), ovary (containing involuting corpus luteum), vagina

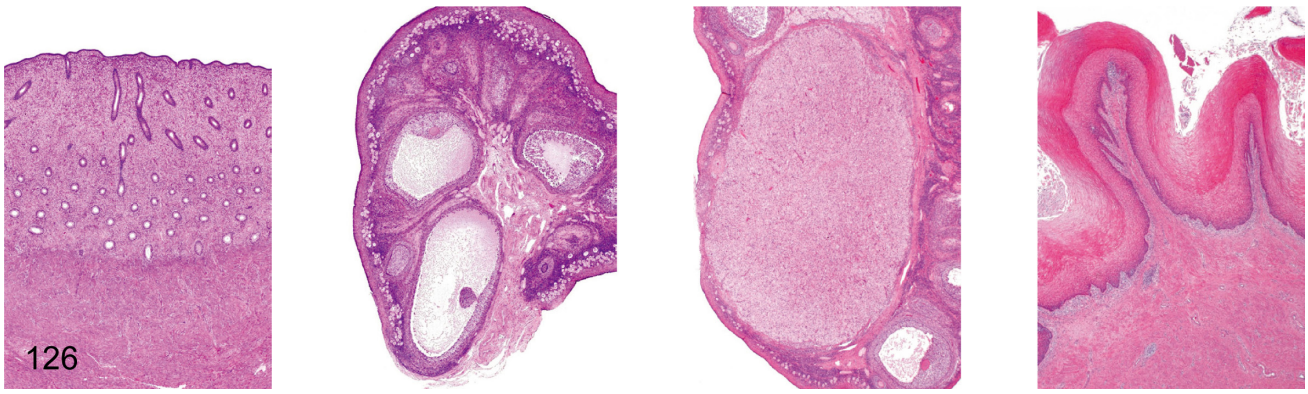

Fig. 126. Female reproductive system: Follicular phase. Uterus, ovary (containing dominant follicle), ovary (containing involuting corpus luteum), vagina

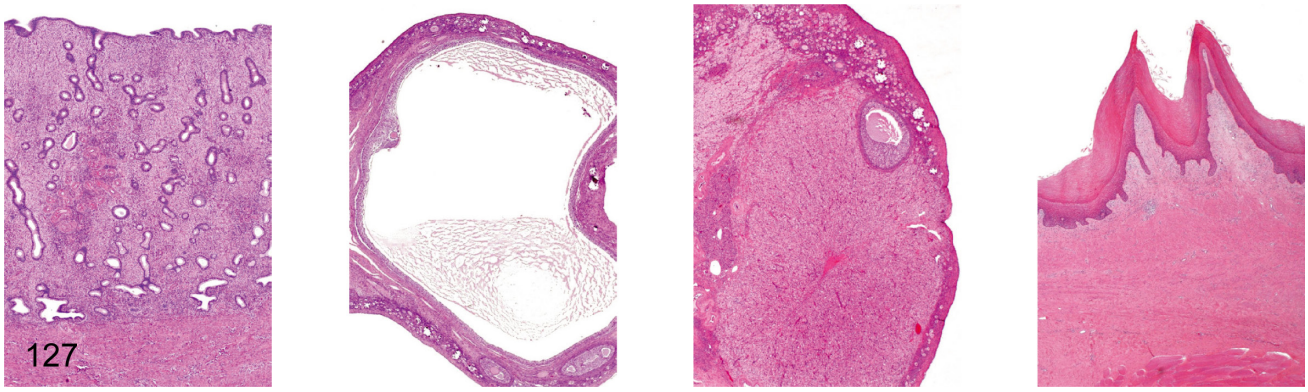

Fig. 127. Female reproductive system: Preovulation. Uterus, ovary (containing dominant follicle), ovary (containing involuting corpus luteum), vagina

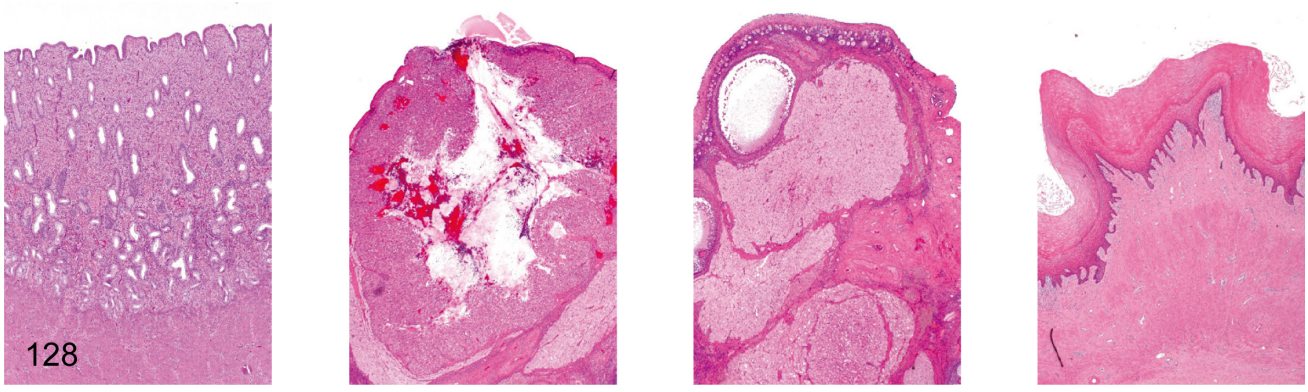

Fig. 128. Female reproductive system: Early luteal phase. Uterus, ovary (containing postovulatory corpus luteum), ovary (containing involuting corpus luteum), vagina

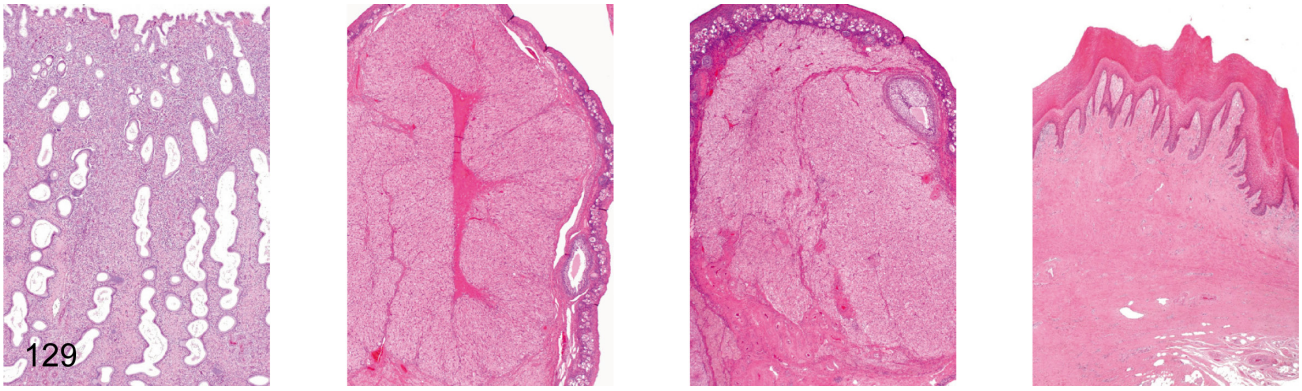

Fig. 129. Female reproductive system: Luteal phase. Uterus, ovary (containing functional corpus luteum), ovary (containing involuting corpus luteum), vagina

Fig. 130. Female reproductive system: Menstruation. Uterus, ovary (containing dominant follicle), ovary (containing menstrual corpus luteum), vagina

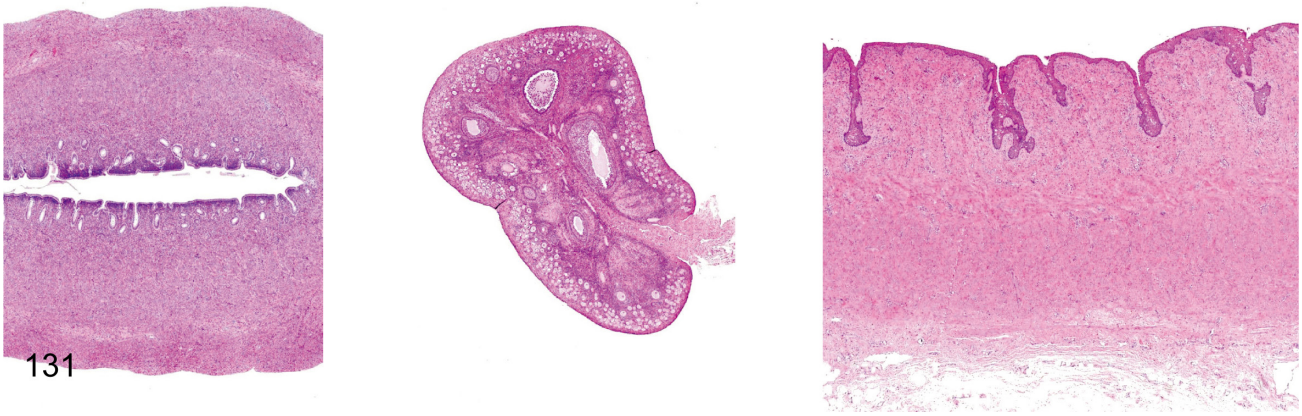

Fig. 131. Female reproductive system: Immature. Immature female reproductive tissues are characterized by a thin endometrium (less than 50% of the mature uterine basal layer) and thin myometrium in the uterus, a small ovary containing a lot of primordial follicle and a few Graafian follicles and thin or no keratinized squamous epithelium in the vagina. It is necessary to distinguish this immature figure from atrophy of the female reproductive system because similar figures are also seen under cachectic conditions.

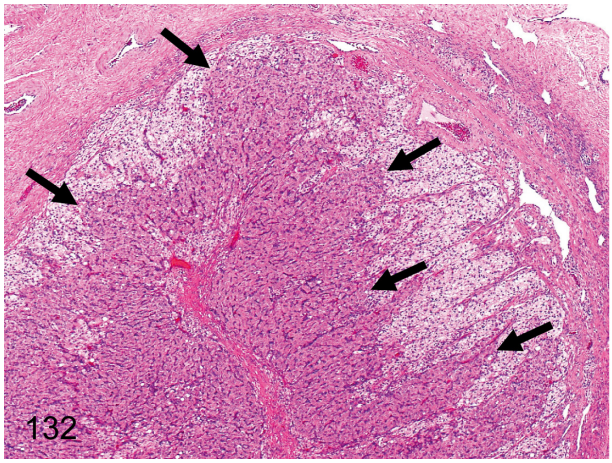

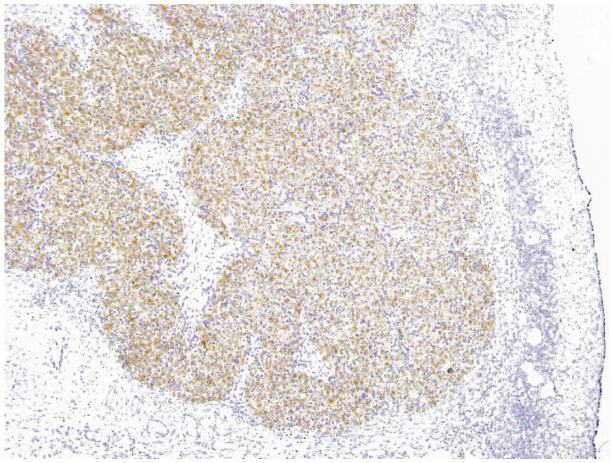

Fig. 132. Ovary: Aberrant corpora luteum. Aberrant corpora lutea (ACL) frequently appear in regressing corpora lutea. They consist of characteristic luteal cells with vesicular nuclei and deeply stained cytoplasm (eosinophilic or basophilic cytoplasm) and abundant capillaries. The luteal cells are positive for inhibin (right). We think that the ACL may have a role in controlling the number of follicles by inhibin secretion for a single ovulation in monkeys.

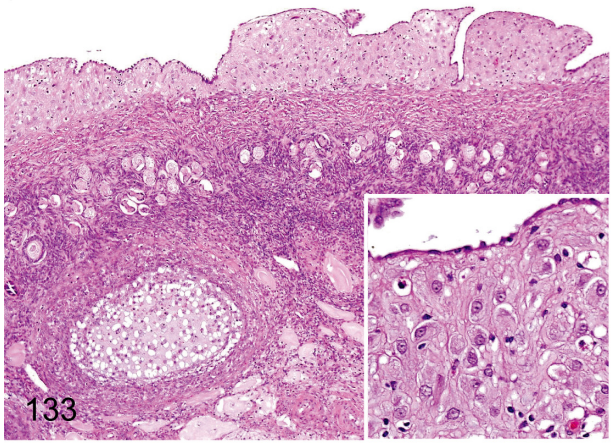

Fig. 133. Ovary: Deciduosis . Extrauterine decidual cell plaque is rare in the subcoelomic mesenchyme. Decidual tissue consists of irregularly shaped and eosinophilic large epithelioid cells. Similar features are well-known as generally occurring changes in women during or after pregnancy.

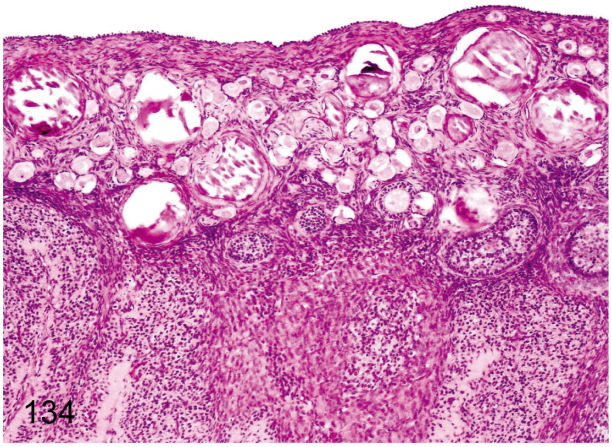

Fig. 134. Ovary: Mineralization. Various numbers of mineralized foci are frequently seen in the ovarian cortex lined by many primordial follicles, especially in young cynomolgus monkeys. They are presumably necrotized oocytes accompanied by follicular atresia.

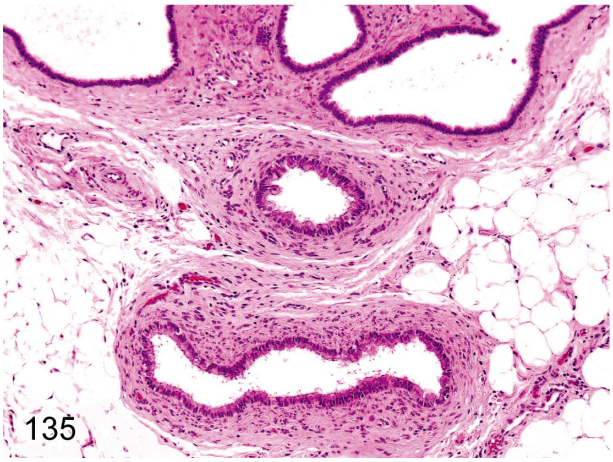

Fig. 135. Ovary: Paroophoritic cyst. These cysts arise from remnants of the paroophoron. Dilated ducts lined by cuboidal or columnar ciliated epithelia occur occasionally in peripheral tissue of the ovaries.

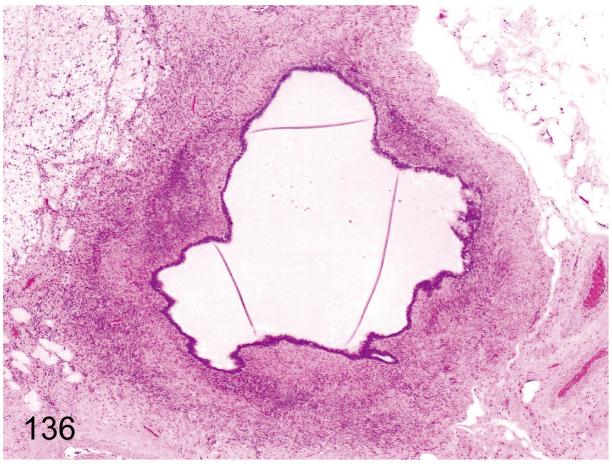

Fig. 136. Ovary: Mesonephric cyst. This cyst arises from remnants of the mesonephric duct. It differs from a paroophoritic cyst in the existence of developed smooth muscle in the pericystic layer.

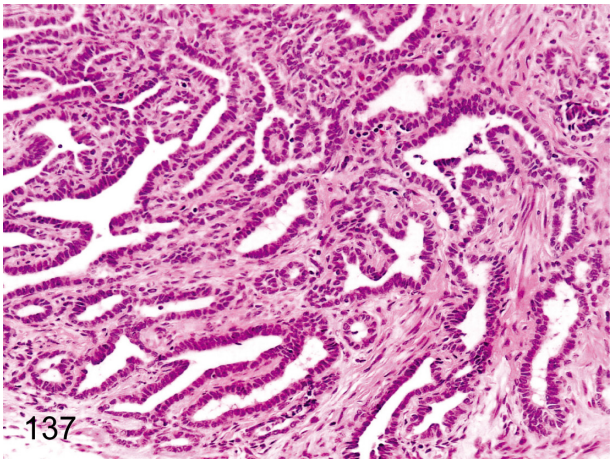

Fig. 137. Ovary: Hyperplasia of the rete ovarii. Remnants of the rete ovarii are frequently seen in the hilum of the ovary and occasionally undergo hyperplastic changes.

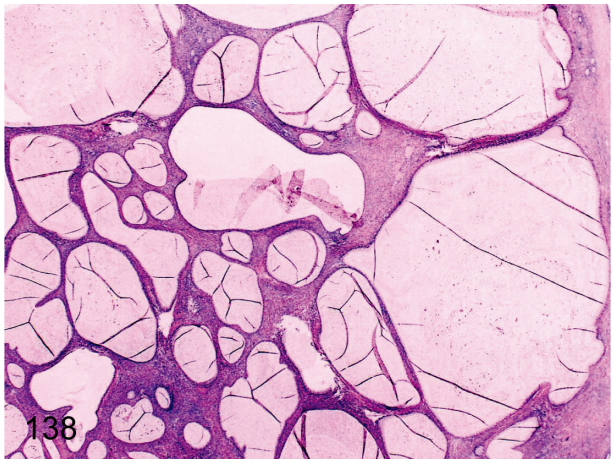

Fig. 138. Ovary: Mucinous cystadenoma. Multiple cysts lined by mucinous epithelia resembling the cervical canal epithelia in the ovarian parenchyma. Details of this rare case have been reported.

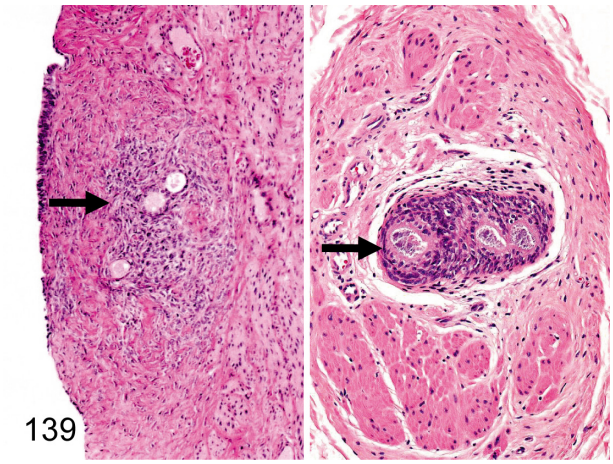

Fig. 139. Ovary: Ectopic ovarian tissue in the uterus or urinary bladder. Ovarian tissue consisting of primordial follicles, primary follicles, preantral follicles and surrounding stromal cells occurs occasionally in the muscle layer or serosa of the uterus (left) but rarely in the urinary bladder (right).

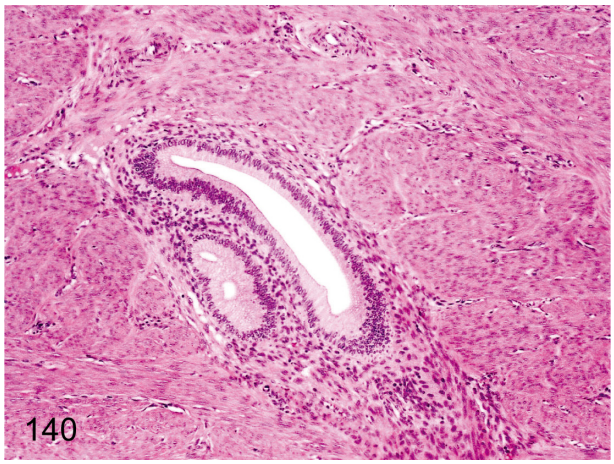

Fig. 140. Uterus: Adenomyosis (endometriosis interna). Endometrial tissue consisting of endometrial glands and stromal cells occurs occasionally in the uterine muscle layer. Endometriosis externa in the intestinal wall, greater omentum and mesenterium has been reported in older cynomolgus monkeys, and we have never observed it in young animals.

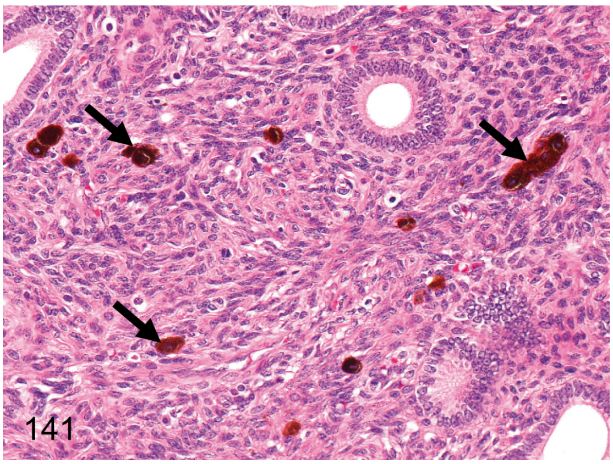

Fig. 141. Uterus: Melanin pigment deposition. Melanin pigments occur occasionally in the endometrium. Melanin pigment deposition (melanosis) can be seen in various organs in cynomolgus monkeys. See also Figs. 144, 173, and 189.

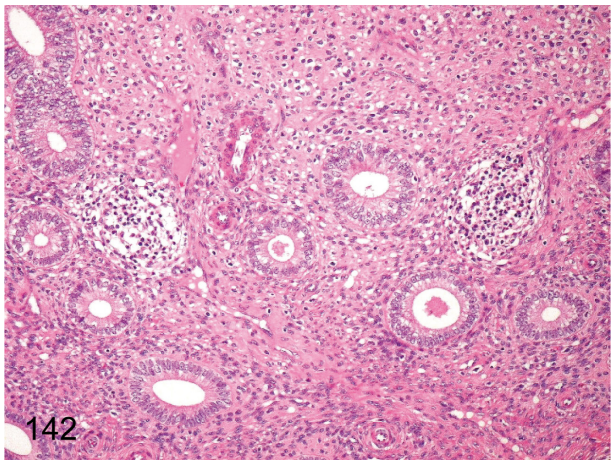

Fig. 142. Uterus: Focal inflammatory cell infiltration in the endometrium. Focal lymphoplasmacytic infiltration occurs occasionally in the endometrium. This lesion differs from estrus cycle-related changes, although some inflammatory cells generally infiltrate into the apical endometrial tissue in the late luteal phase (ischemic phase of uterus).

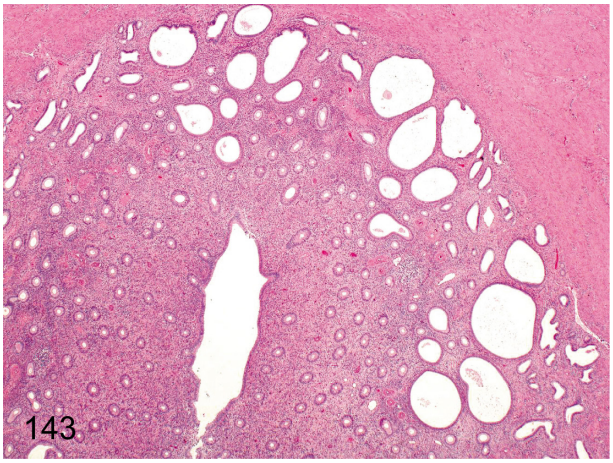

Fig. 143. Uterus: Dilatation of the endometrial gland. Many endometrial glands dilate excessively, so this lesion differs from physiological dilatation during the follicular phase.

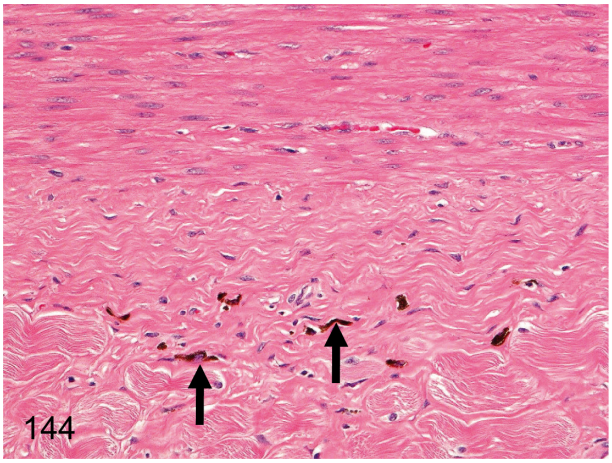

Fig. 144. Vagina: Melanin pigment deposition. Melanin pigments occur occasionally in the muscle layer and/or serosa. Melanin pigment deposition (melanosis) can be seen in various organs in cynomolgus monkeys. See also Figs. 141, 173, and 189.

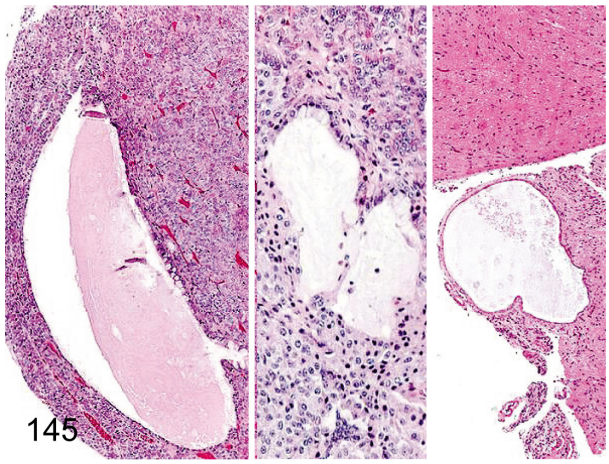

Fig. 145. Pituitary: Cyst. Pituitary cysts are frequently seen in each lobe such as the anterior (left), intermediate (middle) and posterior (right) lobes but are often found in the anterior lobe.

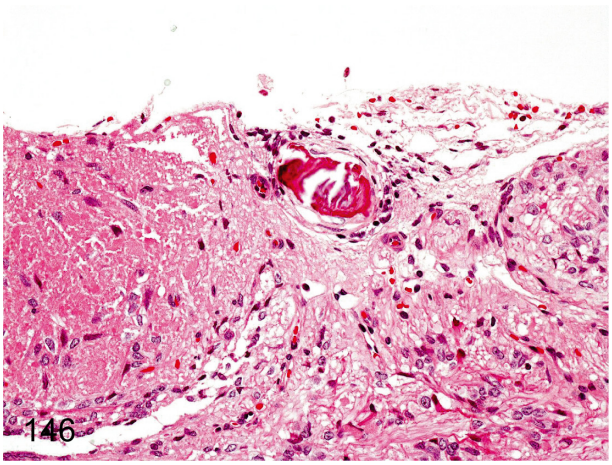

Fig. 146. Pituitary: Mineralization. Mineralization rarely occurs in the pituitary.

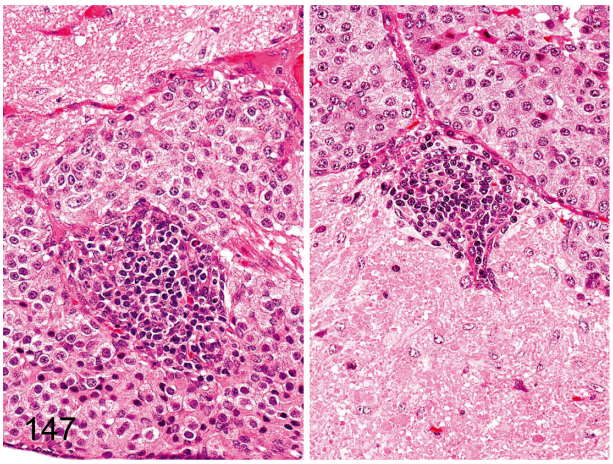

Fig. 147. Pituitary: Focal inflammatory cell infiltration. Focal and slight lymphoplasmacytic accumulation occurs occasionally in each lobe. The left figure is the intermediate lobe, and the right figure is the posterior lobe.

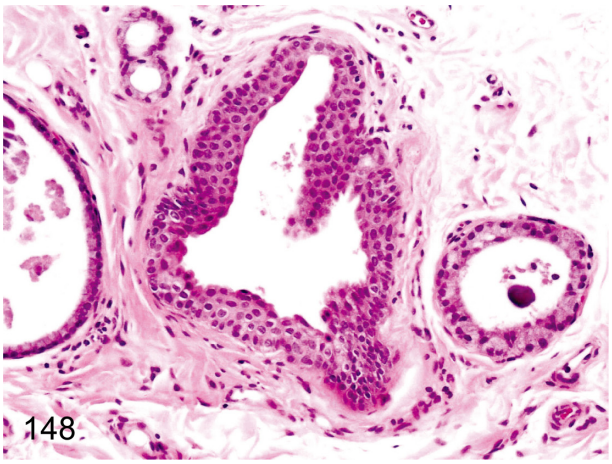

Fig. 148. Thyroid: Ultimobranchial remnant. An ultimobranchial body occurs occasionally. The epithelium is squamous and frequently cystic. The incidence in cynomolgus monkeys is lower than in rats or Beagles.

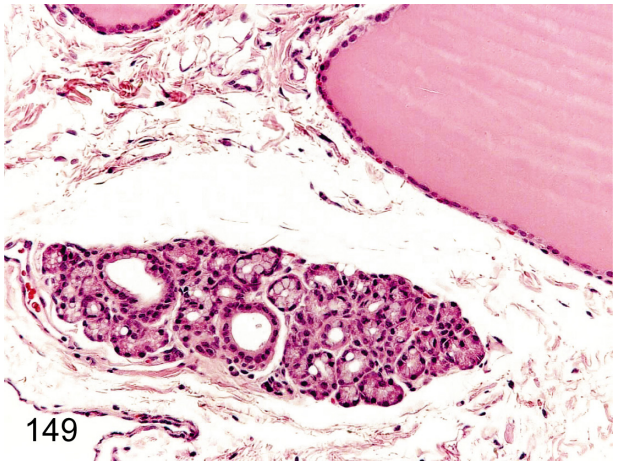

Fig. 149. Thyroid (Parathyroid): Ectopic salivary gland. Salivary acini and ducts can be found in the thyroid and/or parathyroid.

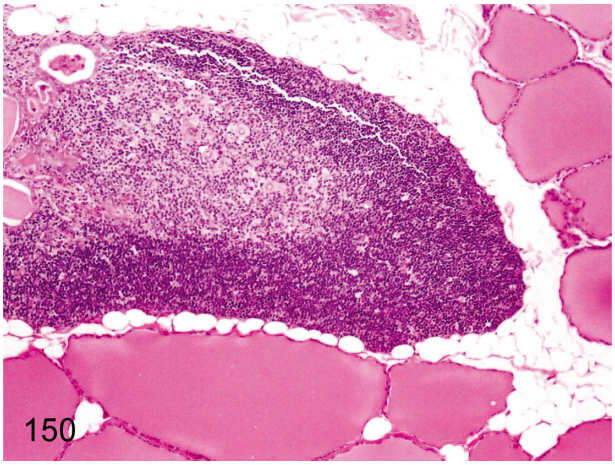

Fig. 150. Thyroid (Parathyroid): Ectopic thymic tissue. Because the parathyroid, thyroid and thymus derive from the same primordium, the pharyngeal cavity, it is comprehensible that the thyroid and/or parathyroid tissue contain thymic tissue. See also Fig. 16.

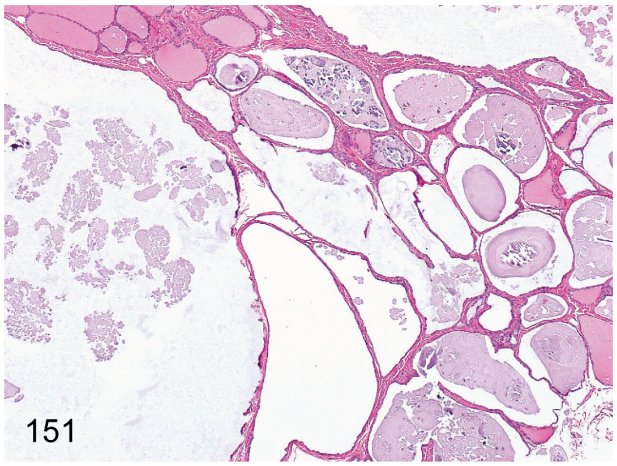

Fig. 151. Thyroid: Cystic dilatation of the follicle. Huge follicles containing weakly basophilic substances occur occasionally. The pathologic meaning and significance of this change are not clear.

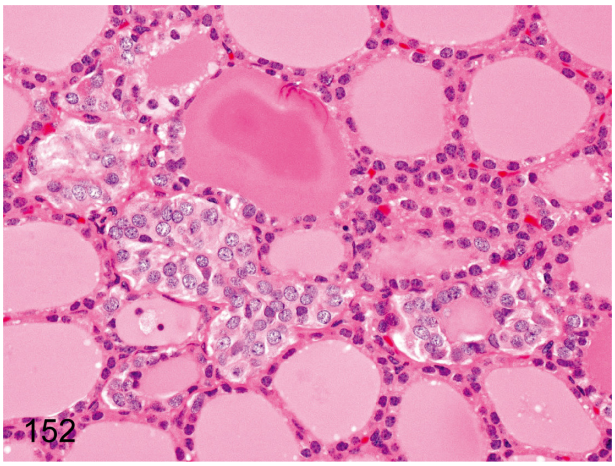

Fig. 152. Thyroid: Focal C-cell hyperplasia. Generally, C-cells are not easily recognizable in the thyroid of cynomolgus monkeys, in contrast to those in Beagles. In this figure, the C-cell hyperplastic focus is small, but even a small focus appears very rarely in cynomolgus monkeys.

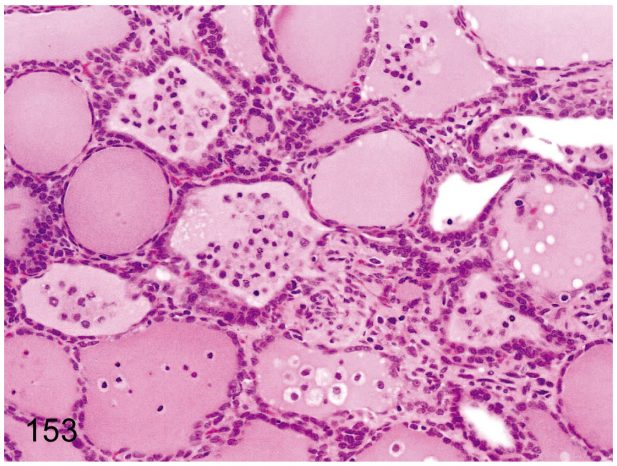

Fig. 153. Thyroid: Infiltration of macrophages in the follicles. Focal follicular atrophy, desquamation of follicular epithelia and infiltration of macrophages in follicles are frequently seen in the thyroid of cynomolgus monkeys.

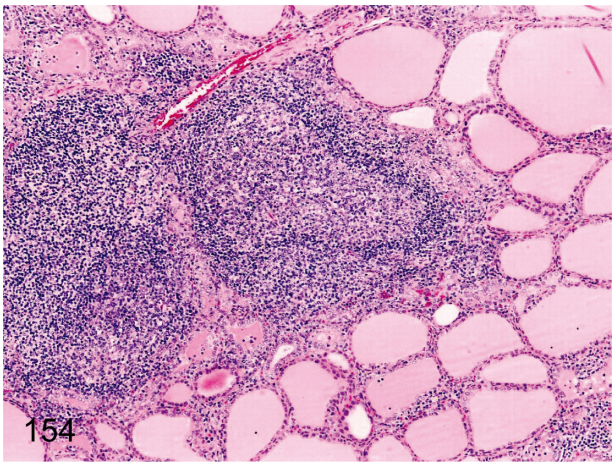

Fig. 154. Thyroid: Focal inflammatory cell infiltration. Focal lymphoplasmacytic infiltration, often with lymph follicle formation in the interstitium, is frequently seen. The incidence and degree of this lesion are lower in cynomolgus monkeys than in Beagles.

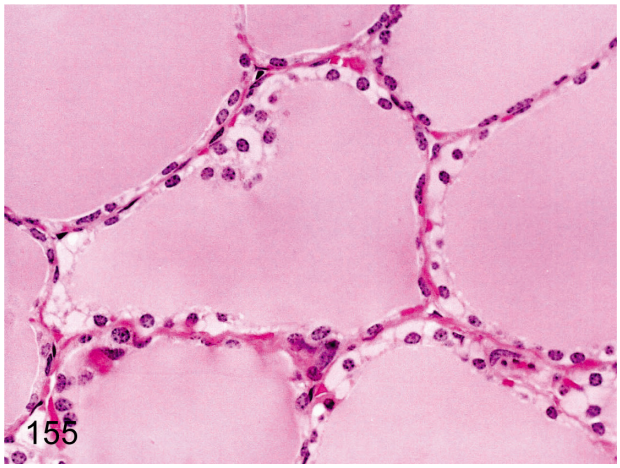

Fig. 155. Thyroid: Hydropic degeneration of follicular cells. Accumulation of pale eosinophilic substances in follicular epithelial cells is rare. Similar changes are caused by dilatation of the endoplasmic reticulum filled with low electron density amorphous substances. See also Figs. 56 and 70.

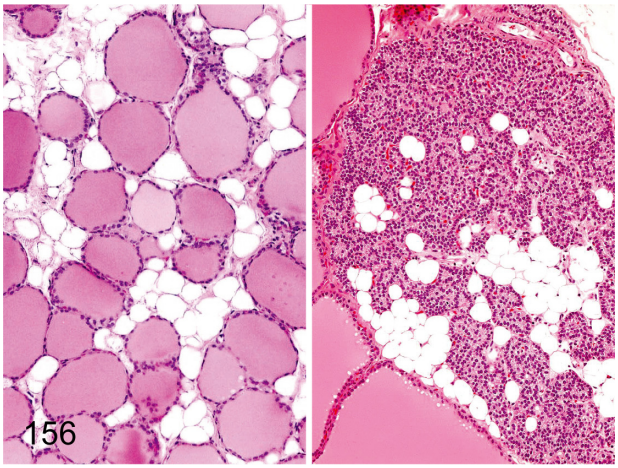

Fig. 156. Thyroid and parathyroid: Fatty infiltration. Adipose cells infiltrate focally or entirely into the interstitium of the thyroid and/or parathyroid.

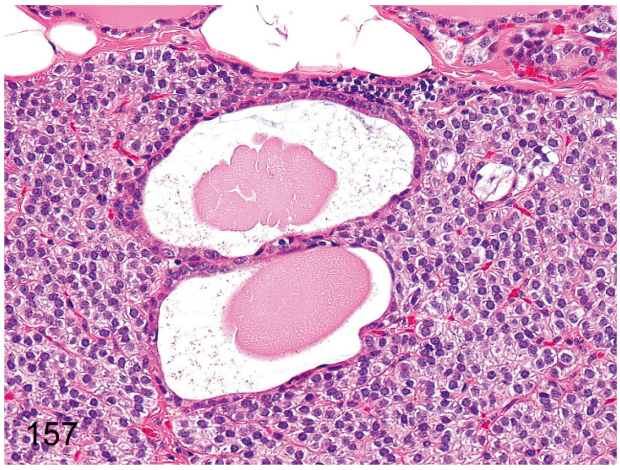

Fig. 157. Parathyroid: Cyst (Kürsteiner's cyst). Cysts are lined by cuboidal epithelia, occasionally ciliated, and contain proteinic substances in the lumens. This cyst is a remnant of the embryonal duct connecting the parathyroid-thymus tissue in the III and IV pharyngeal pouches.

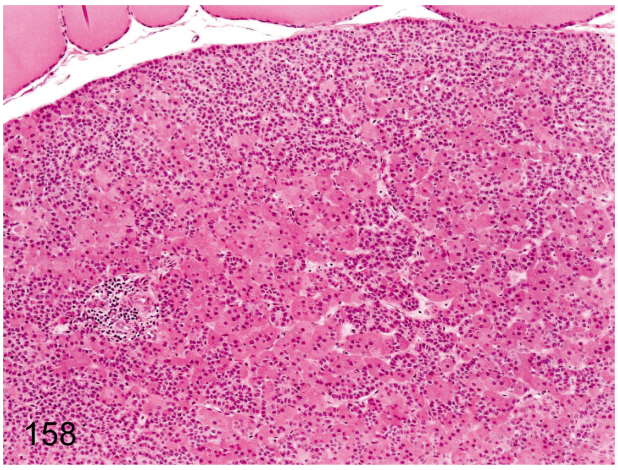

Fig. 158. Parathyroid: Increase in oxyphil cells. The number of oxyphil cells in the parathyroid tends to increase with advancing age; however, this change is rarely seen at a young age. These cells have eosinophilic cytoplasm reflecting a lot of mitochondria.

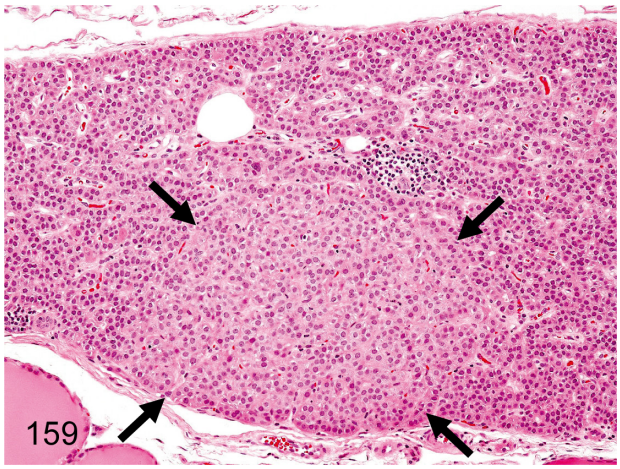

Fig. 159. Parathyroid: Focal hypertrophy of chief cells. Focal hypertrophy of chief cells is rare. This change differs from diffuse hypertrophy caused by hypocalcemia.

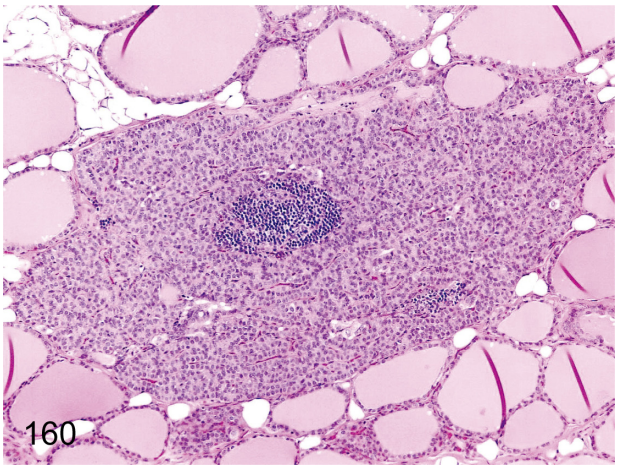

Fig. 160. Parathyroid: Focal inflammatory cell infiltration. Focal lymphoplasmacytic infiltration occurs occasionally in the parathyroid.

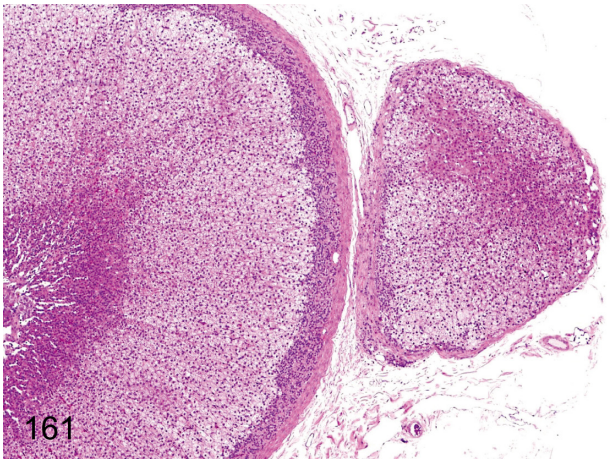

Fig. 161. Adrenal: Accessory adrenocortical tissue. The aberration of adrenocortical tissue separated from the original body and surrounding capsule is called accessory adrenocortical tissue.

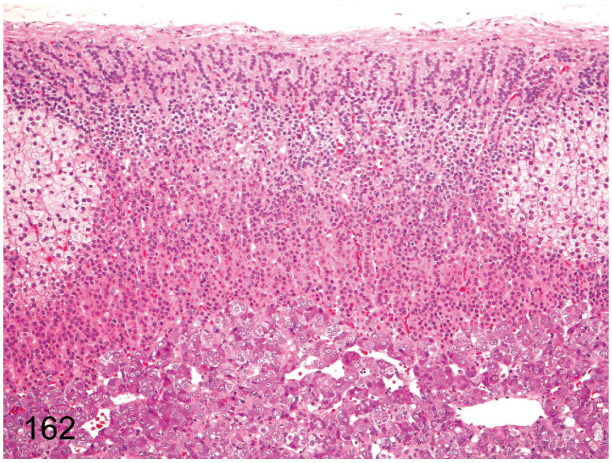

Fig. 162. Adrenal: Normal variance of cortical cells (1). Generally, each of the three adrenocortical zones is obviously distinguishable in cynomolgus monkeys because cells of the zona fasciculata contain numerous fine vacuoles causing a very clear appearance of the cytoplasm. Partial replacement of the zona fasciculata by glomerulosa-like cells occurs occasionally as a normal variance.

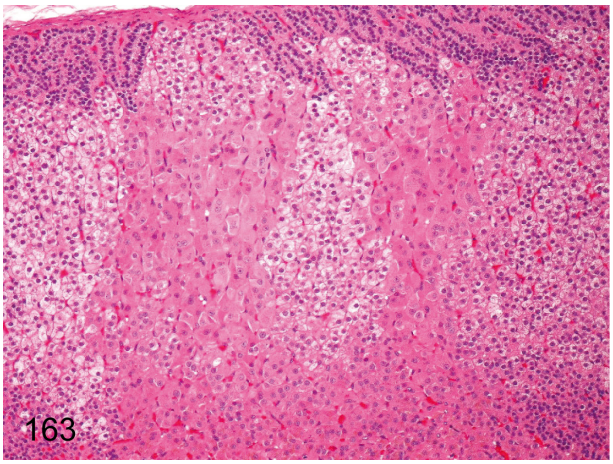

Fig. 163. Adrenal: Normal variance of cortical cells (2). Eosinophilic and hypertrophic cells of the zona fasciculata are focally seen without compressing the adjacent tissue as a normal variance.

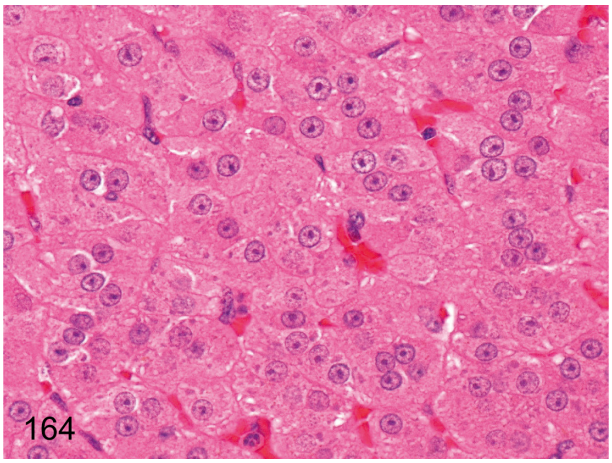

Fig. 164. Adrenal: High magnification of Fig. 163. The hypertrophic cortical cells have eosinophilic cytoplasm containing basophilic granules instead of lipid droplets. Basophilic granules are thought to be rough endoplasmic reticulum, and these changes are the same as for hypertrophic cortical cells under stress conditions. See also Fig. 195.

Fig. 165. Adrenal: Nodular hyperplasia of cortical cells (eosinophilic). A focus consisting of proliferative and hypertrophic eosinophilic cells appears mainly in the zona fasciculata and reticularis. The focus slightly compresses the adjacent cortical tissue. Eosinophilic cells in the focus have few lipid droplets in the cytoplasm.

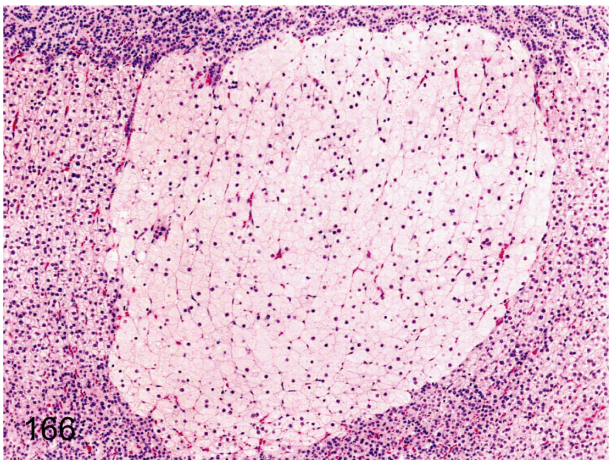

Fig. 166. Adrenal: Nodular hyperplasia of cortical cells (vacuolated). A focus consisting of proliferative and hypertrophic vacuolated cells containing numerous fine lipid droplets originates mainly in the zona fasciculata. The focus slightly compresses the adjacent cortical tissue.

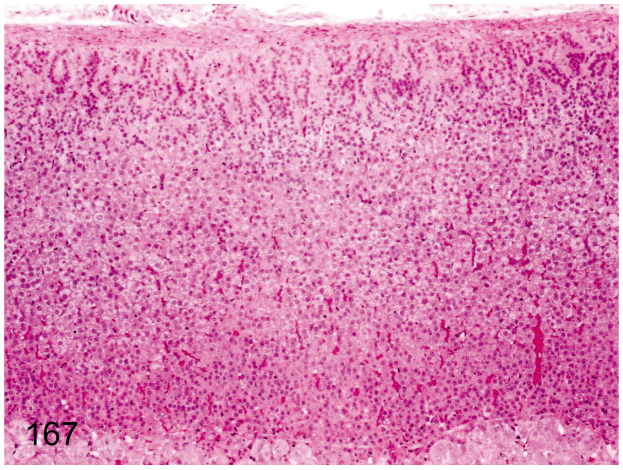

Fig. 167. Adrenal: Decreased lipid droplets in cortical cells. Generally, cells of the zona fasciculata contain numerous fine lipid droplets. If the lipid droplets decrease due to stress, each of the adrenocortical zones is indistinct. Sometimes, cells of the zona fasciculata contain a little fewer lipid droplets under normal conditions.

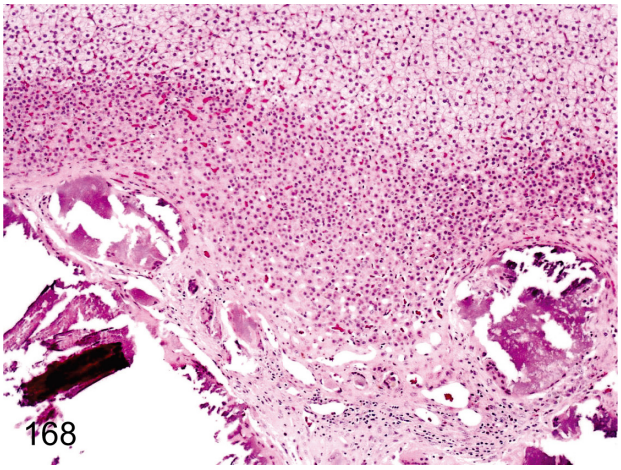

Fig. 168. Adrenal: Mineralization in the corticomedullary junction. Mineralization in the inner cortex is usually seen in monkeys. The change may be dystrophic mineralization presumably caused by preexisting involution, hemorrhage and/or fibrosis in the inner fetal layer during postnatal development.

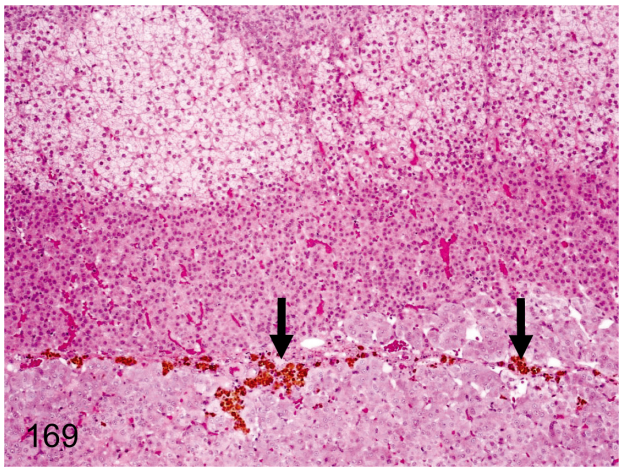

Fig. 169. Adrenal: Pigment deposition in the corticomedullary junction. Brown pigments deposit in the corticomedullary junction. These pigments are mostly hemosiderin.

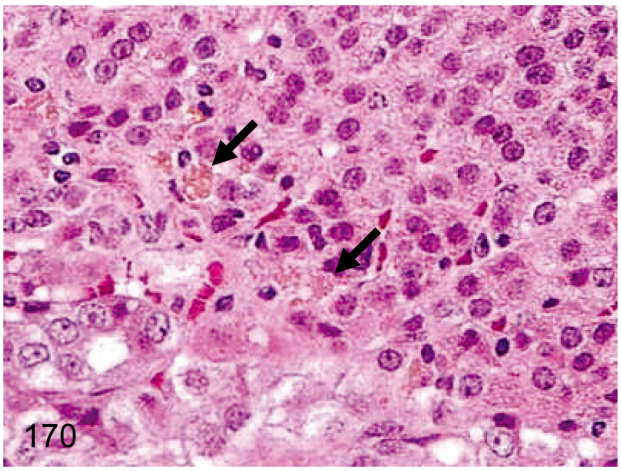

Fig. 170. Adrenal: Pigment deposition in the cells of the zona reticularis. Unlike Fig. 169, yellow-brown pigments in cells of the zona reticularis are mostly lipofuscin.

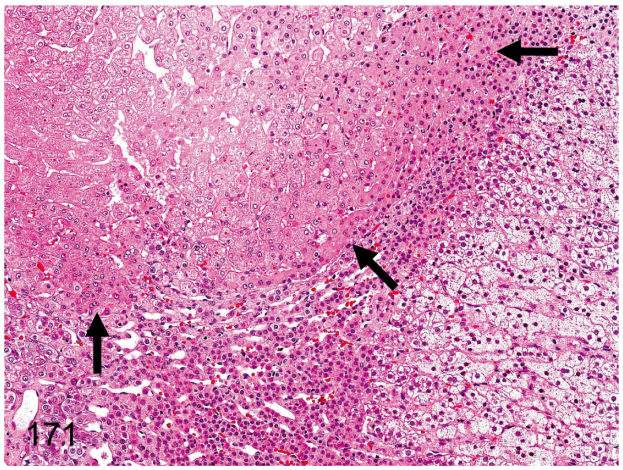

Fig. 171. Adrenal: Adrenohepatic fusion. Grossly, the right adrenal is attached to the right lobe of the liver. The hepatic tissue occasionally occupies a part of the cortex of the right adrenal. There is no capsule surrounding the hepatic tissue.

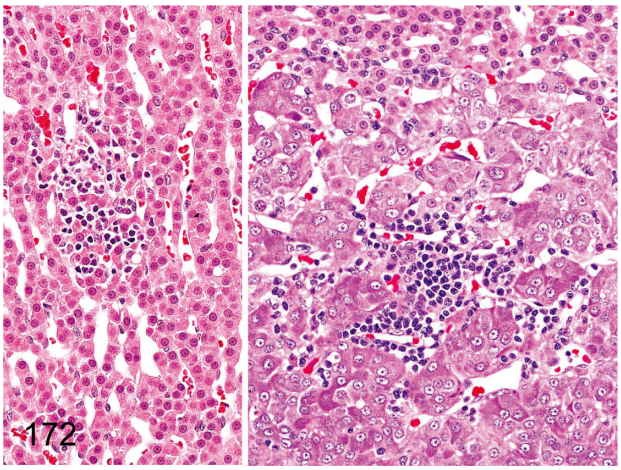

Fig. 172. Adrenal: Focal inflammatory cell infiltration. Focal and slight lymphoplasmacytic infiltration occurs occasionally in the zona reticularis (left) or medulla (right).

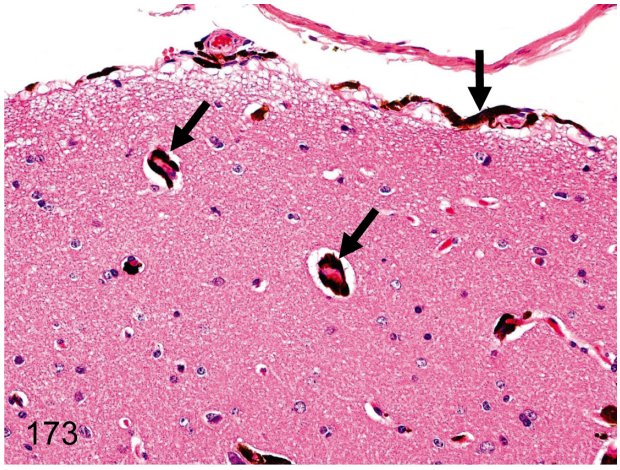

Fig. 173. Brain (Spinal cord): Melanin pigment deposition in the meninx and vascular wall (perivascular tissue) . Melanin pigment deposition is usually seen in the meninges or perivascular tissue. Melanin pigments are common in the various organs in cynomolgus monkeys. See also Figs. 141, 144, and 189.

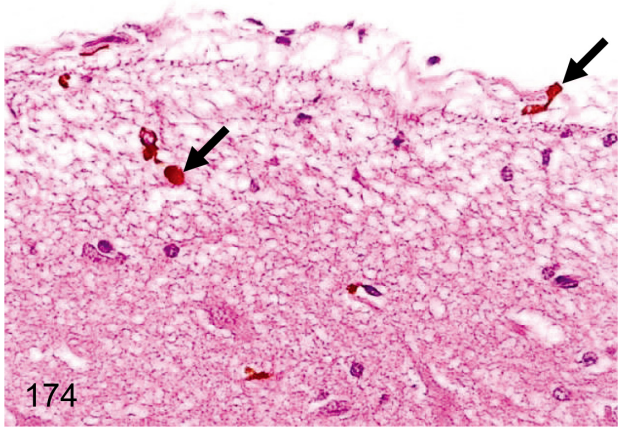

Fig. 174. Brain: Hemosiderin pigment deposition in the meninx or cerebral cortex. Hemosiderin pigments frequently deposit in the meninges or submeningeal cerebral cortex. Extravasation of erythrocytes is most likely the cause of the change, although no changes suggesting the preceding hemorrhage or congestion are evident.

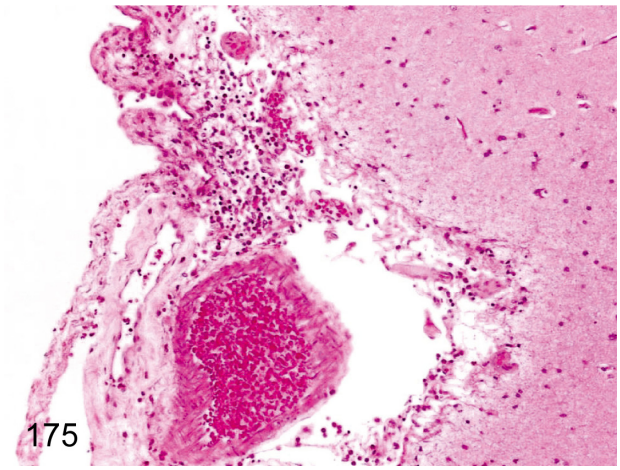

Fig. 175. Brain: Focal inflammatory cell infiltration in the meninx. Focal slight lymphoplasmacytic infiltration occurs occasionally in the meninx.

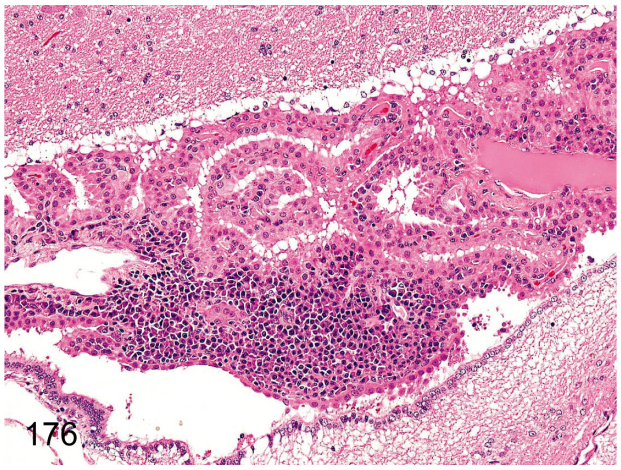

Fig. 176. Brain: Focal inflammatory cell infiltration in the choroid plexus. Lymphoplasmacytes sometimes infiltrate into the interstitium of the choroid plexus.

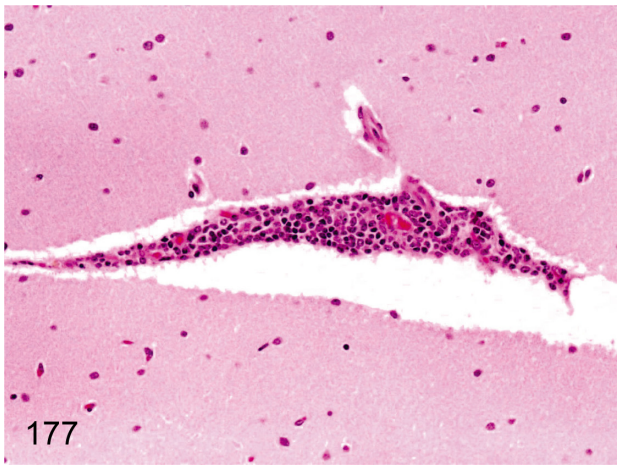

Fig. 177. Brain: Focal perivascular inflammatory cell infiltration. Focal and slight perivascular lymphoplasmacytic infiltration is rare in the parenchyma.

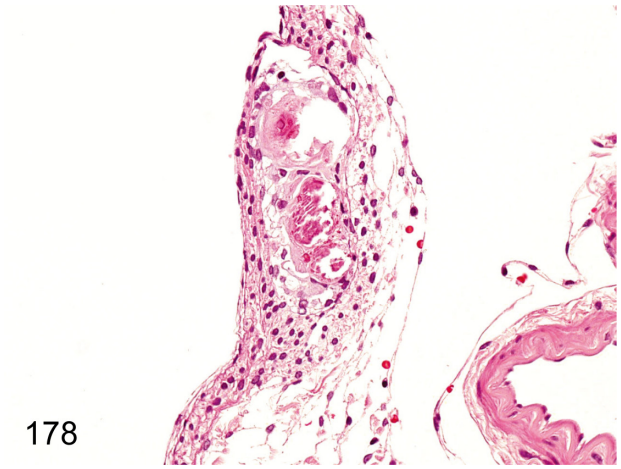

Fig. 178. Spinal cord: Mineralization in the meninx. Focal mineralization in the meninx occurs occasionally.

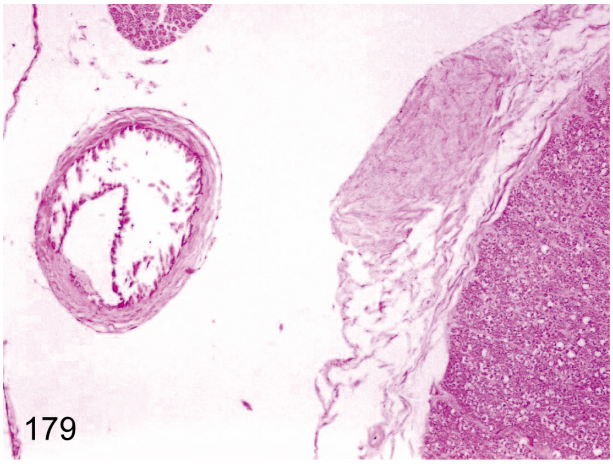

Fig. 179. Spinal cord: Mineralization in the arterial wall. Mineralization in the arterial wall occurs occasionally in the meninx.

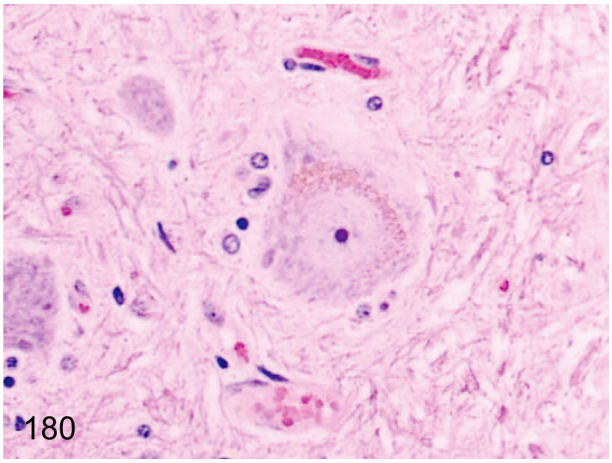

Fig. 180. Spinal cord: Pigment deposition in neuronal cells. Large neuronal cells (motor ventral horn cells) occasionally contain yellow-brown pigments. The pigments are probably lipofuscin.

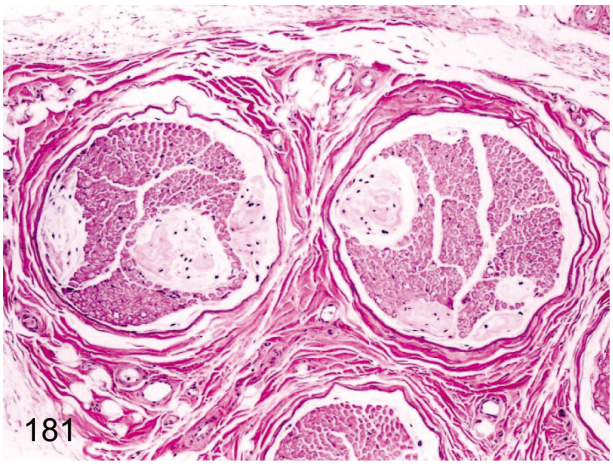

Fig. 181. Sciatic nerve: Renaut body. The irregular fine fibrous structure in the nerve fiber bundles is called the Renaut body. Its function is thought to be protection of the peripheral nerve fibers from pressure damage.

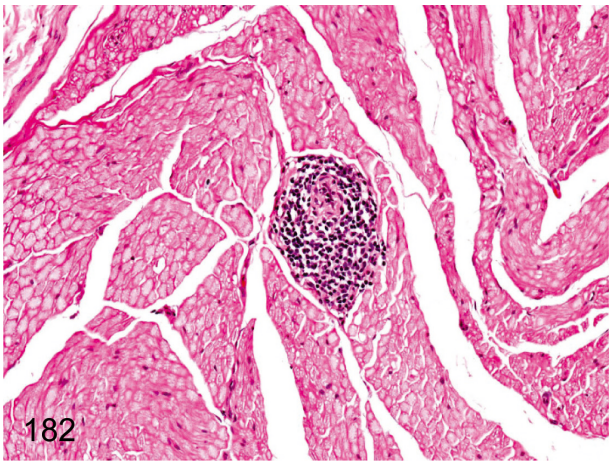

Fig. 182. Sciatic nerve: Focal inflammatory cell infiltration. Focal lymphoplasmacytic infiltration is rarely seen in the sciatic nerve.

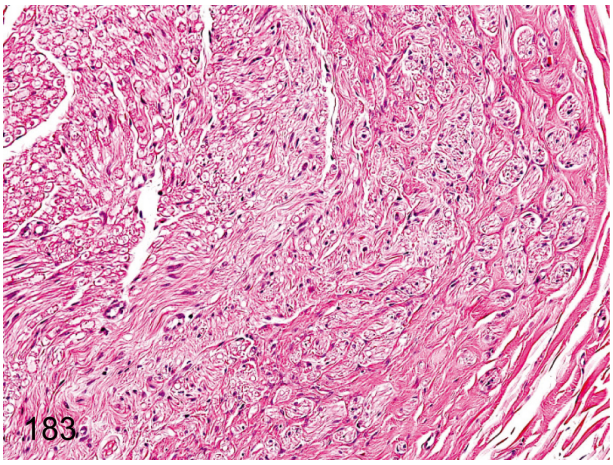

Fig. 183. Sciatic nerve: Focal fibrosis. Focal interfiber fibrosis with decreased nerve fibers is thought to be an end-stage change of peripheral nerve damage.

Fig. 184. Eye: Focal inflammatory cell infiltration in the conjunctiva. Lymphoplasmacytic infiltration is frequently seen in the subepithelium of the conjunctiva.

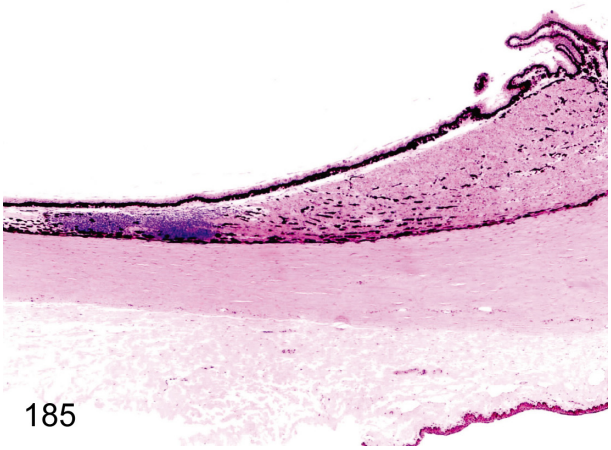

Fig. 185. Eye: Focal inflammatory cell infiltration in the ciliary body. Lymphoplasmacytes infiltrate the ciliary body, usually near the retina.

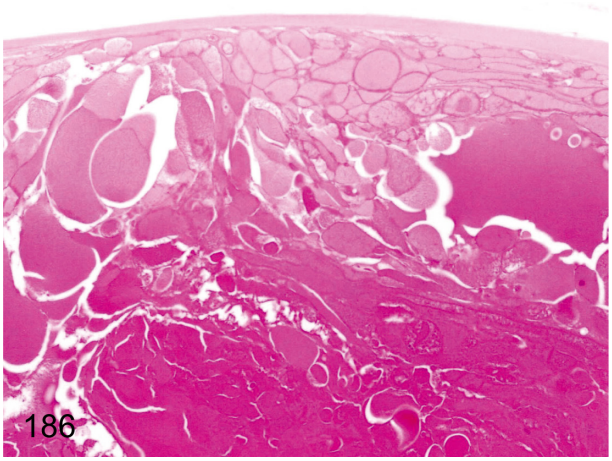

Fig. 186. Eye: Cataract. Swelling and irregular arrangement of lens fibers are characteristic changes of cataract. Intercellular junctions are focally detached in the posterior pole. Cataract is rare in young cynomolgus monkeys.

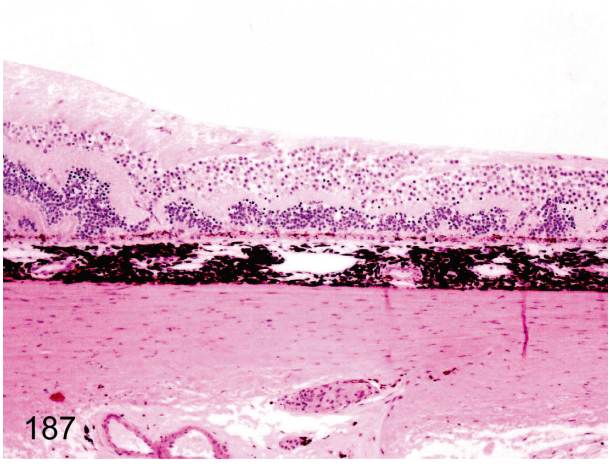

Fig. 187. Eye: Disarrangement of retinal structures . A linear folding of the retinal tissue occurs occasionally. The causes of this lesion may be congenital failures of optic fissure closure (retinal coloboma), dysplasia of retinal structures or focal damage of the retina in the fetal developmental stage.

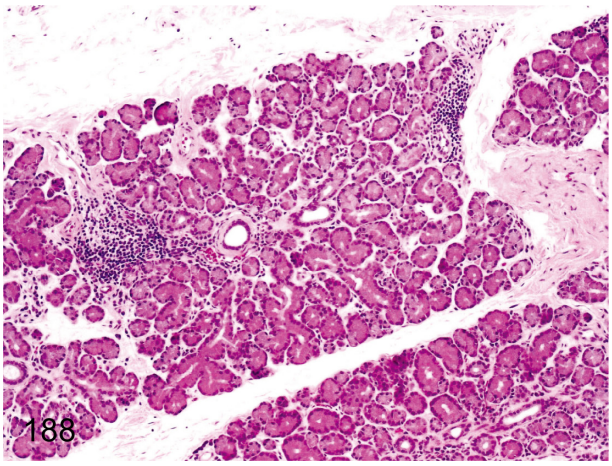

Fig. 188. Lacrimal gland: Focal inflammatory cell infiltration. Focal lymphoplasmacytic infiltration is frequently seen in the lacrimal gland.

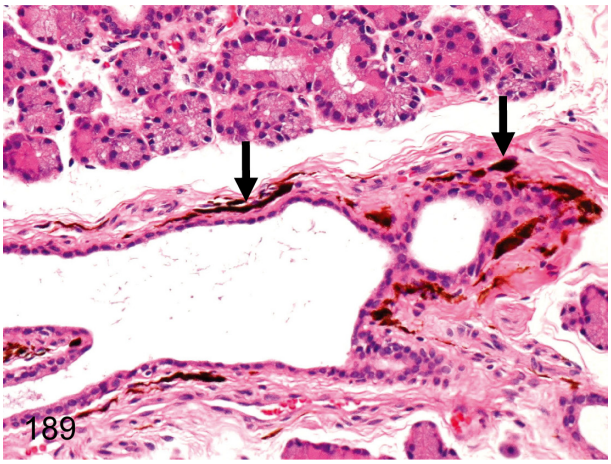

Fig. 189. Lacrimal gland: Melanin pigment deposition. Melanin pigments occasionally deposit in the interstitium around the duct. Melanin pigments deposit (melanosis) in various organs in cynomolgus monkeys. See also Figs. 141, 144, and 173.

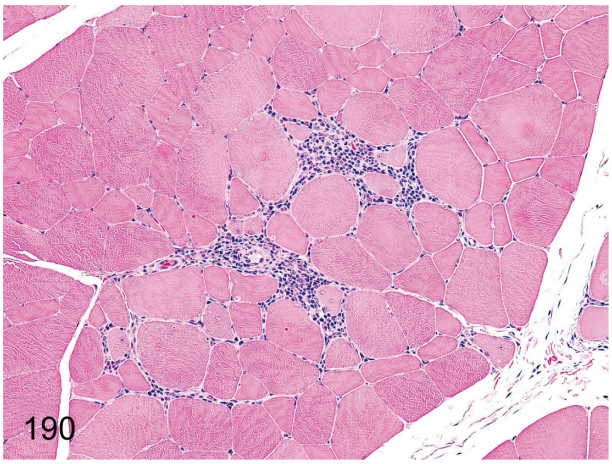

Fig. 190. Skeletal muscle: Focal inflammatory cell infiltration. Infiltration of lymphoplasmacytes and macrophages is infrequently found in intermuscle fibers.

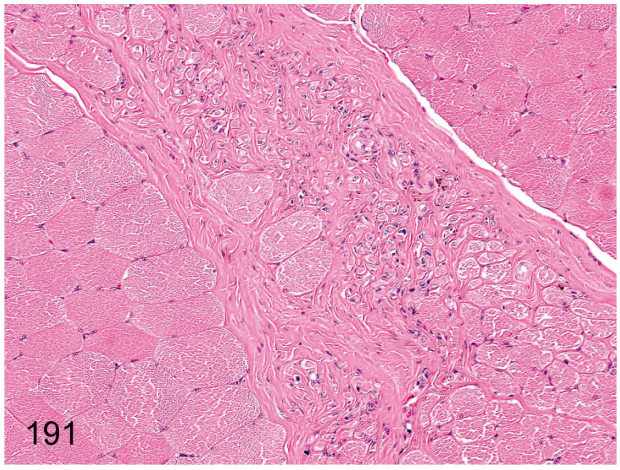

Fig. 191. Skeletal muscle: Focal fibrosis. Focal interfiber fibrosis is probably a result of the degenerative and/or inflammatory lesions such as those shown in Fig. 190. The change contains some regenerative muscle fibers.

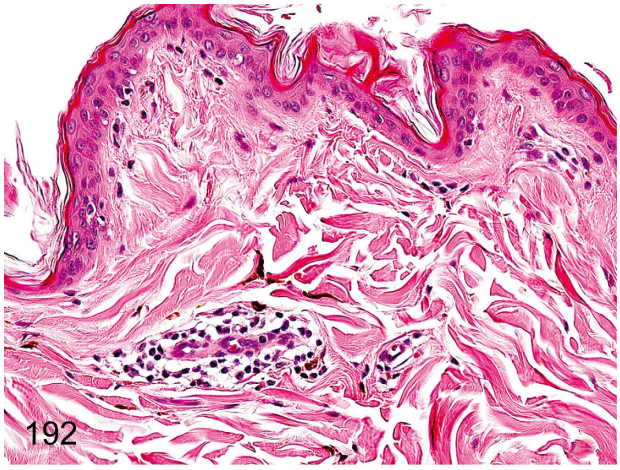

Fig. 192. Skin: Focal inflammatory cell infiltration in the dermis. Accumulation of lymphoplasmacytes is commonly localized but frequently seen in the dermis, especially in the perivascular area.

Stress-induced lesions (Figs. 193-195)

Some stress-induced lesions are observed in moribund or dead cynomolgus monkeys. Lymphoid atrophy, acinar atrophy in the exocrine glands, gelatinous atrophy of the adipose tissue and diffuse hypertrophy of the adrenocortical cells of the zona fasciculata are known to be discriminative. The figures show thymic atrophy (Fig. 193), gelatinous atrophy of the bone marrow adipose tissue (Fig. 194) and diffuse hypertrophy of the adrenocortical cells of the zona fasciculata (Fig. 195).

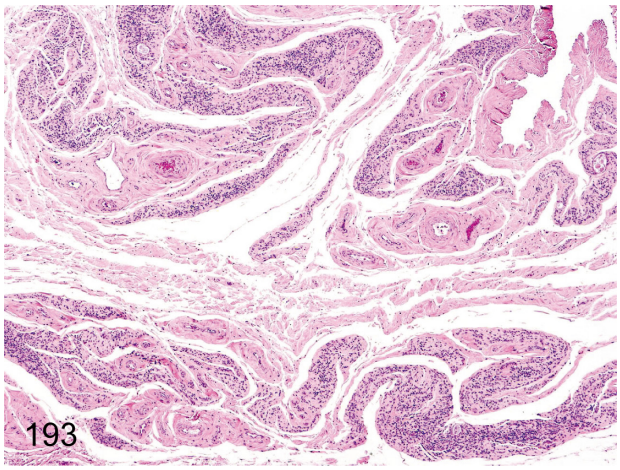

Fig. 193. Thymus: Atrophy.

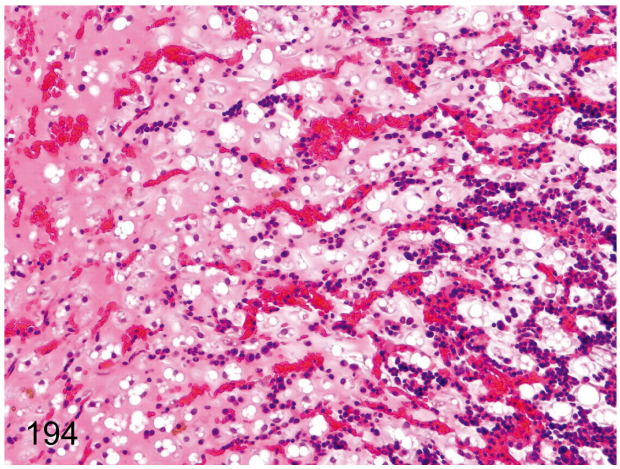

Fig. 194. Bone marrow adipose tissue: Gelatinous atrophy.

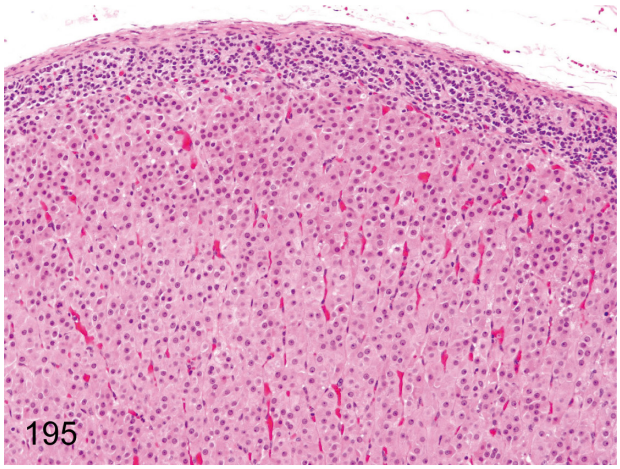

Fig. 195. Adrenal: Diffuse hypertrophy of the adrenocortical cells of zona fasciculata.